EVALUATION OF THE ROBUSTNESS PERFORMANCE OF A FUZZY LOGIC CONTROLLER FOR ACTIVE VIBRATION CONTROL OF A PIEZO-BEAM VIA TIP MASS LOCATION VARIATION

A THESIS SUBMITTED TO
THE GRADUATE SCHOOL OF NATURAL AND APPLIED SCIENCES
OF
MIDDLE EAST TECHNICAL UNIVERSITY

BY

ERDEM RAHMİ ŞENÖZ

IN PARTIAL FULFILLMENT OF THE REQUIREMENTS
FOR
THE DEGREE OF MASTER OF SCIENCE
IN
AEROSPACE ENGINEERING

AUGUST 2019

Approval of the thesis:

EVALUATION OF THE ROBUSTNESS PERFORMANCE OF A FUZZY LOGIC CONTROLLER FOR ACTIVE VIBRATION CONTROL OF A PIEZO-BEAM VIA TIP MASS LOCATION VARIATION

submitted by **ERDEM RAHMİ ŞENÖZ** in partial fulfillment of the requirements for the degree of **Master of Science in Aerospace Engineering Department, Middle East Technical University** by,

Prof. Dr. Halil Kalıpçılar
Dean, Graduate School of **Natural and Applied Sciences** _____

Prof. Dr. İsmail Hakkı Tuncer
Head of Department, **Aerospace Engineering** _____

Assoc. Prof. Dr. Melin Şahin
Supervisor, **Aerospace Engineering, METU** _____

Examining Committee Members:

Prof. Dr. Ozan Tekinalp
Aerospace Engineering, METU _____

Assoc. Prof. Dr. Melin Şahin
Aerospace Engineering, METU _____

Assoc. Prof. Dr. Ercan Gürses
Aerospace Engineering, METU _____

Assist. Prof. Dr. Ali Türker Kutay
Aerospace Engineering, METU _____

Prof. Dr. Metin Uymaz Salamcı
Mechanical Engineering, Gazi University _____

Date: 27.08.2019

I hereby declare that all information in this document has been obtained and presented in accordance with academic rules and ethical conduct. I also declare that, as required by these rules and conduct, I have fully cited and referenced all material and results that are not original to this work.

Name, Surname: Erdem Rahmi Şenöz

Signature:

ABSTRACT

EVALUATION OF THE ROBUSTNESS PERFORMANCE OF A FUZZY LOGIC CONTROLLER FOR ACTIVE VIBRATION CONTROL OF A PIEZO-BEAM VIA TIP MASS LOCATION VARIATION

Şenöz, Erdem Rahmi
Master of Science, Aerospace Engineering
Supervisor: Assoc. Prof. Dr. Melin Şahin

August 2019, 115 pages

This thesis presents a study in which a robust Fuzzy Logic Controller (FLC) is designed to suppress both free and the first resonance of a piezo-beam even if the position of the tip mass located on the beam varies. The cantilever aluminum piezo-beam involves the piezoelectric patches bonded on the surfaces to be used as a sensor and actuator for the vibration control and the displaceable tip mass attached to the free end of the piezo-beam and used to change the system parameters for checking the robustness of the designed controller.

At first, the experimental setup for actively controlled piezo-beam is introduced and the system identification of the piezo-beam for all positions of the tip mass is performed. The frequency response functions are then investigated via the System Identification Toolbox in Matlab in order to be used in the simulation studies.

Then, a FLC is designed via Fuzzy Logic Toolbox in Matlab. The performance of the FLC is the evaluated through various simulation and experimental studies such as free vibration suppression, forced vibration suppression at the first resonance frequency and the forced vibration suppression within the frequency span covering the first resonance of the piezo-beam. Moreover, the performance in the robustness of the FLC is investigated by changing the position of the tip mass.

This thesis shows that the first resonance of the piezo-beam is suppressed by the designed FLC developed for a certain position of the tip mass even if the dynamics of the piezo-beam is changed due to change in the position of the tip mass by providing a certain degree of robustness.

Keywords: Piezo-Beam, Active Vibration Control, Fuzzy Logic Controller

ÖZ

BİR PİEZO-KİRİŞ YAPININ AKTİF TİTREŞİM KONTROLÜNDE BULANIK MANTIK DENETLEYİCİNİN GÜRBÜZLÜK PERFORMANSININ KÜTLE KONUMU DEĞİŞİKLİĞİ İLE DEĞERLENDİRİLMESİ

Şenöz, Erdem Rahmi
Yüksek Lisans, Havacılık ve Uzay Mühendisliği
Tez Danışmanı: Doç. Dr. Melin Şahin

Ağustos 2019, 115 sayfa

Bu tez, bir piezo-kirişin serbest ve zorlanmış ilk rezonans frekansını bastırmak amacıyla tasarlanan Bulanık Mantık Denetleyici (BMD)'nin piezo-kirişin ucundaki kütlenin pozisyonu değiştiğinde de gürbüz bir denetleyici olarak davranmasını amaçlayan çalışmaları sunmaktadır. Alüminyum ankastre piezo-kiriş, titreşim kontrolü için algılayıcı ve uyarıcı olarak kullanılacak piezoelektrik yamaları ve kontrolcünün gürbüzlük denemeleri için sistem parametrelerini değiştirmek üzere kullanılacak olan ve piezo-kirişin serbest ucuna bağlı yer değiştirebilir kütleyi içermektedir.

İlk önce, piezo-kirişi aktif olarak kontrol etmek için kurulan deney düzeneği tanıtılmış ve piezo-kirişin ucundaki kütlenin tüm konumları için sistem tanımlaması deneysel olarak gerçekleştirmiştir. Daha sonra, frekans cevap fonksiyonları benzetim çalışmalarında kullanılmak üzere Matlab'daki System Identification Toolbox aracılığıyla bulunmuştur.

Ardından, bir BMD, Matlab'daki Fuzzy Logic Toolbox aracılığıyla tasarlanmış ve denetçinin performansı, piezo-kiriş yapının serbest, ilk rezonans frekansındaki zorlanmış ve yine ilk rezonans frekansını kapsayan frekans bandı içinde zorlanmış

titreşimlerini sönümlemek için çeşitli benzetim ve deneysel çalışmalarla değerlendirilmiştir. Ayrıca, BMD'nin gürbüz performansı da piezo-kirişin ucundaki kütlenin konumu değiştirilmek suretiyle incelenmiştir.

Bu tez, piezo-kirişin ilk rezonansındaki titreşimlerin, ucundaki kütlenin konumundaki değişiklik nedeniyle dinamiği değişse bile, kütlenin belirli bir konumu için geliştirilen BMD tarafından belli bir gürbüzlük seviyesinde sönümlendiğini göstermiştir.

Anahtar Kelimeler: Piezo-Kiriş, Aktif Titreşim Kontrolü, Bulanık Mantık Denetleyicisi

To my daughter Derin who is now in her mother's belly

ACKNOWLEDGEMENTS

First of all, I would like to express my sincere gratitude to my supervisor Assoc. Prof. Dr. Melin ŞAHİN for giving me an opportunity to work with him, allowing me to benefit from his invaluable comments and experiences and his support in completing my study.

I would like to express my gratitude to Asst. Prof. Dr. Ali Türker Kutay for support and contribution in control design.

I also would like to express my special thanks to Asst. Prof. Dr. Taylan Daş for sharing his invaluable experiences on my study and to Asst. Prof. Dr. Gülesin Sena Daş for sharing her deep knowledge in fuzzy logic.

I am completely indebted to my whole family for their endless patience, encouragement and love. Especially, I would like to thank to my sister Çiğdem Şenöz for being a friend who helps in every time of need.

Special thank and deepest gratitude to my dearest wife carrying our baby Büşra Şenöz for her endless encouragement and love. Without her support, this work would not have been completed.

TABLE OF CONTENTS

LIST OF TABLES

TABLES

LIST OF FIGURES

FIGURES

LIST OF ABBREVIATIONS

ABBREVIATIONS

DC	Direct Current
ER	Electro-Rheostatic
FFT	Fast Fourier Transform
FLC	Fuzzy Logic Controller
FRF	Frequency Response Function
LPV	Linear Parameter Varying
LQG	Linear Quadratic Gaussian
LQR	Linear Quadratic Regulator
LTI	Linear Time Invariant
MR	Magneto-Rheostatic
PD	Proportional Derivative
PID	Proportional Integrated Derivative
PVDF	Polyvinylidene Fluoride Film
PZT	Lead Zirconate Titanate
SMA	Shape Memory Alloy
TF	Transfer Function

LIST OF SYMBOLS

SYMBOLS

A	System matrix
A_d	System matrix in discrete form
A_i	Linguistic values of error for i^{th} rule
B	Controller matrix
B_d	Controller matrix in discrete form
B_i	Linguistic values of change in error for i^{th} rule
C	Output matrix
C_d	Output matrix in discrete form
C_i	Linguistic values of output for i^{th} rule
D	Feed-forward matrix
D_d	Feed-forward matrix in discrete form
e	Error in sensor signal
G_{sc1}	Transfer function between controller and sensor signals for arm position of +64º
G_{sc2}	Transfer function between controller and sensor signals for arm position of +32º
G_{sc3}	Transfer function between controller and sensor signals for arm position of 0º

G_{sc4}	Transfer function between controller and sensor signals for arm position of -32º
G_{sc5}	Transfer function between controller and sensor signals for arm position of -64º
G_{sd1}	Transfer function between disturbance and sensor signals for arm position of +64º
G_{sd2}	Transfer function between disturbance and sensor signals for arm position of +32º
G_{sd3}	Transfer function between disturbance and sensor signals for arm position of 0º
G_{sd4}	Transfer function between disturbance and sensor signals for arm position of -32º
G_{sd5}	Transfer function between disturbance and sensor signals for arm position of -64º
LM_1	Lower member of the first membership function
NB	Linguistic value of negative big
NM	Linguistic value of negative medium
NS	Linguistic value of negative small
PB	Linguistic value of positive big
PM	Linguistic value of positive medium
PS	Linguistic value of positive small
s	Complex variable in Laplace transform
u	Output of the fuzzy logic controller

UM_1	Upper member of the first membership function
UM_2	Upper member of the second membership function
x_e	Fuzzy variable for error
x_u	Fuzzy variable for output
$x_{\Delta e}$	Fuzzy variable for change in error
ZE	Linguistic value of zero
α_{C_i}	Firing strength of linguistic values of output for i^{th} rule
β_C	Maximum firing strength of linguistic values of output
Δe	Change in error in sensor signal
μ_{NB_e}	Membership function of linguistic value of negative big for error fuzzy variable
μ_{NS_e}	Membership function of linguistic value of negative small for error fuzzy variable
μ_{ZE_e}	Membership function of linguistic value of zero for error fuzzy variable
μ_{PS_e}	Membership function of linguistic value of positive small for error fuzzy variable
μ_{PB_e}	Membership function of linguistic value of positive big for error fuzzy variable
$\mu_{NB_{\Delta e}}$	Membership function of linguistic value of negative big for change in error fuzzy variable
$\mu_{NS_{\Delta e}}$	Membership function of linguistic value of negative small for change in error fuzzy variable

$\mu_{ZE_{\Delta e}}$	Membership function of linguistic value of zero for change in error fuzzy variable
$\mu_{PS_{\Delta e}}$	Membership function of linguistic value of positive small for change in error fuzzy variable
$\mu_{PB_{\Delta e}}$	Membership function of linguistic value of positive big for change in error fuzzy variable
μ_{NB_u}	Membership function of linguistic value of negative big for output fuzzy variable
μ_{NS_u}	Membership function of linguistic value of negative small for output fuzzy variable
μ_{ZE_u}	Membership function of linguistic value of zero for output fuzzy variable
μ_{PS_u}	Membership function of linguistic value of positive small for output fuzzy variable
μ_{PB_u}	Membership function of linguistic value of positive big for output fuzzy variable

CHAPTER 1

INTRODUCTION

In aircraft design, using light-weight structures has been an important criterion since beginning of the flight history. Although light-weight structures provide the aircraft many features, they have also low-stiffness characteristics. The flexible structures such as wings of aircraft or rotor blades generally suffer from dynamic loads. Fatigue can also be observed due to resonance in which severe structural vibration occurs due to matching the frequency of dynamic loads with the natural frequency of the structures at a low frequency. In the circumstances, investigation of the vibration characteristic of lightweight structures with low natural frequencies is quite important in the design of aircraft structures.

There are two different approaches to suppress vibrations of structures, namely; passive and active vibration control. Passive vibration control does not consume any power or energy in the form of an actuator. The damping properties of materials used in design or pistons used for dissipating energy are one of the key elements of passive vibration control. Additionally, the stiffness and mass properties of the structures can be changed in order to adjust natural frequencies away from resonance by alternating methods such as relocating mass [1] or making the structure stiffer or changing its geometry [2]. However, passive vibration control method is generally efficient in the high frequency range. On the contrary, active vibration control is more effective than passive one in suppression vibration at low frequency modes which is seen mostly in aerospace structures [3]. Because, external force which is applied by actuators to suppress vibration can be calculated accurately with real-time measurement of the motion, force or acceleration etc. by sensors on systems. Hereby, active vibration control methods are generally preferred more than passive methods due to the stability performance and robustness issues although active ones need input energy [4].

In active vibration control, mainly an actuator and a sensor are needed. In the aerospace structures, this need can be provided with using smart materials as a space-saving and lightweight solution. Smart materials have ability to change their property such as shape or size by external stimuli such as electric current, stress, or temperature [5]. One of example to smart materials are shown in Figure 1.1.

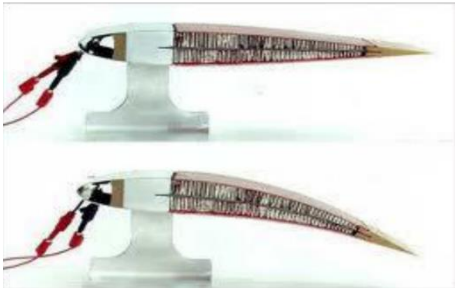

Figure 1.1. Shape Change of Smart Material with External Electric Current [5]

Active vibration control systems can be designed with various control algorithms which are created in order to calculate desired output signal with using measured input signal. Proportional-integrated-derivative (PID), linear quadratic control, H-infinity control, neural networks, genetic algorithms and fuzzy control are the most preferred control strategies used in active vibration control [6]. PID controller is one of the classic controller methods where actuator output signal is calculated by multiplied by gains with input and its numerical derivation and equivalent of integration. Linear quadratic and H-infinity controllers are basic optimization-based methods. Neural networks, genetic algorithms and fuzzy controller are soft computing approaches which are referred to as computational intelligence. With the selection of one or more of these controllers, the controller design is made for the active vibration control system.

1.1. Background of the Study

In this section, the background of the study is mentioned in four parts. The first part is about types of the vibration control. In this particular part, active vibration control is compared with passive one. The second part is related to smart structures especially

piezoelectric materials. The third part contains control strategies in active vibration control systems. The feature of the fuzzy logic controller (FLC) which is used in the study is discussed in depth. In the last part, the previous research studies related to active vibration control in Department of Aerospace Engineering at METU are presented. Consequently, the major parts of the background of the study are remarked.

1.1.1. Vibration Control: Active Vibration Control

In order to prevent undesirable vibrations on aerospace structures such as helicopter blades and wind turbine blades, passive control systems are preferred as one of vibration control method. Many applications of passive control method on the aerospace structure generally include a tuned mass damper. In the helicopter blades, the pendulum absorbers which are considered as one of passive control method have been used for reducing amplitudes of vibration at resonance as shown in Figure 1.2 [7]. Similarly, a tuned mass damper is used for reduction of vibration in wind turbine [8]. Besides tuned mass dampers, constrained-layer damping treatments reduce mechanical vibration in naval vessels and aircraft without significantly adding mass and thickness to structures [9]. Additionally, the design optimization or modification such as adding stiffener or removing mass from the structure can be evaluated as another passive control method.

Although the passive method is preferred due to simplicity and cost, it has disadvantages which are additional weight to structures and limited effectiveness at low frequency range [10]. Reverse situation may be observed when a shift in frequency of vibration source or a structural change occurs such as change in location of lamped mass on structure or loss in weight.

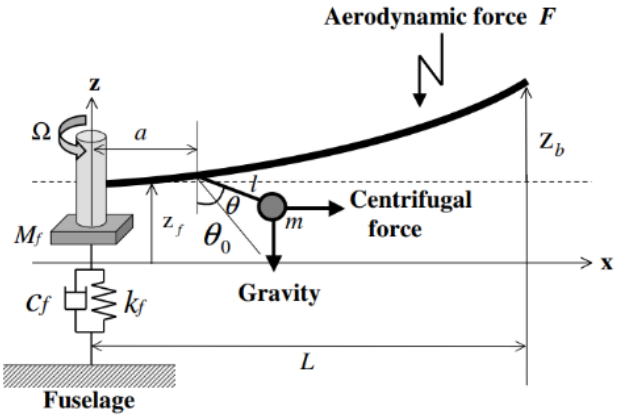

Figure 1.2. Model for a Blade, a Pendulum Absorber and a Rotor Mount [7]

Researchers have studied for last two decades active vibration control of aerospace structures. Active control techniques in vibration suppression can be applied at many areas on helicopters [11]. One example to active vibration control in a helicopter rotor is shown in Figure 1.3. With the applications of piezoelectric patches and piezo-actuators, active vibration control have been used in flexible aerospace structures [12], [13], [14]. Piezo-beams and piezo-plates are used to illustrate the flexible aerospace structures in order to analyze the performance of active vibration control. In the literature, there are many researches on a review state-of-the-art of active vibration suppression systems of flexible beams [15] and plate-like structures [16].

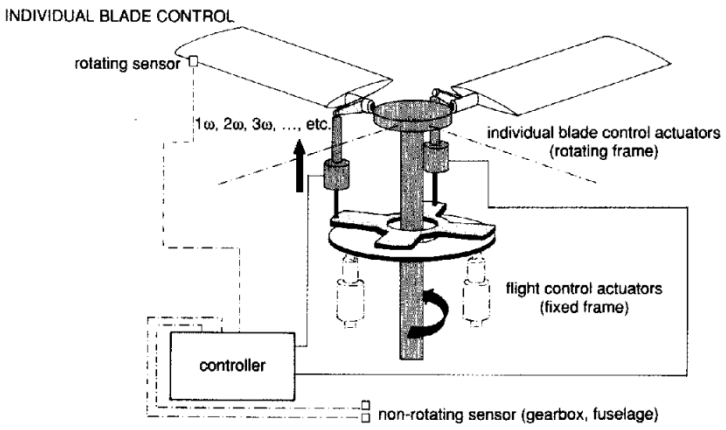

Figure 1.3. Example of Active Vibration Control in a Helicopter Rotor [11]

The active vibration control can achieve better control performance due to external control energy when compared with passive control. The other important features of active vibration control methods are to provide effectiveness over a wider frequency span and is effective at low frequency range. Additionally, components of an active vibration control unit have lower weight and save more space to the system. Pearson, Goodall and Lyndon [11] mentioned the advantages of active systems on passive ones; supplying or absorbing energy using actuators, producing control forces as a function of variables which may be remotely measured and modifying the control system to achieve different performance conditions.

1.1.2. Smart Materials: Piezoelectric Materials

Smart materials are defined as materials that have reactions to variations in environmental conditions. When the environmental conditions such as temperature, electricity, pressure or light change, smart materials react like change in their shape, color or rigidity [5]. Different varieties of smart materials have been used in many applications with their advantages. Electro-rheostatic (ER) and magneto-rheostatic (MR), shape memory alloy (SMA) and piezoelectric materials are the most popular types of smart materials [17].

ER and MR materials are fluids whose viscosity can change when materials are exposed to an electric or magnetic field. ER and MR fluids have been developed for use in engine mount design and car suspension system to reduce noise and vibration [18].

SMAs are metals which can be exposed to solid-to-solid phase transformation and can return to initial shape when heated to specific temperature. They have been widely used as an actuator in aerospace, robotic, biomedical and defense industries. A harmonic movable tooth drive system integrated with SMAs as a rotational motion actuator is one of the examples to the applications of SMA [19].

Piezoelectric materials have been widely used as smart materials. The main property of piezoelectric materials that make them “smart” is to ability to generate an electric charge in response to applied mechanical stress which is called as the piezoelectric effect. Furthermore, one of the distinctive properties of the piezoelectric effect is that it can be reversible which is called as the converse piezoelectric effect (generation of stress or deformation in shape when an electric field is applied). Therefore, piezoelectric materials can be used both as sensors with direct piezoelectric effect and actuators with converse piezoelectric effect. The direct and converse effects are shown in Figure 1.4.

The advantages of piezoelectric materials increase the popularity of them in wide range of applications where precision of control, size and lightness are important specifications. Some significant advantages can be listed as follows [20]:

- Quick in response with wide range bandwidth
- Easily bonded the surface of the structure or molded within the structure
- Small-sized with high energy density
- Cheap and commercially available

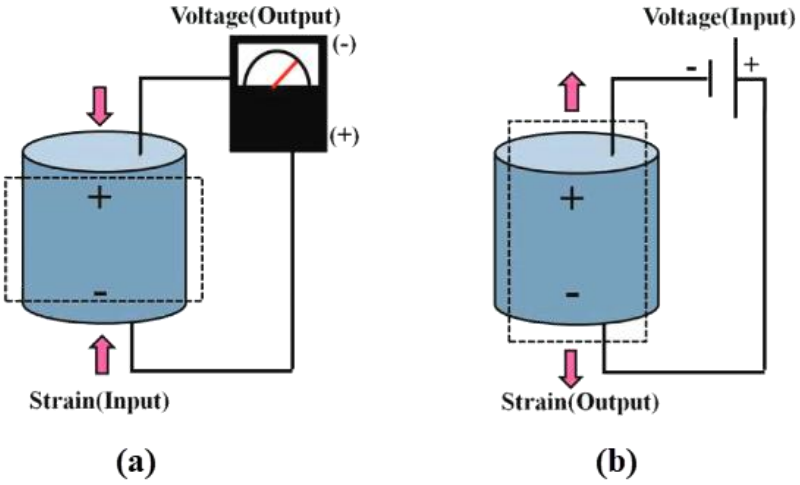

Figure 1.4. Piezoelectric Effect (a) Direct (b) Converse [21]

There are two common type of piezoelectric materials which are piezoceramics and polymer piezoelectric film. Polyvinylidene Fluoride film (PVDF) is a polymer piezoelectric film which is manufactured by solidification from a molten phase stretched in a particular direction. The most known and used type of piezoceramics is Lead Zirconate Titanates (PZTs) which are manufactured by powder technologies. PZTs have a permanent dipole moment oriented along its long axis due to undergoing a paraelectric to ferroelectric phase transition during cooling process of manufacturing [22]. In active control applications, PZTs are preferred to PVDF due to its high elastic modulus.

In this thesis, PZT patches are used as smart materials due to the ability to be used as surface bonded sensors and actuators and their advantages such as quick response and lightweight.

1.1.3. Control Algorithms: Fuzzy Logic Control

In the active vibration control applications, several control strategies have been developed by the researchers with in the last decades [23]. In many studies related to active vibration control, classical control strategies such as constant gain, amplitude velocity feedback [24], positive position feedback [25] have been employed. PID, also evaluated as classical controllers, and H_∞ controllers [26] have been used in active vibration suppression. Linear quadratic regulator (LQR) [27], and linear quadratic Gaussian (LQG) [28] control methods are optimal control algorithms where control forces are determined by minimizing a cost function. Wang and Inman compare positive position feedback, PID and LQR controllers in terms of their energy consumption [29]. These controller algorithms suffer from failing to suppress vibration when the frequency of the excitation differs slightly from the natural frequency of the structures [30]. Kircali [31] and Sahin et al. [32] have implemented H_∞ and μ-synthesis controllers for robust performance of the systems in the presence of uncertainties. Although the control strategies mentioned above can provide suitable solution for many problems related to vibration suppression, most of them need a

mathematical model of the system in order to define parameters of the controllers. Additionally, the performance of them are adversely affected by changing operating conditions and it is difficult to adjust the parameter of controller for operating conditions. The soft computing control systems such as neural network, genetic algorithms and fuzzy logic are suited for plants whose exact mathematical model is hard to be achieved. Qiu et al. have employed a back propagation neural network to tuning parameters of proportional-derivative (PD) controller online in order to minimize the effect of the nonlinearities as an example for soft computing control systems [33]. Kwak and Sciulli have shown that the fuzzy logic control has been designed for the active structure with collocated sensors and actuators without any knowledge of the structure [34].

The basis of fuzzy controllers is based on the fuzzy set theory. The theory has been established in 1965 by Zadeh [35]. In contradiction to classical set theory, fuzzy set is specified by a membership function which assigns to each object a membership value in interval between zero and one. In other words, fuzzy set is a mathematical model which is based on the generalization of the classical set and its characteristic function.

Researchers have studied the fuzzy set theory and its applications in many research fields especially control theory. In 1974, Mamdani has implemented the fuzzy control algorithm in order to control a steam engine by means of "IF-THEN" rules, expressed as fuzzy conditional statements [36]. Fuzzy logic is based on human thinking and natural language. Basically, the sets in fuzzy logic derive from the approximate assumptions that humans guess. From this point of view, the main parts of fuzzy logic controls are the set created by human guess and the rules based on linguistic control. FLCs are designed by converting the human's linguistic control strategies based on expert knowledge and experience into a soft computing control algorithm.

FLCs do not need a mathematical model of the plant, it can be applied to many systems where conventional control theory is not applicable due to lack of mathematical models. Because, their algorithm can be constituted by converting the linguistic

control strategy based on expert knowledge in engineering. It is very useful when the analyses made for designing a controller are too complex or when the available information for analysis are inaccurate, or uncertain. Since, it does not have the complicated mathematical calculations, it is easy to understand and to modify.

Fuzzy logic control theory can be applied not only linear but also non-linear systems. Because the actuators used in active vibration control systems have non-linear characteristics, FLCs are used as non-linear controllers. Wenzhong et al. have used a fuzzy logic system in order to suppress the primary disturbance which is non-linear sensor function with non-linear piezoelectric actuators [37].

Researchers found FLCs easy to use in control applications in smart structures equipped with piezoelectric sensor and actuators. Teng et al. have applied fuzzy theory to structural active control without theoretical deduction and complicated calculation [38]. Lin and Liu have demonstrated a novel vibration absorption scheme using fuzzy logic which can significantly enhance the performance of a flexible structure with a resonant response [39]. Tairidis et al. [40] and Marinaki et al. [41] have used a genetic algorithm in order to optimize the parameters of the fuzzy controller. Zoric et al. have studied on active control of smart beams for free vibrations using particle-swarm optimized self-tuning FLC in order to improve robustness and performance of the FLC [42]. Wei et al. have designed dual-mode controllers combining fuzzy logic and proportional integral control for suppressing the lower amplitude vibration near the equilibrium point significantly [43].

Consequently, FLCs have been improved with various researches and therefore become more common in active vibration control applications of piezo-structures because of simple creation, non-linearity characteristics, and compatibility with different operating conditions.

1.1.4. Research Studies related to Active Vibration Control in the Department of Aerospace Engineering at METU

In the Structural Laboratory in the Department of Aerospace Engineering at Middle East Technical University, there are many experimental studies related to the structural modelling characteristics and active vibration control [32]. In these experimental studies, system model of cantilever beam-like and plate-like structures with surface bonded PZT patches are identified by using strain gauges or laser displacement sensor. For plate-like structure applications, optimum locations of the PZT patches as sensors and actuators for suppression of the first three resonance modes of the are determined [44].

There are many different controller designs in order to suppress the free and forced vibrations of the structures with PZT patches as actuators and sensors. At first, H_∞ and sliding mode controller models are obtained to be used in vibration suppression [45], [46]. Then, active vibration control is achieved by designing of LQG controller [47] and fractional controller [48]. Moreover an LPV based fractional controller is designed for the vibration suppression of the smart beam with variable mass [49].

The mass location variation mechanism on the free end of the beam-like structures are designed for performance evaluation of robustness of the controller for vibration suppression of the structures with different modal parameters. The performance of a linear controller with a neural network based adaptive element for active vibration suppression of the piezo-beam with the mass location variation mechanism is also investigated [50], [51].

1.2. Motivation to the Study

Having motivated from the previous studies related to the piezo-beam with variable mass, in this thesis, the FLC is designed and implemented in order to achieve the vibration suppression of the piezo-beam even if the system parameters has been changed with the mass location variation mechanism. Performance evaluation of a

FLC which is designed for certain system parameters of the piezo-beam is made according to the results of the system response for all cases where the piezo-beam has different system parameters.

1.3. Limitation of the Study

The limitations of the study are presented in the following list as;

- The nonlinearity due to hysteresis characteristics of PZT patches and adhesive between beam and PZT patches are neglected in the simulation results.
- Noise level due to hardware setup and cabling has limitations in the experimental work and is handled by using a low pass filter.
- The working frequency range is selected only at around the first resonance frequencies of the piezo-beam for different system parameters which can be changed with the mass location variation mechanism.

1.4. Objective of the Study

The objectives of the study are presented in the following list as;

- Obtaining the system parameters of the piezo-beam via experimental setup by using System Identification Toolbox in Matlab.
- Suppressing free and forced vibration at the first resonance frequency of the piezo-beam by designing and implementing a FLC in both simulation and experimental studies.
- Designing various FLCs with different parameters such as the number of rules, the overlap ratio and core location of the membership functions to compare the robustness on the vibration suppression of the piezo-beam via mass location variation mechanism.

By achieving these aforementioned objectives, this thesis contributes the evaluation of robustness of various designed FLCs on the vibration suppression of a piezo-beam via mass location variation to the current literature.

1.5. Outline of the Study

In Chapter 1, background studies about vibration control techniques, smart structures and control algorithms are mentioned. The research studies, related to Active Vibration Control in the Department of Aerospace Engineering at METU, are also presented as background studies. Followed by, the motivation, limitation and the objective of the study are given.

In Chapter 2, first, the experimental setup which consists of the piezo-beam with piezoelectric patches and its hardware setup is introduced. Then, the system model parameters are identified separately for different excitation signals and various arm positions. Additionally, the first resonance frequency of the piezo-beam with various arm positions are compared with each other. Finally, the estimated transfer functions are obtained to be used in the simulation for the comparison of the performances of the FLCs with experimental results.

In Chapter 3, the fuzzy logic control algorithm is introduced in details while designing the intended FLC according to the experimental studies in the fundamental resonance frequency of the piezo-beam corresponding to a certain arm position of the mass location variation mechanism. The simulation and experimental results of suppression of the free and forced vibration are then represented for this particular arm position.

In Chapter 4, the performances in the robustness of the designed controllers are evaluated by changing the arm position through mass location variation mechanism. The experimental studies for various FLCs which are designed by chancing the number of the rules, the overlap ratio and core location of the membership functions for those predefined arm positions are then performed and compared with each other regarding their robustness performances in the suppression of the forced vibration of a piezo-beam at its first resonance for corresponding arm position.

All obtained results are discussed and the outcomes are summarized in Chapter 5 by also providing a future work for this particular research study.

CHAPTER 2

EXPERIMENTAL SETUP AND SYSTEM IDENTIFICATION OF THE PIEZO-BEAM STRUCTURE

2.1. Introduction

In this chapter, the experimental setup which aims to control free and forced vibration at the first resonance frequency of the piezo-beam are introduced and the system identification of the piezo-beam using an experimental setup is defined. First, the experimental setup with the piezo-beam and hardware equipment for data acquisition and signal processing are briefly introduced. Then, how the system parameters of the setup are obtained is explained in details. Finally, the mathematical models of the system for various arm positions of the mass location variation mechanism are derived in order to simulate the performance of the controller.

2.2. Experimental Setup

The experimental setup established for the vibration control research studies in the Department of Aerospace Engineering at METU is also used in this particular study. The setup consists of the piezo-beam on which PZT patches have been surface bonded, the real-time target machine for both data acquisition and signal processing and the high voltage amplification system.

2.2.1. Piezo-Beam Structure

The piezo-beam shown in Figure 2.1 is a cantilever aluminum beam on which four PZT patches are bonded. The beam, with a size of 300 mm x 30 mm x 2 mm, is hold with a clamp in vertical position. Four pieces of Sensor Technology BM500 with dimensions of 25 mm x 25 mm x 0.5 mm is used as PZT patches bonded on the

surfaces of the beam. In the bonding process, a good insulation layer between the aluminum beam and PZT patches was provided due to preventing the electrical fields of signals from each other.

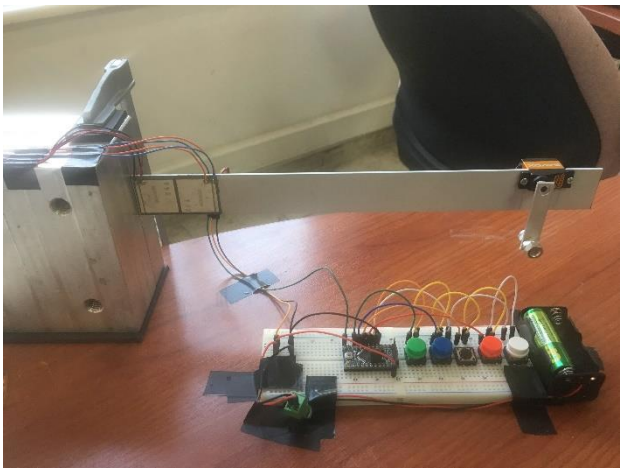

Figure 2.1. The Piezo-Beam in the Department of Aerospace Engineering at METU

One of the PZT patches in the experimental setup is used as a sensor PZT which is labeled as “S”, one of them is used as a disturbance PZT labeled as “D”, and the other two of them are used as controller PZTs labeled as “C1” and “C2”. The PZTs were bonded on the both sides which are near the clamped end of the beam as shown in Figure 2.2. The reason for the PZTs to be bonded close to the fixed end is that the PZTs generate or sense the maximum strain near the fixed end for controlling the first mode of the beam [52].

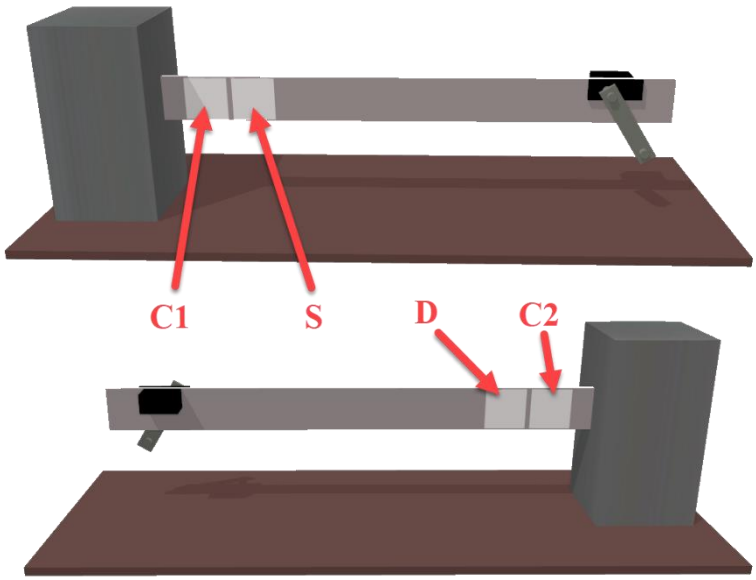

Figure 2.2. Presentation of PZTs Label on the Reference View from Both Sides of the Piezo-Beam Modal

The sensor PZT takes advantage of direct piezoelectric effect while the disturbance PZT and the controller PZTs act as actuators with properties of converse piezoelectric effect. Additionally, controller PZTs are attached to the beam by the bimorph connection. In the bimorph connection, they are not only bonded collocated, but also the cables of them are connected with opposite polarization. When bimorph connection is applied to the collocated PZTs, they are called bimorph actuators. In the bimorph actuators, one patch contracts and the other expands, therefore; the resulting strain in opposite direction affect the bending mode of the beam when voltage is applied. Therefore, the beam can be deformed in bending mode by the bimorph actuators for control of bending modes.

The mass location variation mechanism, where the arm can be rotated by the servomotor, is placed at the free end of the piezo-beam in order to obtain different modal characteristics of the piezo-beam through the rotating the arm. The arm on which the tip mass is can be driven to five different positions by servomotor as shown in Figure 2.3 when the related one from five different push buttons on the controller board setup is pushed. Thanks to the mass location variation mechanism, because there can be five different modal characteristics of the piezo-beam, the performance in the

robustness of a controller which is designed for a certain modal characteristic with a determined arm position can be compared with the other four system models in various arm positions.

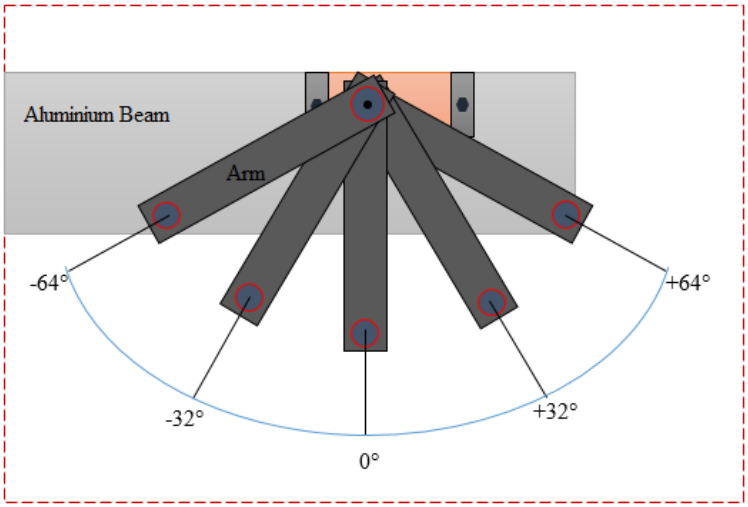

Figure 2.3. Different Arm Positions [51]

2.2.2. Real-Time Target Machine

In this experimental setup, Speedgoat Education Real-Time Target Machine connected to a host PC where MATLAB Simulink and Toolboxes installed is used for data acquisition and signal processing. The target machine is equipped with an input/output module "Speedgoat I/O 102" where the limit of voltage range of both analog inputs and outputs signal is to ±10 V.

A Simulink model is created in Simulink Real-Time for the real-time testing by use of the driver block of the I/O module in Simulink. The input and output signal connections are made with the driver block in the Simulink model. In the I/O module and its driver block as shown in Figure 2.4, channel (1) of analog input module is used for the sensor PZT while channel (1) and channel (2) of analog output module are used for the disturbance PZT and the controller PZTs, respectively.

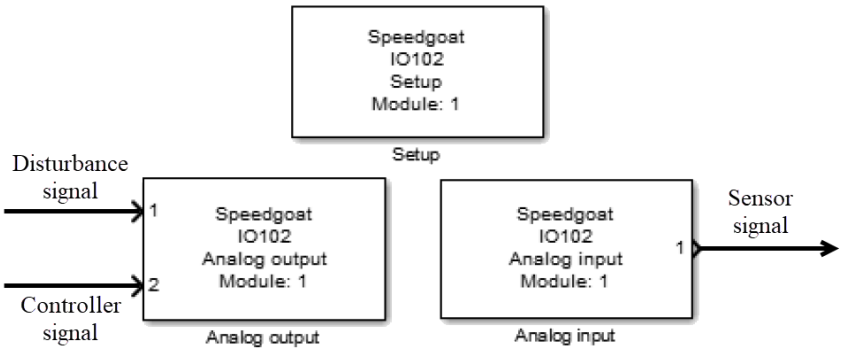

Figure 2.4. The Driver Blocks of Speedgoat I/O 102

2.2.3. High-Voltage Amplification System

High-voltage is required to operate both the disturbance and the controller PZTs which are used as actuators with a sufficient signal to noise ratio. Sensortech SA10 high-voltage power amplifier, powered by Sensor SA21 High-Voltage power supply, is used in order to increase voltage of the disturbance and actuator signals to 15 times. Although Speedgoat I/O 102 module can produce ±10 V, limit of input voltage of the power amplifier is ±9 V. For this reason, a saturation block with ±9 V is added to secure the voltage range. Consequently, the voltage generated by the disturbance and controller PZTs is limited in the range of ±135 V.

The sensor PZT can produce higher voltage than output voltage limit of the I/O module which is ±10 V. For providing a solution, LM324N IC op-amp, powered by ± 10V power supply, is used in order to decrease voltage generated by the sensor PZT to 4.7 times. Because voltage limit of sensor signal is ±10 V defined by the I/O module, voltage generated by the sensor PZT has the limit in range of ±47 V.

2.2.4. Schematic of the Experimental Setup

The schematic representation of the experimental setup can be seen in Figure 2.5.

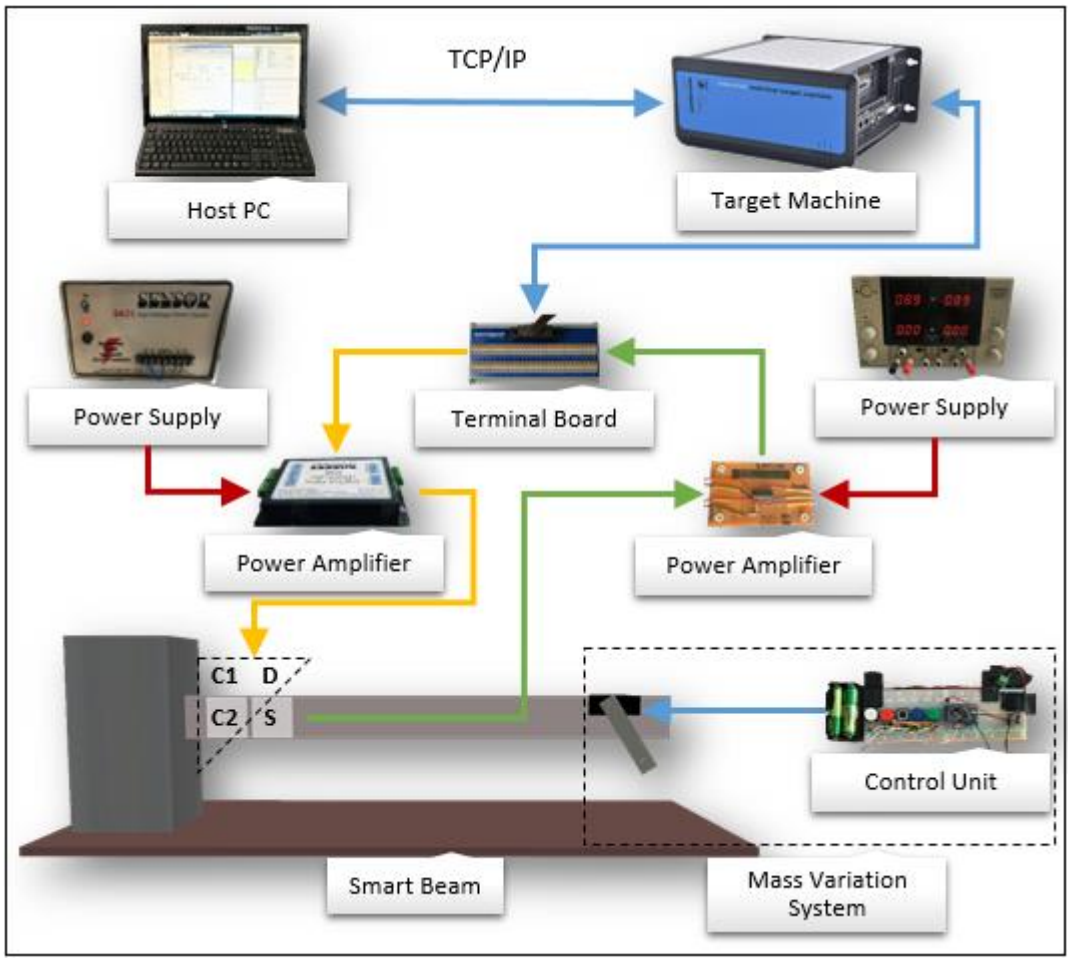

Figure 2.5. Schematic Sketch of the Experimental Setup

2.3. System Identification

A frequency response function (FRF) of the piezo-beam is required to be identified in order to simulate the designed controllers and obtain simulation results in order to compare with experimental results. In the experimental setup, as there are two input and one output signals on the piezo-beam, two transfer functions as parameters of the system model both between the disturbance and sensor signals and between the controller and sensor signals are investigated. Additionally, the transfer functions of the system should be obtained for various arm positions. Finally, in order to simulate the performance of a controller, it is necessary to obtain transfer functions for five different positions of the arm.

2.3.1. Excitation Characteristic and Time Response

In order to obtain a transfer function, the system should be excited by an input signal and output signal should be logged as a response of the system. In this experimental setup, there are two different input signals which are the controller and disturbance signal. The same excitation characteristic is applied separately as an input signal of controller and disturbance PZT in order to obtain the transfer functions by recording the sensor signal as output for the different positions of the arm.

A logarithmic sweep signal is applied as an excitation frequency. The properties of the sweep excitation are given in Table 2.1. Since it is already known from the previous study on the piezo-beam [51] that the mode of the piezo-beam is around 14.5 Hz, frequency of the signal is varying from 5 to 35 Hz with logarithmic increment.

The duration of the sweep excitation is set to 20 s in order to have the frequency resolution of Fast Fourier Transform (FFT) be as 0.05 Hz.

Table 2.1. *Parameters of the Sweep Excitation Signal*

Frequency Sweep	Logarithmic
Initial Frequency	5 Hz
Target Frequency	35 Hz
Sweep Time	20 s
Number of Sweeps	1
Sample Time	0.1 ms
Voltage	±5 V

Simulink models in Figure 2.6 and Figure 2.7 are prepared in order to observe and log input-output data for model identification between controller and sensor signals and between disturbance and sensor signals, respectively. In both figures, the chirp block is multiplied by the gain of 5. The chirp block which generates input signal is connected with the controller signal port (2) of the analog output driver block of

I/O 102 in Figure 2.6 for the transfer functions between the controller and sensor signals. For the ones between the disturbance and sensor signals, the chirp block is connected with the disturbance signal port (1) as shown in Figure 2.7. Then, the sensor signal is logged via analog input driver block of I/O 102.

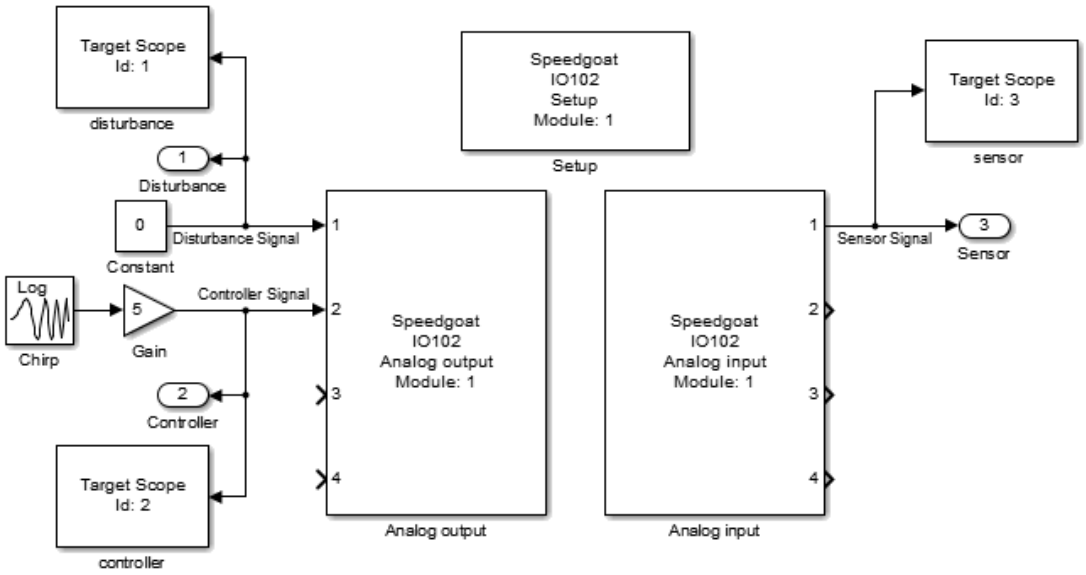

Figure 2.6. Simulink Model for System Identification when Controller Signal is applied as an Input

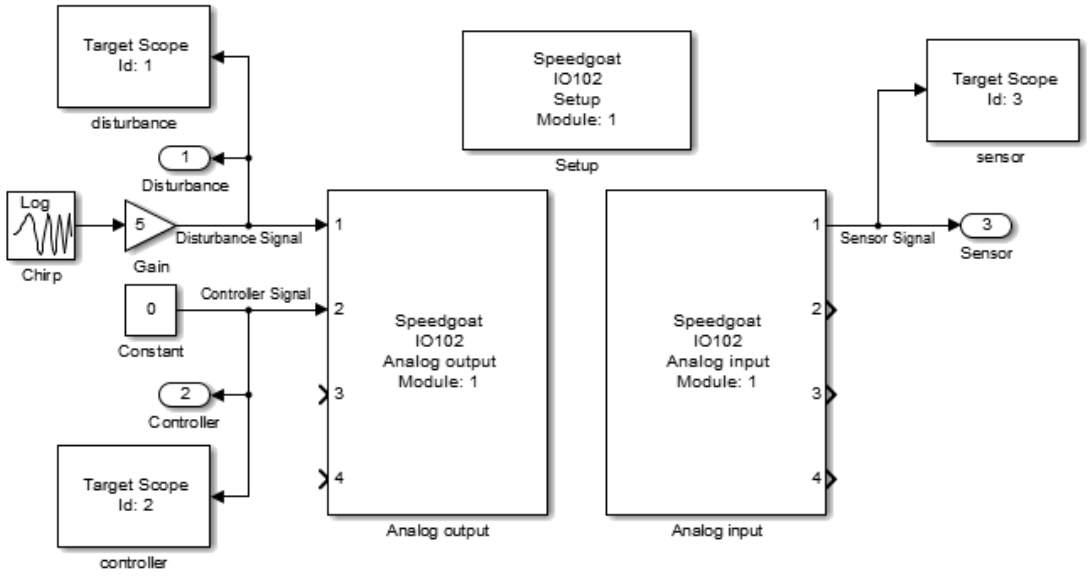

Figure 2.7. Simulink Model for System Identification when Disturbance Signal is applied as an Input

The both controller and disturbance signals as excitation signals and the time responses of the piezo-beam for all cases with different arm positions are plotted in Figure 2.8 and Figure 2.9. The excitation signals are the same for all the cases. Even in time domain, time responses show that the first resonance frequency of the piezo-beam increases when the arm rotates from +64° to -64° (towards to fixed end).

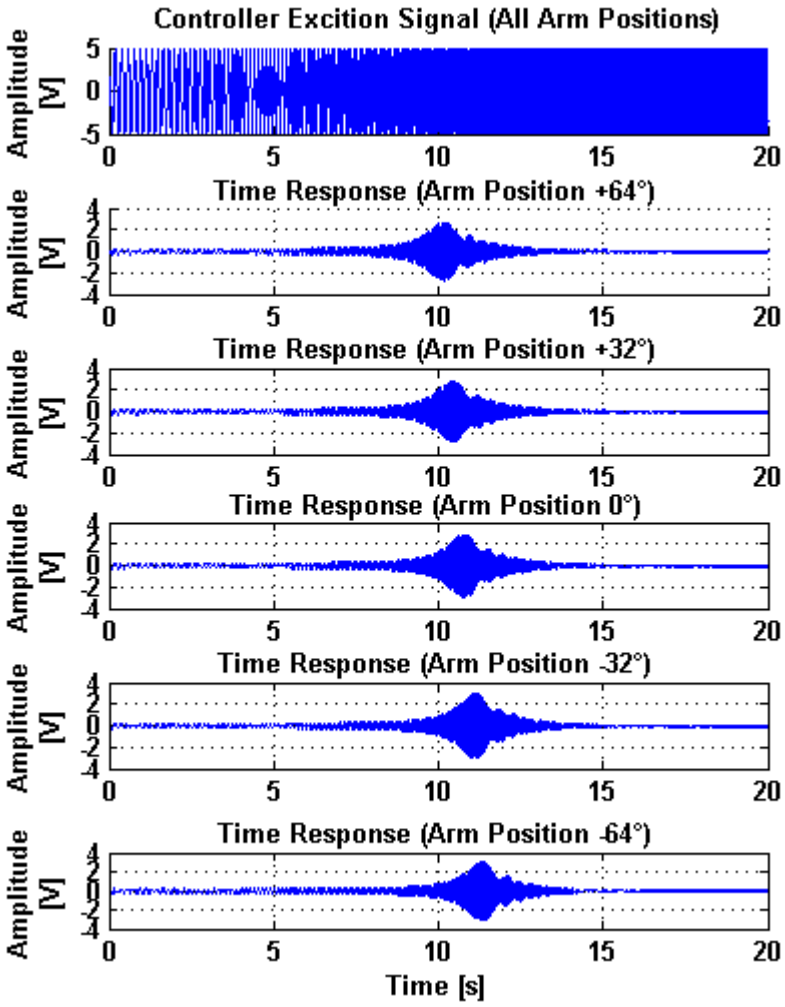

Figure 2.8. Time Responses of Controller Excitation Signal

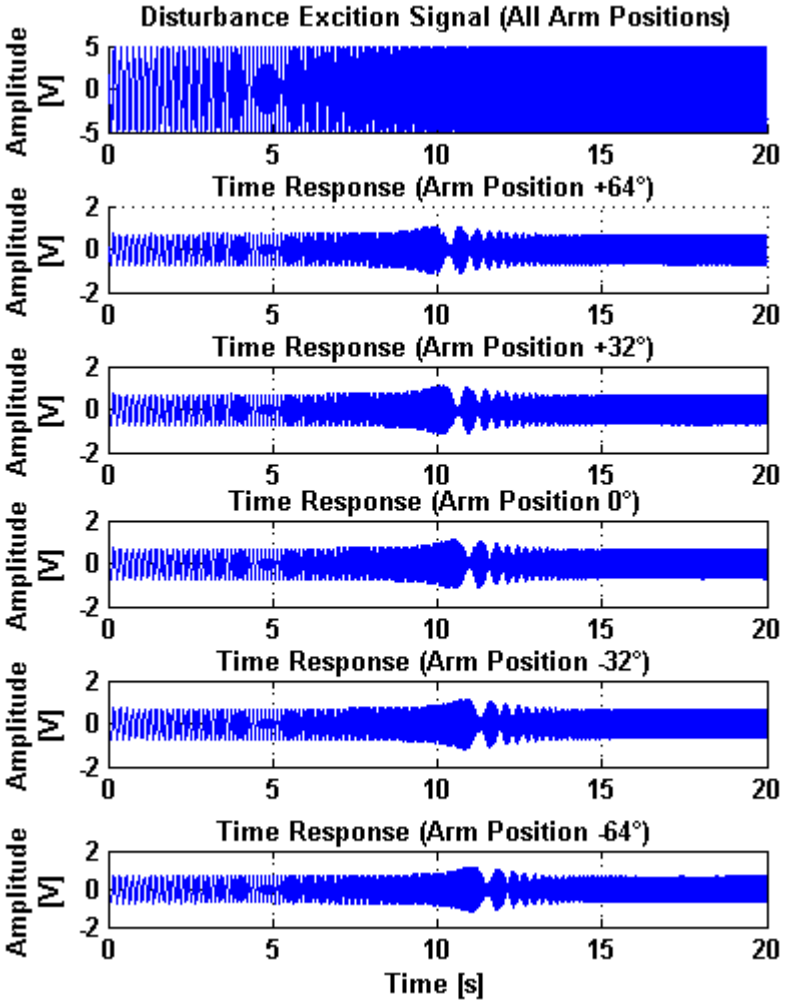

Figure 2.9. Time Responses of Disturbance Excitation Signal

2.3.2. FRFs between the Excitation and the Response Signal

The time domain signals gathered with sampling frequency of 10 kHz are converted to frequency domain and analyzed to obtain FRFs between the excitation and response signals in the range of 5 to 35 Hz.

MATLAB function *tfestimate* is used to plot FRFs. The signals are windowed with a window of 131072 (2^{17}) samples or 13.1 s. Also, FFT length is determined as 131072. Therefore, frequency resolution of transfer functions is 0.076 Hz/bin. Additionally, 90% overlap of the window is used in order to reduce noise with averaging more

windows in the limited time span. In the other words, the window is shifted 1.31 s after each average. In this way 6 windows which can be averaged are obtained with 20 s of signal and 90% overlap of the windows.

The FRFs between the controller and sensor signals for different arm positions from +64° to -64° are plotted in Figure 2.10 with the range of 5-35 Hz.

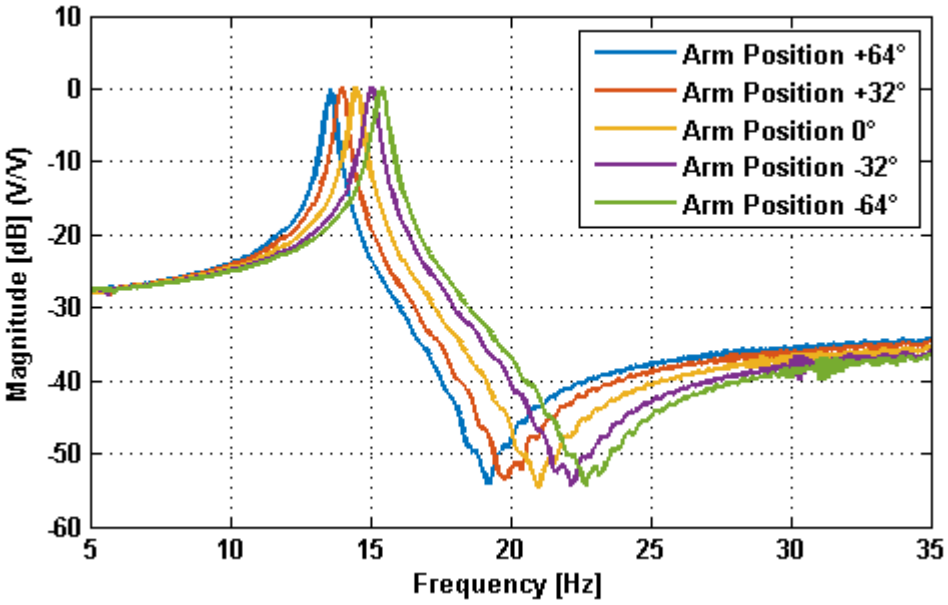

Figure 2.10. FRFs between Controller and Sensor Signals for Different Arm Positions

The first resonance frequencies of the piezo-beam for different arm positions and their corresponding peak magnitudes of the controller and sensor signals are tabulated in Table 2.2. The peak magnitudes in the FRFs show magnitude ratios between the two signals at the resonance. As analyzed in time domain data in the Section 2.3.1, the first resonance frequency increases when the arm rotates towards to fixed end (i.e. from +64° to -64°).

Table 2.2. *The First Resonance Frequencies and Corresponding Magnitude Ratios of Controller and Sensor Signals for Different Arm Positions*

Arm Position	Resonance Frequency [Hz]	Peak Magnitude [dB] (V/V)
+64°	13.58	-0.1067
+32°	13.96	0.0964
0°	14.50	0.2045
-32°	15.03	0.2221
-64°	15.41	0.2649

The FRFs between the disturbance and sensor signals for different arm positions are also plotted in Figure 2.11.

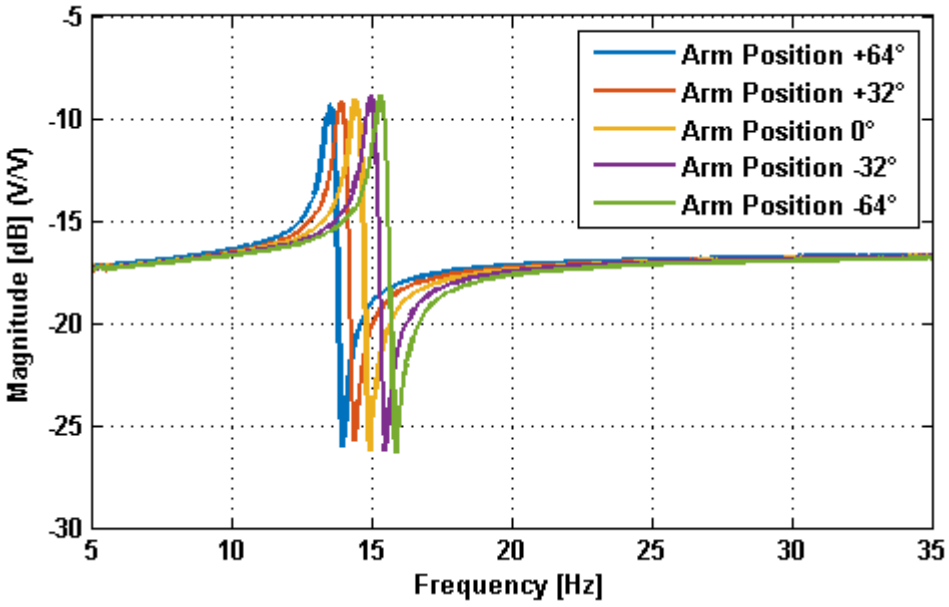

Figure 2.11. FRFs between Disturbance and Sensor Signal with Different Arm Positions

Table 2.3 is also created for the first resonance frequencies of the piezo-beam for different arm positions and their corresponding peak magnitudes of the disturbance and sensor signals. It is shown that the same first resonance frequencies are obtained by using different input signal channels which are designated as the controller and disturbance signals. The reasons for the low peak magnitudes in the FRFs between the

disturbance and the sensor signals with respect to the FRFs between the controller and the sensor signals are from the fact that there are two controller PZTs and they are connected in bimorph configuration.

Table 2.3. *The First Resonance Frequencies and Corresponding Magnitude Ratios of Disturbance and Sensor Signals for Different Arm Positions*

Arm Position	Resonance Frequency [Hz]	Peak Magnitude [dB] (V/V)
+64°	13.58	-9.547
+32°	13.96	-9.351
0°	14.50	-9.208
-32°	15.03	-9.089
-64°	15.41	-9.224

2.3.3. Continuous Transfer Functions of Identified Model

Transfer functions in Laplace domain should be estimated in order to be used as plants in controller design stage. The transfer functions of identified models are estimated by using MATLAB function *tfest* or MATLAB System Identification Toolbox. Because optimal order of the estimated transfer function is third order in order to represent only the first resonance region which is the frequency range of 5-35 Hz, the number of poles and zeros is selected as three for the continuous transfer functions.

Transfer functions between the controller and sensor signals and their corresponding fitting ratios, which indicate the agreement between response of the model and measured output in time domain, for different arm positions are tabulated in Table 2.4.

Table 2.4. *Estimated Continuous Time Transfer Functions between Controller and Sensor Signals and Fitting Ratios in Time Domain for the Different Arm Positions*

Arm Position	**Continuous Time Transfer Function**	**Fitting Ratio**
+64°	$G_{sc1}(s) = \frac{0.01983s^3 - 0.1098s^2 + 287.2s - 3255}{s^3 + 1.572s^2 + 7295s + 35.2}$	96.62%
+32°	$G_{sc2}(s) = \frac{0.01913s^3 - 0.1088s^2 + 303.1s - 3476}{s^3 + 1.609s^2 + 7719s + 44.11}$	96.74%
0°	$G_{sc3}(s) = \frac{0.01845s^3 - 0.09243s^2 + 326s - 3757}{s^3 + 1.7s^2 + 8315s + 66.67}$	96.82%
-32°	$G_{sc4}(s) = \frac{0.01769s^3 - 0.08339s^2 + 349.6s - 4090}{s^3 + 1.808s^2 + 8937s + 76.39}$	96.91%
-64°	$G_{sc5}(s) = \frac{0.01734s^3 - 0.07675s^2 + 367.8s - 4270}{s^3 + 1.88s^2 + 9371s + 35.78}$	96.87%

The estimated transfer functions (TF) are compared with FRFs obtained with experimental data for all different arm positions in Figure 2.12. In the resonance frequency regions of all different arm positions, the bode diagrams almost coincidence and the peak magnitudes at the corresponding resonance frequencies are also very close to each other.

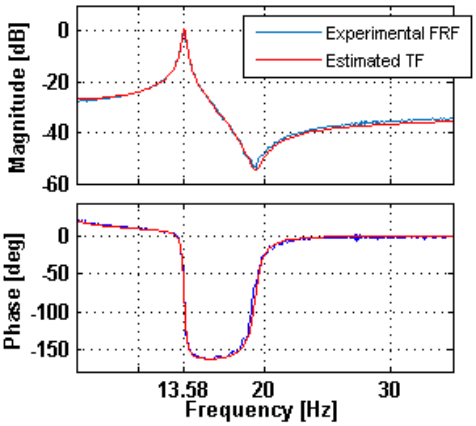

a) Arm Position +64°

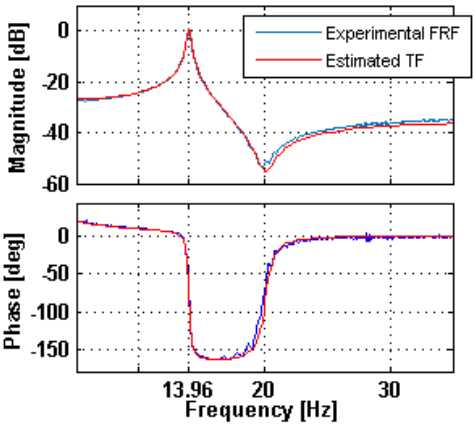

b) Arm Position +32°

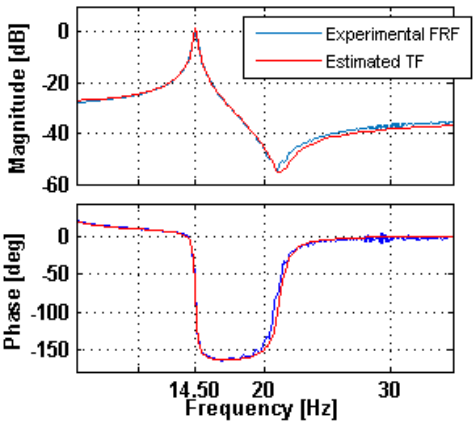

c) Arm Position 0°

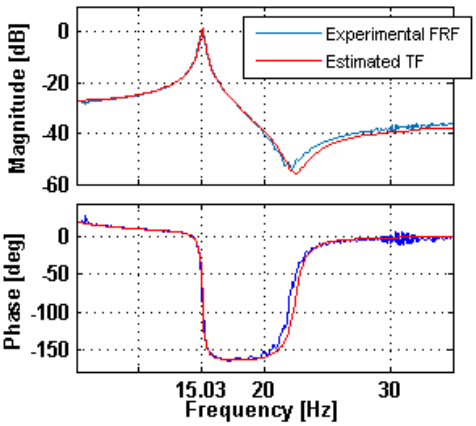

d) Arm Position -32°

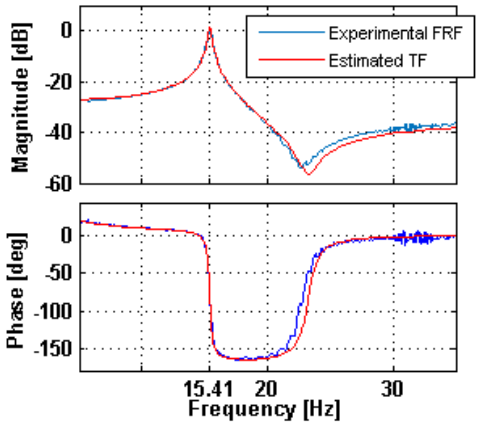

e) Arm Position -64°

Figure 2.12. FRF of Experimental Data and Estimated Transfer Function between Controller and Sensor Signals for the Different Arm Positions (Bode Diagrams)

The same procedure is applied for obtaining transfer function between the disturbance and sensor signals. The transfer functions and their corresponding fitting ratios are tabulated in Table 2.5.

Table 2.5. *Estimated Continuous Time Transfer Functions between Disturbance and Sensor Signals and Fitting Ratios in Time Domain for the Different Arm Positions*

Arm Position	**Continuous Time Transfer Function**	**Fitting Ratio**
+64°	$G_{sd1}(s) = \frac{0.0135s^3 - 2.011s^2 + 1027s - 16850}{s^3 + 1.367s^2 + 7319s + 16.07}$	87.84%
+32°	$G_{sd2}(s) = \frac{0.0134s^3 - 1.977s^2 + 1076s - 17650}{s^3 + 1.413s^2 + 7744s + 15.31}$	87.50%
0°	$G_{sd3}(s) = \frac{0.0134s^3 - 1.967s^2 + 1161s - 19050}{s^3 + 1.479s^2 + 8345s + 15.98}$	87.57%
-32°	$G_{sd4}(s) = \frac{0.145s^3 + 0.6568s^2 + 1368s + 3930}{s^3 + 23.03s^2 + 9006s + 191400}$	89.46%
-64°	$G_{sd5}(s) = \frac{0.144s^3 + 0.6483s^2 + 1422s + 3976}{s^3 + 22.94s^2 + 9447s + 199400}$	89.43%

The estimated transfer functions are compared with FRFs of experimental data for all different arm positions in the bode diagrams in Figure 2.13. All estimated transfer functions almost coincidence with the corresponding FRFs for different arm positions. Although there are small differences in the magnitudes for the frequencies before the resonance for the arm position of +64°, +32° and 0°, the region is not in the case of the study.

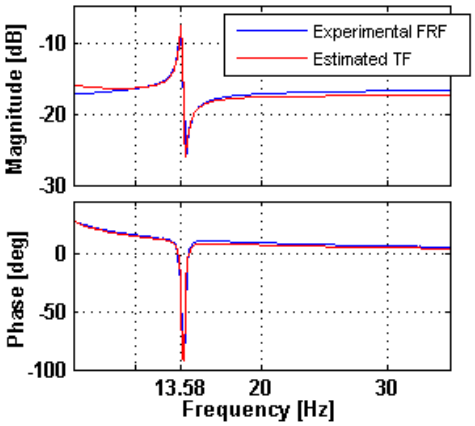

a) Arm Position +64°

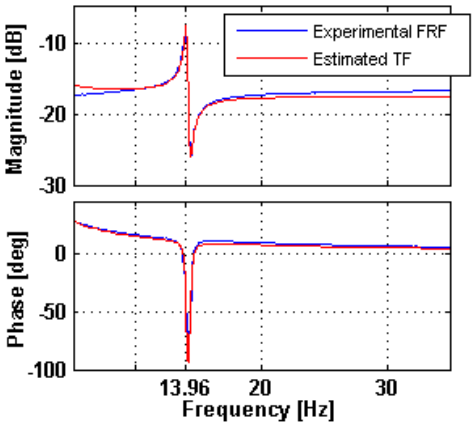

b) Arm Position +32°

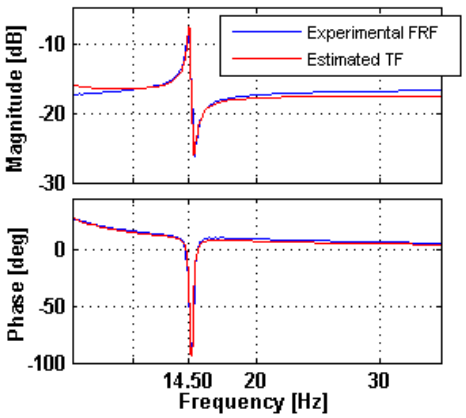

c) Arm Position 0°

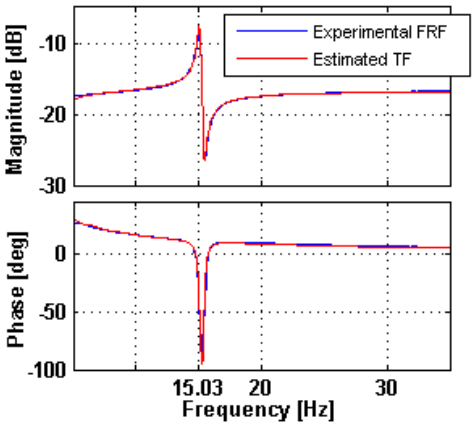

d) Arm Position -32°

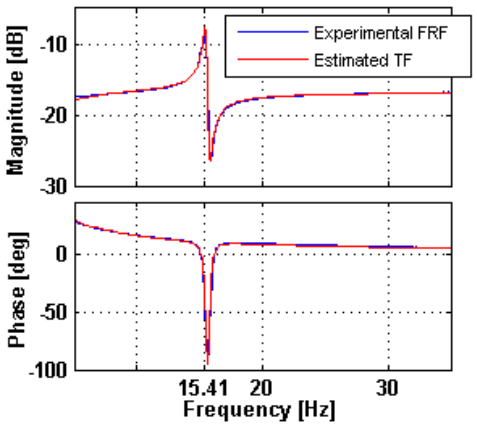

e) Arm Position -64°

Figure 2.13. FRF of Experimental Data and Estimated Transfer Function between Disturbance and Sensor Signals for the Different Arm Positions (Bode Diagrams)

2.4. Conclusion

This chapter consists of two main sections which are Experimental Setup and System Identification. First, the piezo-beam with four piezoelectric patches and its hardware setup are mentioned in the Experimental Setup section. Additionally, the mass location variation mechanism at the free end of the piezo-beam are introduced. Second, the model of the piezo-beam is identified in the System Identification section by time domain and frequency domain analyses where the controller and disturbance signals are used as an excitation input and the sensor signal is as an output. It can be seen the obtained FRFs that the first resonance frequencies of the piezo-beam for the arm positions from +64° to -64° are increased from 13.58 Hz to 15.41 Hz. The transfer functions between the controller and sensor signals and the transfer functions between disturbance and sensor signals for all different arm positions are estimated in order to simulate the performances of the designed controllers. The estimated transfer functions are then compared with the FRFs of experimental data by the figures and fitting ratios in time domain.

CHAPTER 3

DESIGN OF A FUZZY LOGIC CONTROLLER FOR A CERTAIN ARM POSITION

3.1. Introduction

In this chapter, suppression of the first resonance of the piezo-beam whose arm position is 0° is achieved by the help of a designed FLC. First, the FLC is designed in details and tested in the experimental setup. Then the controller is also simulated according to the estimated model which is obtained in the previous chapter. Following this, the results of the simulation and those of the experimental ones are compared with each other.

3.2. Open-Loop Analysis and Plant Model of the Piezo-Beam

Before designing a FLC, open loop analysis should be made for defining the amplitude range of input of the controller and observing noise level at the experimental setup and then, the plant model for the simulation study is derived.

3.2.1. Open-Loop Analysis for the Experimental Study

In this part, the experimental studies are performed for observing the noise level and defining the amplitude of the sensor signal at the first resonance frequency. Additionally, a study is done to define the cut-off frequency of a low pass filter.

In order to analyze the noise level and to obtain the bias term for the sensor signal, an experiment is performed by the Simulink model in Figure 3.1 without providing any signal to the piezo-beam.

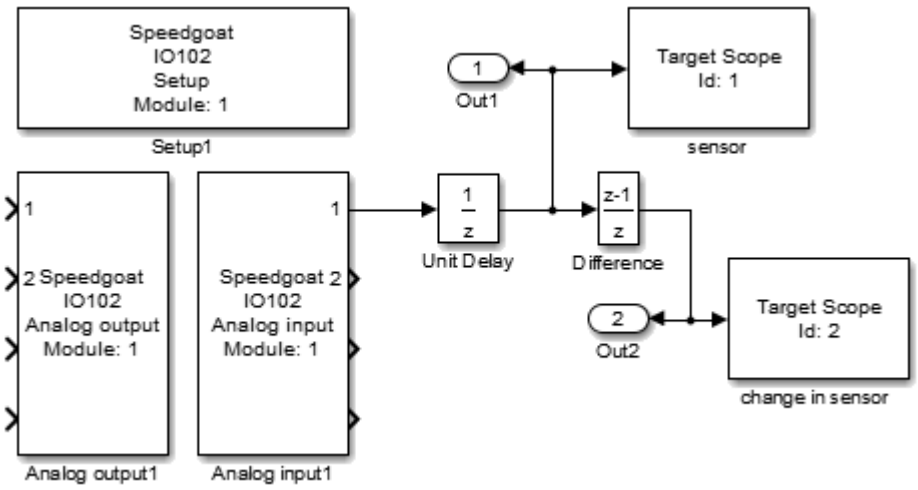

Figure 3.1. Simulink Model for Observing the Noise Level and Finding the Bias Term

From the Simulink model, the sensor signal which is the output port of the block of the Analog Input Module, and the change in sensor signal which is found as the difference from previous signal data is obtained and plotted in Figure 3.2.

(a)

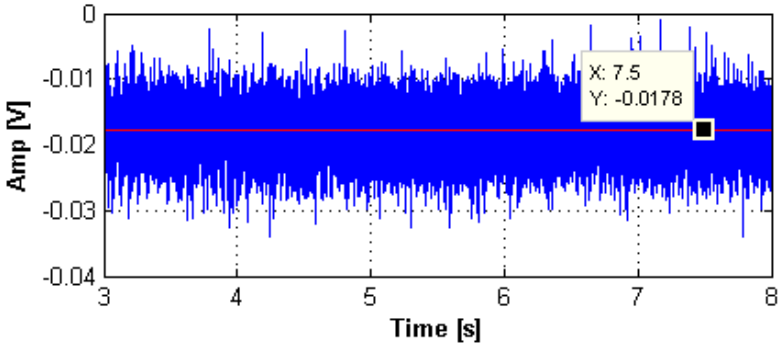

(b)

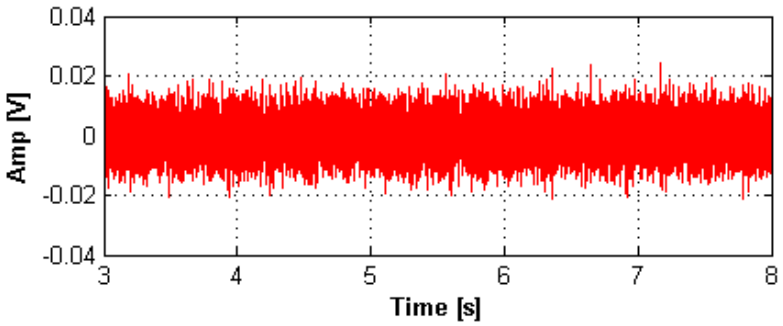

Figure 3.2. Time Responses of the Sensor Signal (a) and the Change in Sensor Signal (b) without Giving any Signal to the Piezo-Beam

It is observed that there is a DC offset of -0.0178 V (mean value of the signal) on the sensor PZT patch. This value should be reduced to zero with the addition of the bias block in the Simulink model. Additionally, there are noise levels at around of 0.008 and 0.018 V (RMS values) for sensor signal and change in sensor signal, respectively.

Simulink model shown in Figure 3.3 is created in order to obtain the amplitude of 0.5 V for the sensor signal when applying the sine wave at the first resonance to disturbance signal, which is the first input port of the Analog Output block. The time responses of the sensor signal and the change in sensor signal are obtained as shown in Figure 3.4. Although signal-to-noise ratio is high for this sensor signal, it is very low for the change in sensor signal. Therefore, a low pass filter should be used for the noise.

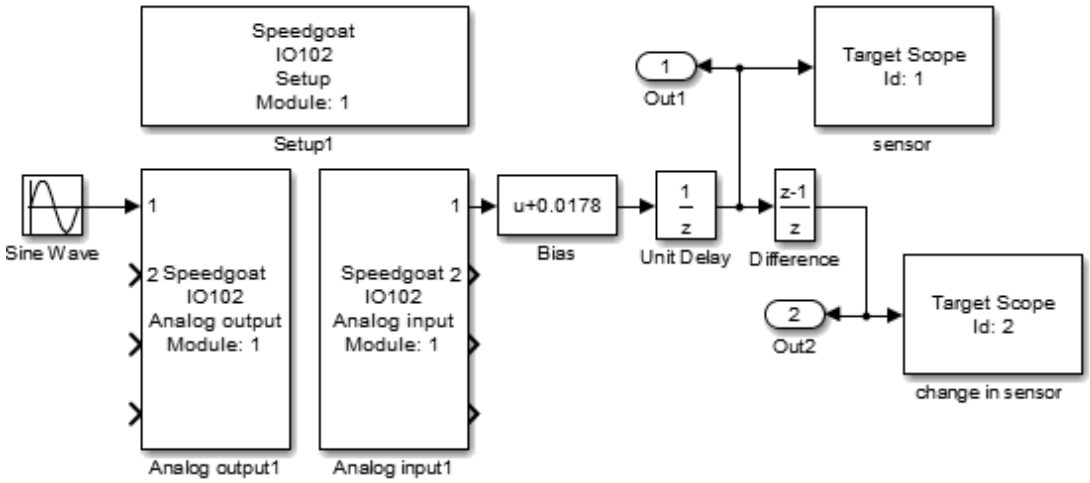

Figure 3.3. Simulink Model for the Time Response at the First Resonance of the Piezo-Beam

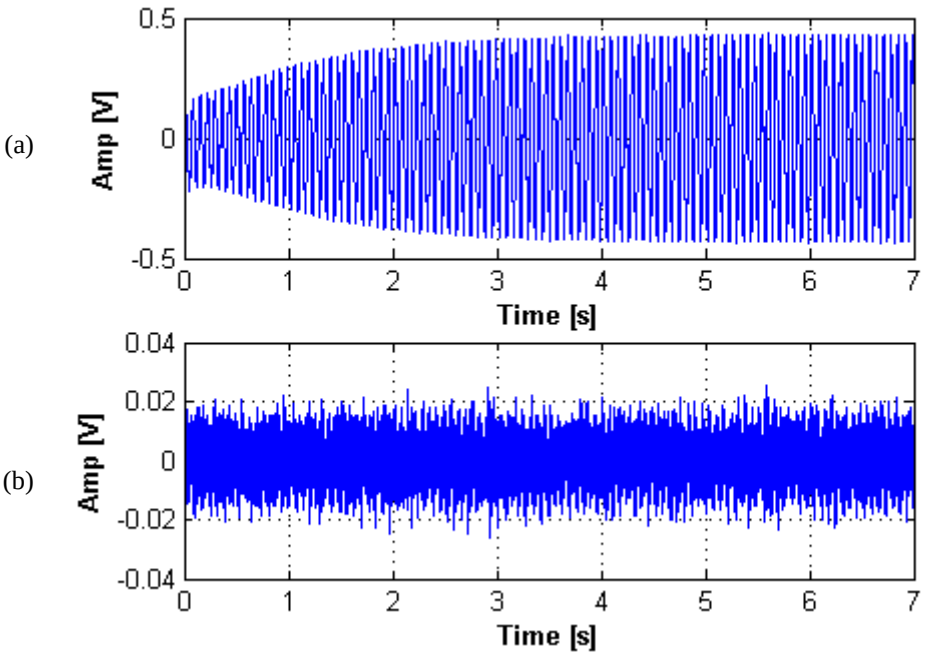

Figure 3.4. Time Response of the Sensor Signal (a) and the Change in Sensor Signal (b) at the First Resonance of the Piezo-Beam

The Butterworth low-pass filter with cut-off frequency of 100 Hz is used to eliminate the noise and to increase the signal-to-noise ratio. The selection of the low-pass filter is explained in details in the Appendix A. The Simulink model for the low-pass filter is shown in Figure 3.5. The time responses with low noise are plotted in Figure 3.6 and a high signal-to-noise ratio in the change in sensor signal is obtained.

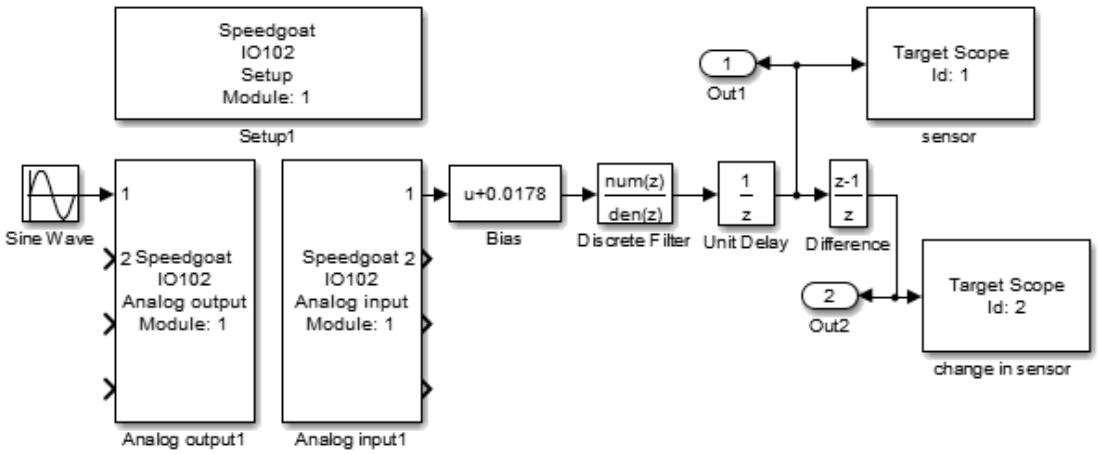

Figure 3.5. Simulink Model for the Time Response at the First Resonance of the Piezo-Beam with the Low-Pass Filter

(a)

(b)

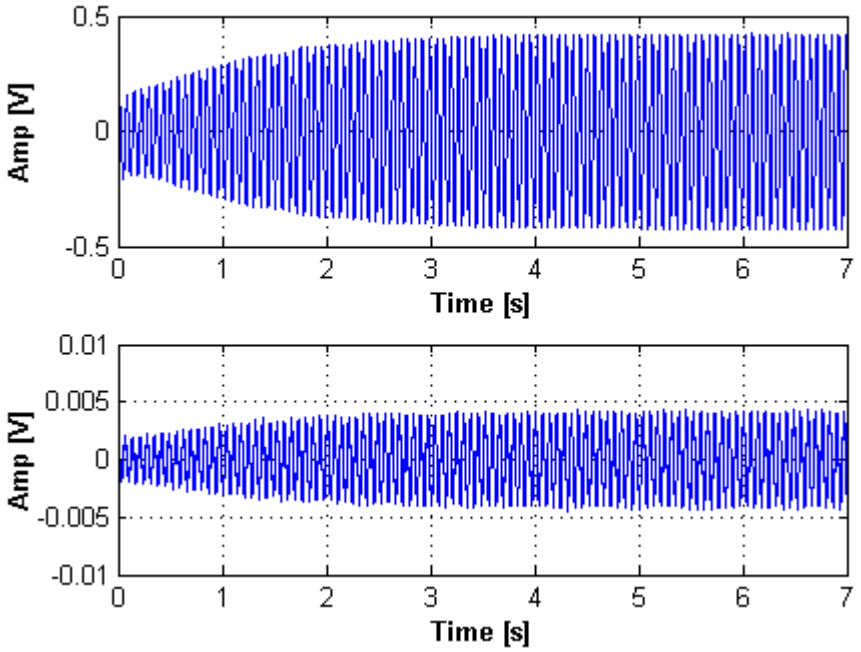

Figure 3.6. Time Response of the Sensor Signal (a) and the Change in Sensor Signal (b) at the First Resonance of the Piezo-Beam with the Low-Pass Filter

Stabilization of the vibration amplitude occurs at 4 seconds after start of experiment. The maximum voltages of the sensor signal and the change in sensor signal which is used for design of a FLC are 0.45 and 0.045 V, respectively.

3.2.2. Plant Model for the Simulation Study

In simulation of the designed controller, a plant which is mathematical modelling of a dynamic system is needed. The plant models are derived as the transfer functions in the previous chapter. However, the transfer function of the plant model should be converted into linear time invariant (LTI) state-space model for the simulation studies which will then be compared with experimental ones.

The controller will be designed according to the experimental study of forced vibration of the piezo-beam for the arm position of 0°. Therefore, the continuous time state space model is calculated from the transfer function $G_{sc3}(s)$ of the case where the arm position is 0°. The model consists of the state equation which is given in Equation 3.1

and the output equation which is given Equation 3.2. In the equations, x, u and y are the state, input and output vectors, respectively.

$$\dot{x} = Ax(t) + Bu(t) \tag{3.1}$$

$$y = Cx(t) + Du(t) \tag{3.2}$$

The "system" matrix A, "controller" matrix B, "output" matrix C and "feed-forward" matrix D are calculated from the transfer function $G_{sc3}(s)$, as follows:

$$A = \begin{bmatrix} -1.7 & -8315 & -66.67 \\ 1 & 0 & 0 \\ 0 & 1 & 0 \end{bmatrix}$$

$$B = \begin{bmatrix} 1 \\ 0 \\ 0 \end{bmatrix}$$

$$C = [-0.1238 \quad 172.5883 \quad -3758.2]$$

$$D = 0.0185$$

The state-space model of the plant in discrete version is derived from the continuous time state space model for the sampling time of 0.1 ms. The discrete time state equations are given in Equation 3.3 and 3.4, as follows:

$$x(k+1) = A_d x(k) + B_d u(k) \tag{3.3}$$

$$y(k) = C_d x(k) + D_d u(k) \tag{3.4}$$

Where the discrete versions of the matrices are found as follows:

$$A_d = \begin{bmatrix} -19.63 & -8339 & -149700 \\ 1 & 0 & 0 \\ 0 & 1 & 0 \end{bmatrix}$$

$$B_d = \begin{bmatrix} 1 \\ 0 \\ 0 \end{bmatrix}$$

$$C_d = [-2.8242 \quad 56.5769 \quad -23452]$$

$$D_d = 0.1629$$

For the forced vibration suppression case, sine wave with amplitude of ±0.5 Volt and frequency of 14.50 Hz is applied as input of the plant. The Simulink model, shown in Figure 3.7, is created for observing the response of the plant to the forced vibration.

According to Figure 3.8, the output of the plant model is stabilized to the constant amplitude vibration of ±0.5 V in 6 seconds. The results regarding the values of the sensor signal obtained from the experimental and simulation studies are closed to each other.

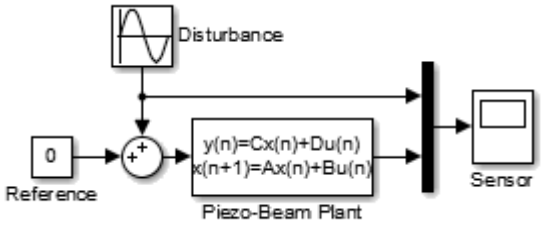

Figure 3.7. Simulink Model of the Open Loop System for Forced Vibration Simulation

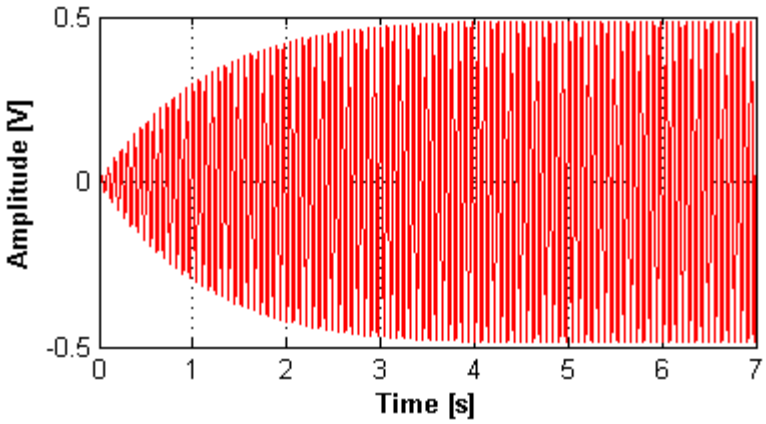

Figure 3.8. Time Response of the Open-Loop System to the Forced Vibration at the First Resonance

3.3. Design of a FLC

The scope of this section is to design a FLC in order to suppress the free and forced vibration at the first resonance frequency of the piezo-beam. While plant is being vibrated by the disturbance PZT, the sensor PZT collects data from the piezo-beam in order to calculate error to reference signal which is zero due to vibration suppression. The error and its difference from previous one, which is called change in error, are the input of the FLC, which is built using the Fuzzy Logic Toolbox in Matlab. The output of the FLC which is controller signal is applied by controller PZT. The representation of the controlled plant is given in Figure 3.9.

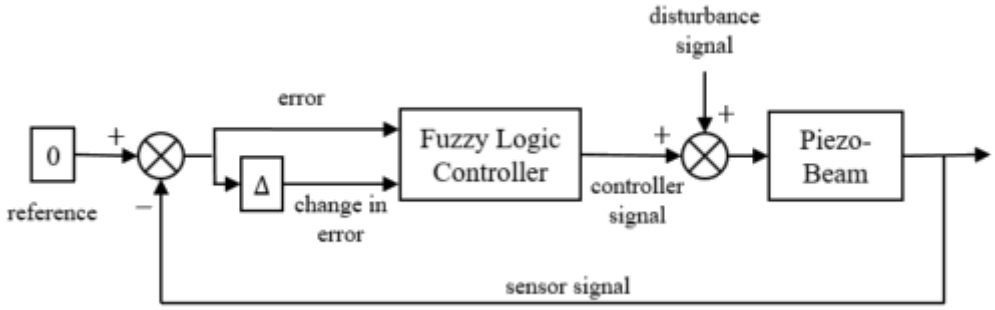

Figure 3.9. The Representation of the Controlled Plant

The main concept of fuzzy logic control is based on using IF-THEN rules as linguistic directives which are composed of human expertise as a basis for control. By help of those rules, the output of the controller can be calculated from the two-input data. As an example of IF-THEN rules, i-th rule can be written as follows

$$R^i: \quad if \quad x_e \; is \; A_i \quad and \quad x_{\Delta e} \; is \; B_i \quad then \quad x_u \; is \; C_i \tag{3.5}$$

where x_e and $x_{\Delta e}$ are input fuzzy variables corresponding to the error e and the change in error Δe, which are the crisp (unfuzzy) input variables of the FLC. x_u is output fuzzy variable corresponding to the controller signal u, which is the crisp output variable. A_i, B_i and C_i are the linguistic values for the fuzzy variables x_e, $x_{\Delta e}$ and x_u, respectively.

The structure of fuzzy logic control can be divided into four sections; fuzzification, rule base, inference engine, and defuzzification as shown in Figure 3.10. Design of a FLC is explained in details in these sections.

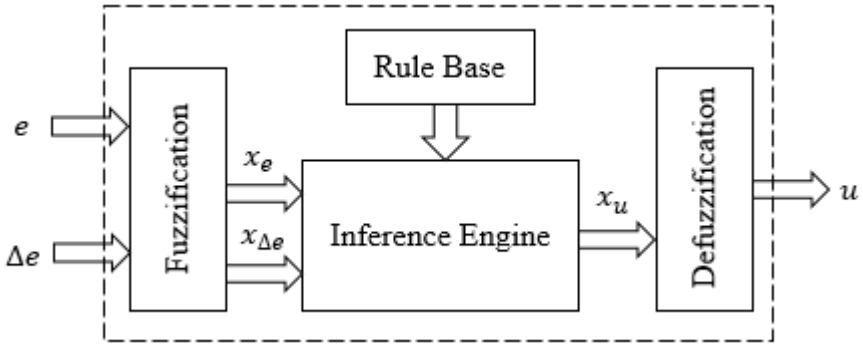

Figure 3.10. Schematic Representation of FLC System

3.3.1. Fuzzification

Fuzzification is the process of changing crisp value, real scalar value, of inputs of the controller into membership values for each linguistic value [53]. This is achieved with membership functions. Membership functions of each linguistic value determine the degrees of membership of each crisp value of input.

In the fuzzification process, defining the range of input and output crisp data is the first design step. The range for input variables is selected by observing the data in the response of open-loop system in Figure 3.8. The range for error is taken from -0.6 to 0.6 V. The range for change in error is found as from -0.006 to 0.006 V. Finally, the range of controller signal is selected as from -10 to 10 V.

The crisp data error e and change in error Δe are converted into a membership value for each linguistic value which is also called fuzzy set. Determining the number of the linguistic values for each input and output is the second design step of FLC. As a result of literature research [54], [38], it is observed that the fuzzy controllers with five linguistic values are used for active vibration control applications. Therefore, in this thesis, input and output fuzzy variables are defined in the fuzzy space in the form of five linguistic values, which are namely NB (negative big), NS (negative small), ZE (zero), PS (positive small) and PB (positive big).

The membership functions are used in order to present the linguistic values with membership degrees for both input fuzzy variables. In the third design step, the

membership functions are defined for the fuzzy set of both input and output variables. There are different types of membership functions in the literature. The most three popular types of membership function are triangular, trapezoid and Gaussian functions. According to the results of the comparison study between these three popular functions, the FLC with the triangular function shows better performance concerning both the transient and the steady-state behaviors [55]. Therefore, in this thesis, the triangular membership function is used for all fuzzy sets. The membership functions of each fuzzy set for error e input fuzzy variable are $\mu_{NB_e}(e)$, $\mu_{NS_e}(e)$, $\mu_{ZE_e}(e)$, $\mu_{PS_e}(e)$ and $\mu_{PB_e}(e)$ as shown in Figure 3.11 (a). The membership functions of each fuzzy set for change in error Δe input fuzzy variable are $\mu_{NB_{\Delta e}}(\Delta e)$, $\mu_{NS_{\Delta e}}(\Delta e)$, $\mu_{ZE_{\Delta e}}(\Delta e)$, $\mu_{PS_{\Delta e}}(\Delta e)$ and $\mu_{PB_{\Delta e}}(\Delta e)$ as shown in Figure 3.11 (b). Finally, the membership functions of each fuzzy set for controller signal u output fuzzy variable are $\mu_{NB_u}(u)$, $\mu_{NS_u}(u)$, $\mu_{ZE_u}(u)$, $\mu_{PS_u}(u)$ and $\mu_{PB_u}(u)$ as shown in Figure 3.11 (c).

(a)

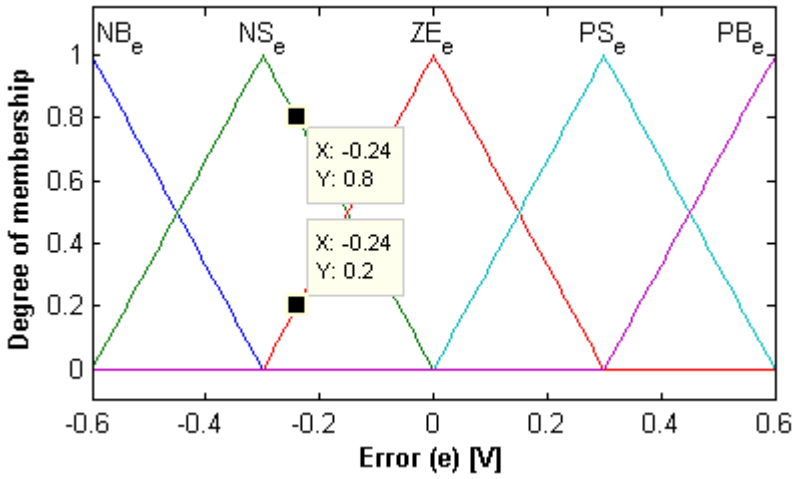

(b)

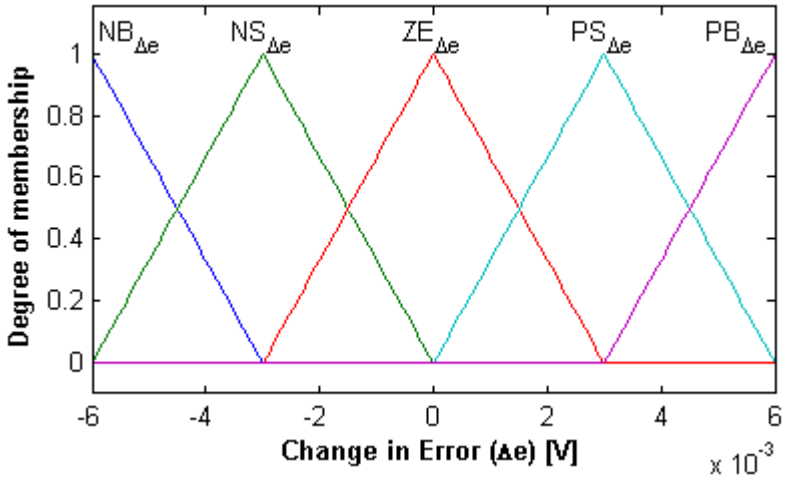

(c)

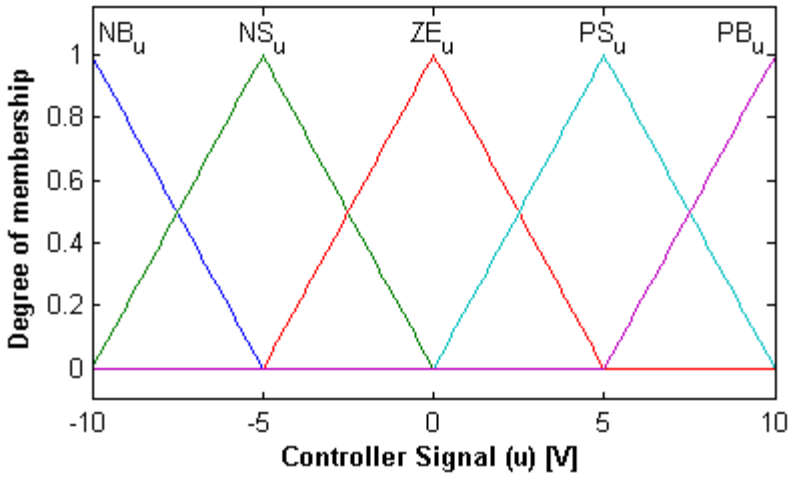

Figure 3.11. Membership Functions of the Inputs as (a) the Error and (b) the Change in Error and the Output as (c) the Control Signal

The degree of membership of each fuzzy set for a crisp input can be calculated from the membership function. For example; in Figure 3.11 (a), if a crisp value of -0.24 V is taken as error input, then the degree of membership of fuzzy set $\mu_{NS_e}(-0.24)$, will be 0.8 and $\mu_{ZE_e}(-0.24)$, will be 0.2 and the other fuzzy sets will be zero. In other words, error value of -0.24 V is described as negative small error with probability of 0.8 and zero error with probability of 0.2 in linguistic terms.

3.3.2. Rule Base

The rule base contains a set of rules which are composed by the knowledge that human experts may have about how to control the plant. The rules are formed by the "if-then" sentences as shown in Equation 3.5.

The number of rules depends on the number of memberships in the fuzzy set of the inputs. In this thesis, twenty-five fuzzy rules can be composed of the combinations of five linguistic values of both inputs.

The form of fuzzy rule tables where all rules are presented for active vibration control of structures are generally similar in the literature except a few rules. In this thesis, rule table are designed based on the study about vibration absorber using a fuzzy controller in a piezo-beam [39]. The rule table are presented in Table 3.1.

Table 3.1. *Fuzzy Logic Rule Table*

Controller signal (x_u)		**change in error** $(x_{\Delta e})$				
		NB	***NS***	***ZE***	***PS***	***PB***
error (x_e)	***NB***	*NB*	*NB*	*NB*	*NS*	*NS*
	NS	*NS*	*NS*	*NS*	*ZE*	*ZE*
	ZE	*NS*	*NS*	*ZE*	*PS*	*PS*
	PS	*ZE*	*ZE*	*PS*	*PS*	*PS*
	PB	*PS*	*PS*	*PB*	*PB*	*PB*

For instance, the ninth rule presented by the second row and the fourth column in *Table 3.1* is written as in Equation 3.6

$$R^9: \quad if \quad x_e \; is \; NS \quad and \quad x_{\Delta e} \; is \; PS \quad then \quad x_u \; is \; ZE \tag{3.6}$$

3.3.3. Inference Engine

Inference engine is a mapping process of the fuzzified inputs as received from the fuzzification process to a fuzzy output for the defuzzification process using logical operations and if-then rules. A degree of membership of the output fuzzy set is determined based on the degrees of membership of the input fuzzy sets found in fuzzification process and the fuzzy rules.

In the inference engine, at first, the fuzzy rules are evaluated with combining the degrees of membership of the input fuzzy sets by intersection ("and") operator used in fuzzy set. "min" operation, expressed mathematically in Equation 3.7, is used for "and" operator. The result of calculation with "min" operation is called the firing strength, which is the degree to which input fuzzy set of a fuzzy rule is satisfied.

$$\alpha_{C_i} = \min\left(\mu_{A_i}(e), \mu_{B_i}(\Delta e)\right) \tag{3.7}$$

After evaluating the firing strengths α_{C_i} of linguistic values C_i for each rule i, they should be combined to obtain final single fuzzy values for each linguistic value of the output fuzzy set by "max" operation calculating the maximum firing strength of all the twenty-five rules. The resulting membership function is obtained by combining the final fuzzy values for each linguistic value, given as follows

$$\beta_C = \max_{0 \le i \le 25} (\alpha_{C_i}) \tag{3.8}$$

In order to show how to apply the rules and find the resulting membership for the output fuzzy set, random crisps values of -0.24 for error and 0.0018 for change in error, are selected. According to membership functions, shown in Figure 3.12 (a), the fuzzy variable x_e has the linguistic values NS_e and ZE_e with degrees of the

membership 0.8 and 0.2, respectively. As shown in Figure 3.12 (b), the fuzzy variable $x_{\Delta e}$ has the linguistic values $ZE_{\Delta e}$ and $PS_{\Delta e}$ with the membership values 0.4 and 0.6, respectively. Both linguistic values of the input fuzzy variables are involved in the eighth, ninth, thirteenth and fourteenth rules, are shown in Equations from 3.9 to 3.12.

(a)

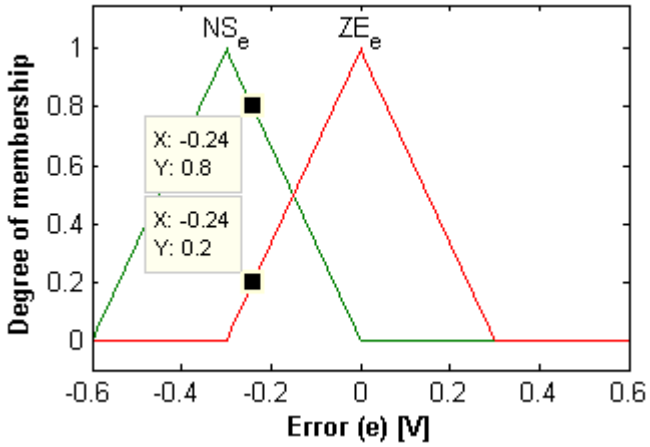

(b)

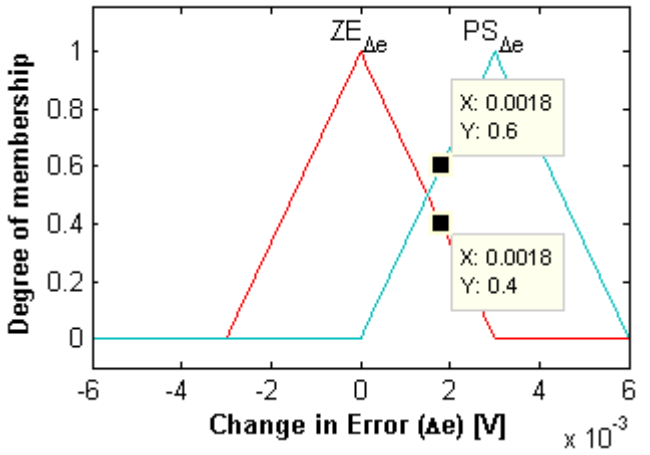

Figure 3.12. The Degrees of Membership of the Linguistic Values for (a) $e = -0.24$ and (b) $\Delta e = 0.0018$

$$R^8: \quad if \quad x_e \; is \; NS_e \quad and \quad x_{\Delta e} \; is \; ZE_{\Delta e} \quad then \quad x_u \; is \; NS_u \tag{3.9}$$

$$R^9: \quad if \quad x_e \; is \; NS_e \quad and \quad x_{\Delta e} \; is \; PS_{\Delta e} \quad then \quad x_u \; is \; ZE_u \tag{3.10}$$

$$R^{13}: \quad if \quad x_e \; is \; ZE_e \quad and \quad x_{\Delta e} \; is \; ZE_{\Delta e} \quad then \quad x_u \; is \; ZE_u \tag{3.11}$$

$$R^{14}: \quad if \quad x_e \; is \; ZE_e \quad and \quad x_{\Delta e} \; is \; PS_{\Delta e} \quad then \quad x_u \; is \; PS_u \tag{3.12}$$

"min" operation is applied for each rule to find firing strengths of linguistic values of output fuzzy variable for each rule as follows

$$(\alpha_{NS_u})_8 = \min\left(\mu_{NS_e}(-0.24), \mu_{ZE_{\Delta e}}(0.0018)\right) = \min(0.8,0.4) = 0.4 \quad (3.13)$$

$$(\alpha_{ZE_u})_9 = \min\left(\mu_{NS_e}(-0.24), \mu_{PS_{\Delta e}}(0.0018)\right) = \min(0.8\,, 0.6) = 0.6 \quad (3.14)$$

$$(\alpha_{ZE_u})_{13} = \min\left(\mu_{ZE_e}(-0.24), \mu_{ZE_{\Delta e}}(0.0018)\right) = \min(0.2\,, 0.4) = 0.2 \quad (3.15)$$

$$(\alpha_{PS_u})_{14} = \min\left(\mu_{ZE_e}(-0.24), \mu_{PS_{\Delta e}}(0.0018)\right) = \min(0.2\,, 0.6) = 0.2 \quad (3.16)$$

"max" operation is applied to combine the firing strengths of the same linguistic values

$$\beta_{NS_u} = \min\left((\alpha_{NS_u})_8\right) = 0.4 \quad (3.17)$$

$$\beta_{ZE_u} = \max\left((\alpha_{ZE_u})_9, (\alpha_{ZE_u})_{13}\right) = 0.6 \quad (3.18)$$

$$\beta_{PS_u} = \min\left((\alpha_{PS_u})_{14}\right) = 0.2 \quad (3.19)$$

After obtaining the final single fuzzy values for each linguistic value as shown in the Figure 3.13, the resulting membership function is plotted in the Figure 3.14.

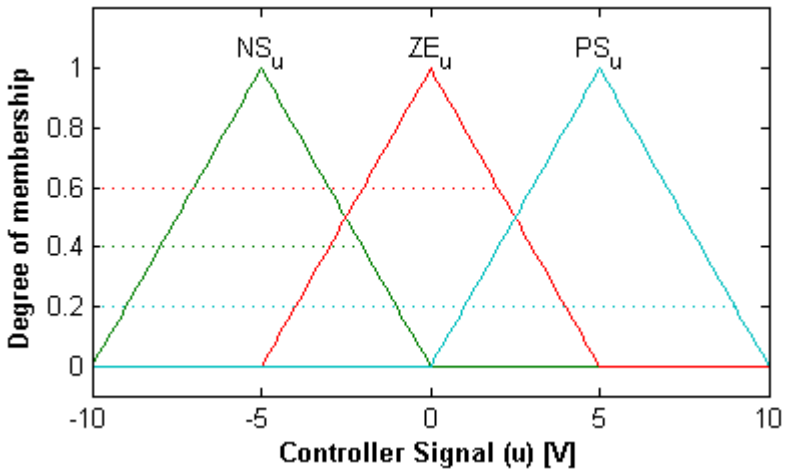

Figure 3.13. The Final Single Fuzzy Values for Each Linguistic Value for $e = -0.24$ and $\Delta e = 0.0018$

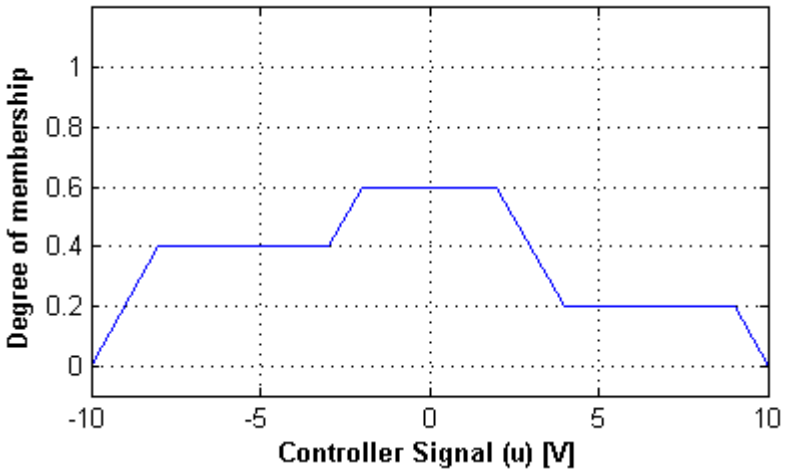

Figure 3.14. The Resulting Membership Function for $e = -0.24$ and $\Delta e = 0.0018$

3.3.4. Defuzzification

In the defuzzification process, the resulting membership for output fuzzy set obtained by combining all the membership functions in the inference engine must be defuzzified to obtain a crisp value for controller signal, u. The centroid of area method can be used as a defuzzification method to defuzzify the output fuzzy variable. According to this method, the crisp value is obtained by calculating the centroid of the area which is under the resulting membership function.

After obtaining the crisp values for the range of the input crisp values, the surface graph is represented in Figure 3.15 for the designed FLC.

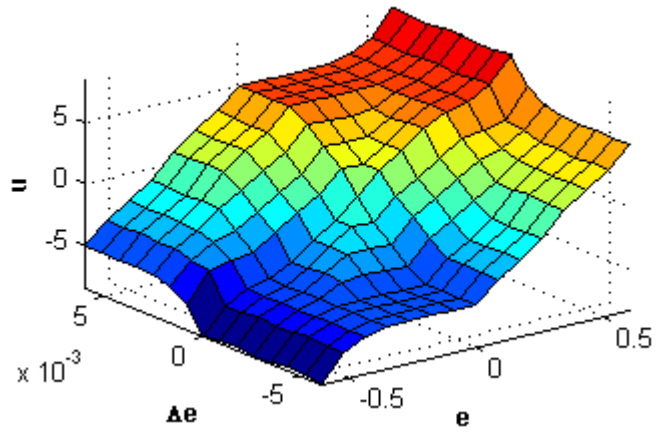

Figure 3.15. The Surface Graph of the FLC

For the example given in previous section, the crisp value is obtained by calculating the centroid of the area which is under the resulting membership function obtained by inference engine process. The screenshot of "Rule Viewer" of Fuzzy Logic Toolbox in Matlab for $e = -0.16$ and $\Delta e = 0.0018$ is given in Figure 3.16 by indicating the crisp value and the resulting membership function. Also, the thick red line in the resulting membership function represents the horizontal position of the centroid of area.

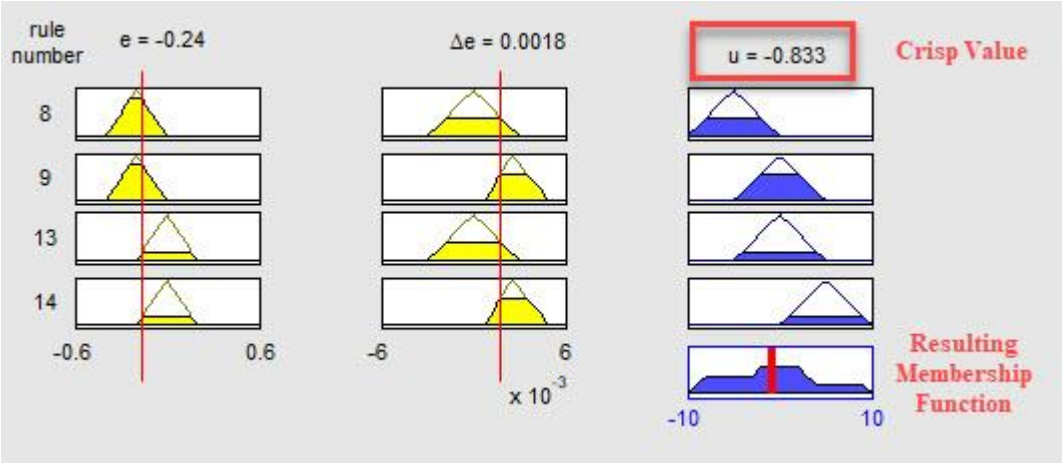

Figure 3.16. Visualization of Inference Engine and Defuzzification Processes for $e = -0.16$ and $\Delta e = 0.0018$

3.4. Performance Analysis of the FLC

The performance of the FLC is evaluated via simulation and experimentally obtained results in both free and forced vibration at the first resonance frequency of the piezo-beam when the arm position of the mass location variation system is 0°. Finally, FRFs of the controlled plant with the 0° arm position are plotted in the range of the frequency span covering the first resonance frequency for simulation and experimental results.

In the Simulink model, a subsystem model which includes the FLC is created as shown in *Figure 3.17*. The error is the input of the subsystem of the controller. At first, the low-pass filter with the cut-off frequency of 100 Hz which is defined in Section 3.2.1 is applied to the error signal for noise reduction. Then, "change in error" is calculated by taking difference between the current and previous error. The error and change in error are taken as input of the FLC designed in the previous section. The controller signal, u, is obtained by applying another low-pass frequency with cut-off frequency of 50 Hz to the output of the controller which is calculated via the Fuzzy Logic Toolbox. The reason to apply the low-pass filter is that the output of the controller has high frequency content due to non-linearity of the FLC. The selection of the low-pass filter for the output of the FLC is explained in details in Appendix B.

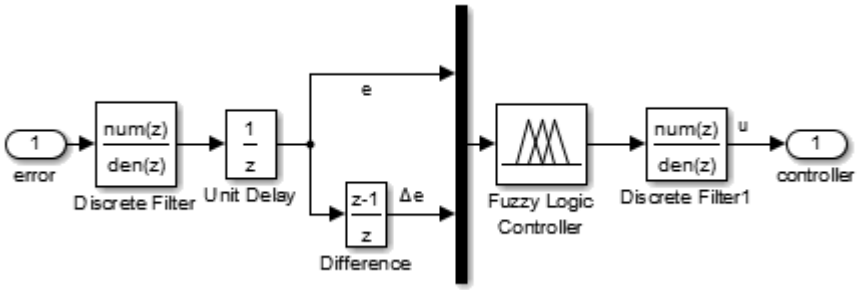

Figure 3.17. Simulink Subsystem Model of the FLC

In the simulation studies, the Simulink model in Figure 3.18 is created for the closed loop system of the plant of the piezo-beam. The output of the plant represents the signal from the sensor PZT. The difference between reference signal which is zero and the sensor signal is defined as "error". The controller signal is calculated from the

error signal via the created subsystem of the FLC. The controller signal is transmitted to the plant as representing the signal from the controller PZTs.

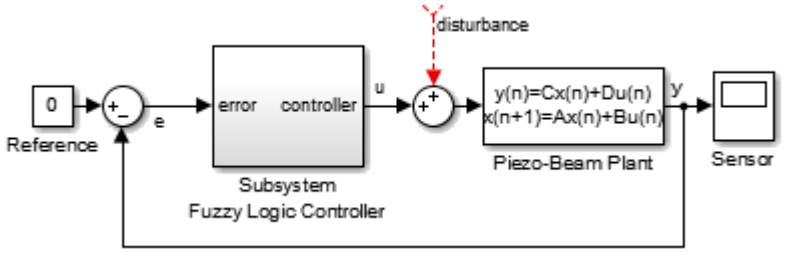

Figure 3.18. Simulink Model of the Closed Loop System (Simulation Study)

On the other hand, in the experimental studies, the Simulink blocks of the Speedgoat Setup Module, Analog Output Module and Analog Input Module are used in the Simulink model shown in Figure 3.19 in order to communicate with the PZTs on the piezo-beam. The sensor signal is the first output port of the block of the Analog Input Module. However, unlike the simulation studies, the bias term is used to eliminate the DC offset of -0.0178 V, found in the Section 3.2.1. The controller signal is calculated as in the simulation studies via the created subsystem of the controller. The controller signal enters the second port of the block of the Analog Output Module. When a disturbance signal is used for experimental studies, the signal is connected to the first port of the Analog Output block.

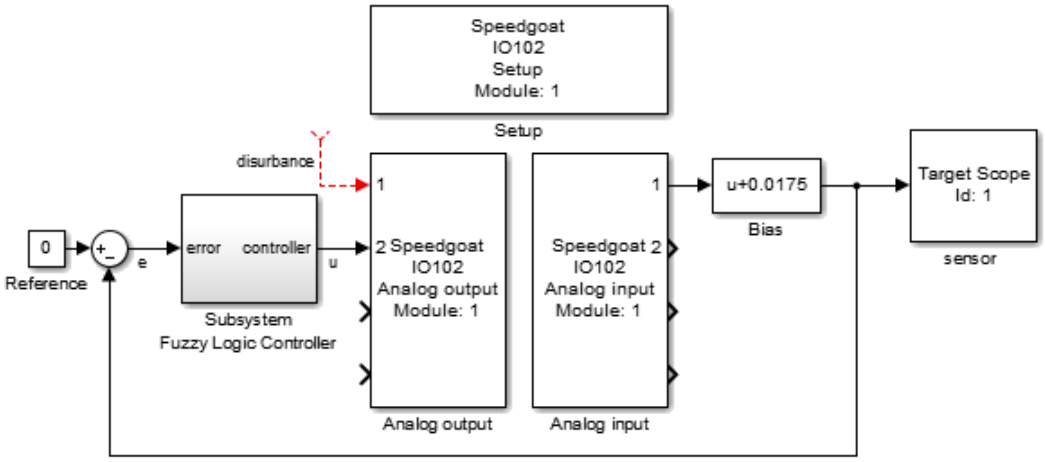

Figure 3.19. Simulink Model of the Closed Loop System (Experimental Study)

3.4.1. Studies for the Free Vibration Suppression

The Simulink model in Figure 3.18 is used for simulating the free vibration suppression. The initial conditions are entered to plant block in the Simulink model in order to simulate the tip displacement of 1 mm for free vibration of the piezo-beam. The tip displacement of 1 mm generates a voltage of 0.5 V in the sensor signal in the experimental setup. Therefore, the amplitude of sensor signal begins to decrease from ±0.5 V.

Uncontrolled plant has the settling time of 4.75 seconds with taking the error band of ±0.01 V (2% of the initial tip displacement). The settling time of the plant is decreased to 1.35 seconds by the fuzzy controller as shown in Figure 3.20.

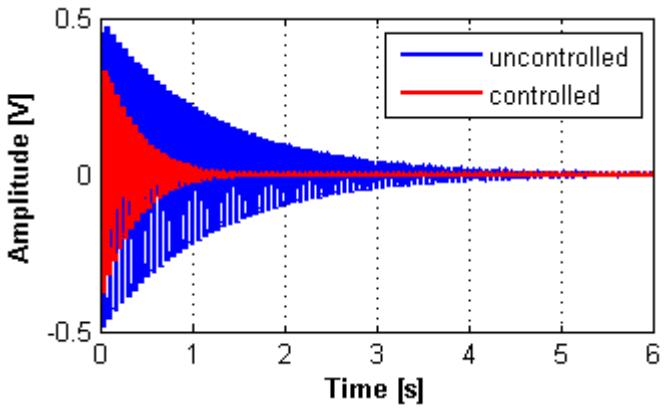

Figure 3.20. The Free Vibration (Simulation Study)

On the other hand, The Simulink model in Figure 3.19 is used without any disturbance signal for the experimental study of the free vibration suppression. The initial displacement of 1 mm is applied on the tip of the piezo-beam and then 0.5 V is recorded as the sensor signal. In this way, the free vibration is applied both in the uncontrolled and the controlled cases for the piezo-beam.

The time responses of the free vibration suppression by the FLC is given in Figure 3.21. While the uncontrolled piezo-beam has the settling time of 4.7 seconds, the controlled piezo-beam has the settling time of 1.3 seconds.

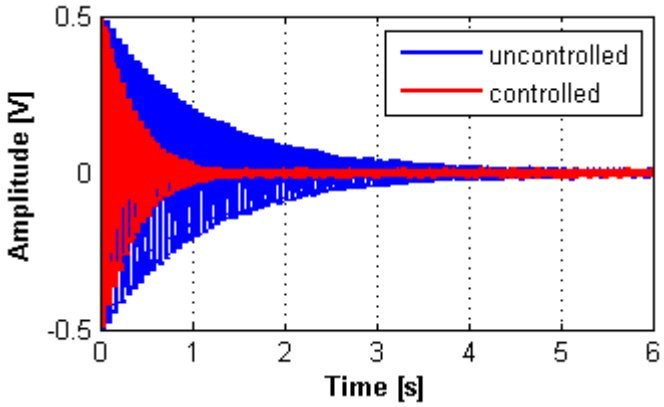

Figure 3.21. Free Vibration (Experimental Study)

When the results are compared, simulation and experimental studies are in good agreement for the free vibration suppression case. The settling time in simulation is decreased by the ratio of 72%. On the other hand, the settling time in experimental study is also decreased by the same ratio of 72%.

In the previous study having the same experimental setup, the settling time was obtained as a ratio of 92% by using the LQR controller [50]. It is observed that the FLC has a lower performance than the LQR controller on the free vibration suppression.

3.4.2. Studies for the Forced Vibration at the First Resonance Frequency

The Simulink model, in Figure 3.22, is created for simulating the forced vibration suppression at the first resonance frequency of the piezo-beam. Unlike the free vibration, the system has the disturbance signal which is sinusoidal input at the first resonance frequency of the piezo-beam. The controller is activated by the switch to suppress the vibration due to disturbance signal after 6 s when the output of the plant, i.e. the sensor signal, is stabilized. Then the calculated controller signal is sent to plant with the addition of the disturbance signal.

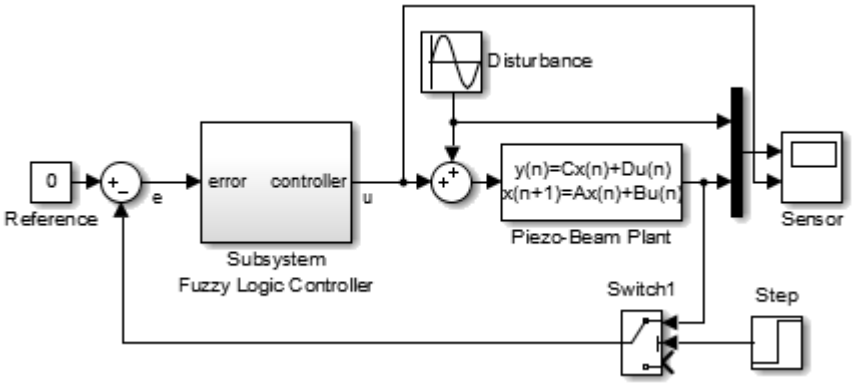

Figure 3.22. The Simulink Model of the Closed Loop System for Forced Vibration at the First Resonance Frequency (Simulation Study)

The result of the simulation is given in Figure 3.23. At this particular resonance frequency, uncontrolled plant has vibration with an amplitude of 0.50 V. When controller is on at sixth second, the amplitude begins to decrease. The amplitude is stabilized at the value of 0.0404 V within 1.14 seconds after the controller is on. Therefore, the ratio of the forced vibration suppression at the resonance frequency is 91.9%.

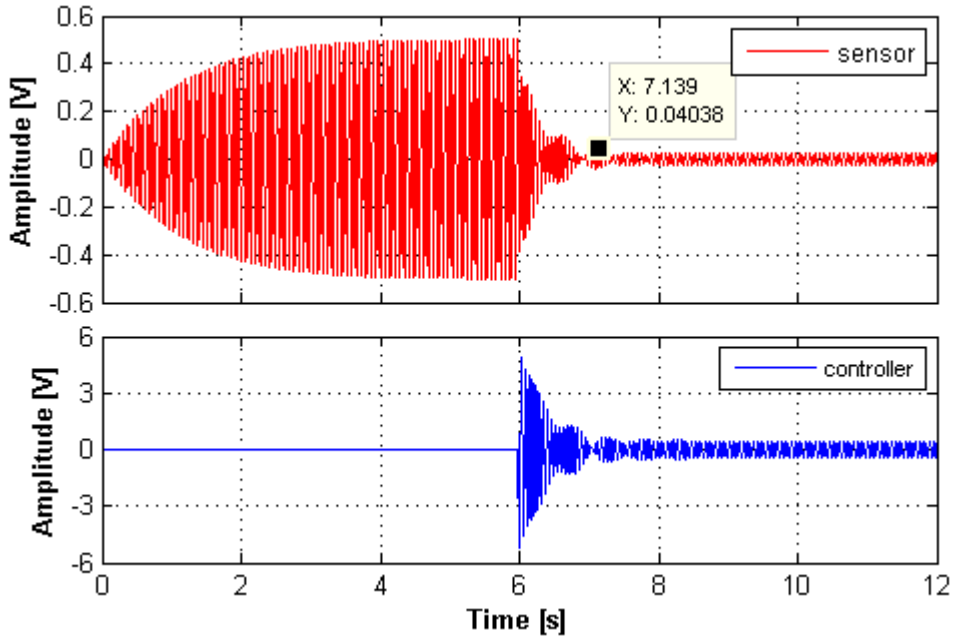

Figure 3.23. The Time Response of the Forced Vibrations of the Piezo-Beam at the First Resonance Frequency (Simulation Study)

On the other hand, the Simulink model in Figure 3.24 is created for the experimental study of the forced vibration suppression at the first resonance of the piezo-beam. A sinus signal with the frequency of 14.5 Hz is applied to the first port of the IO102 Analog output block for resonating the piezo-beam by the disturbance PZT. Until, the measured value of the sensor signal is be stabilized, the disturbance signal is applied without controller. After 6th seconds, the controller is activated by the switch for the vibration suppression.

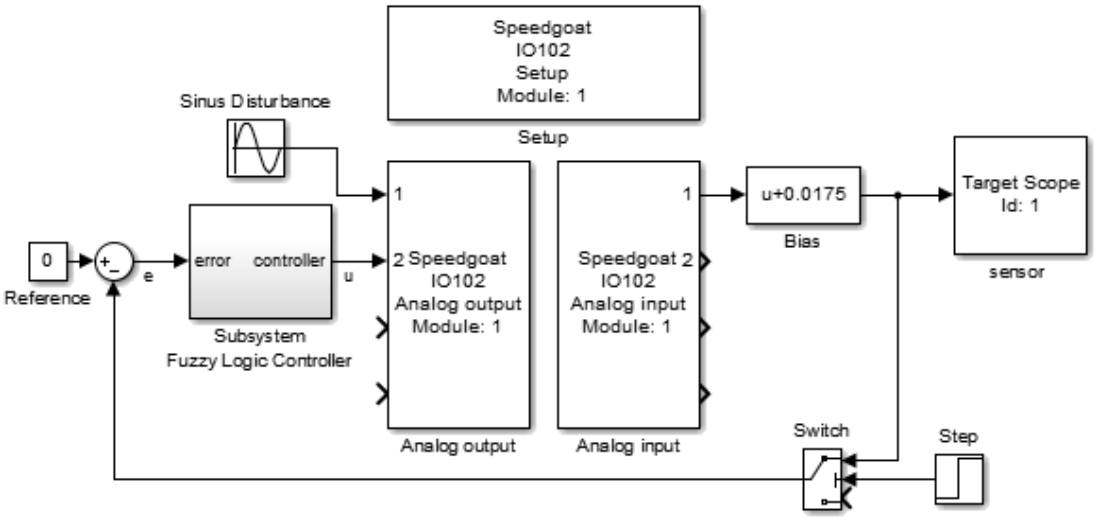

Figure 3.24. The Simulink Model of the Closed Loop System for Forced Vibration at the First Resonance Frequency (Experimental Study)

The result of the experimental study is given in Figure 3.25. Uncontrolled plant has vibration with an amplitude of 0.5 V. Controlled plant decreased the amplitude of the vibration to 0.0431 V at 1.14 seconds after the controller is turned on. The ratio of the forced vibration suppression at the resonance frequency is 91.4%.

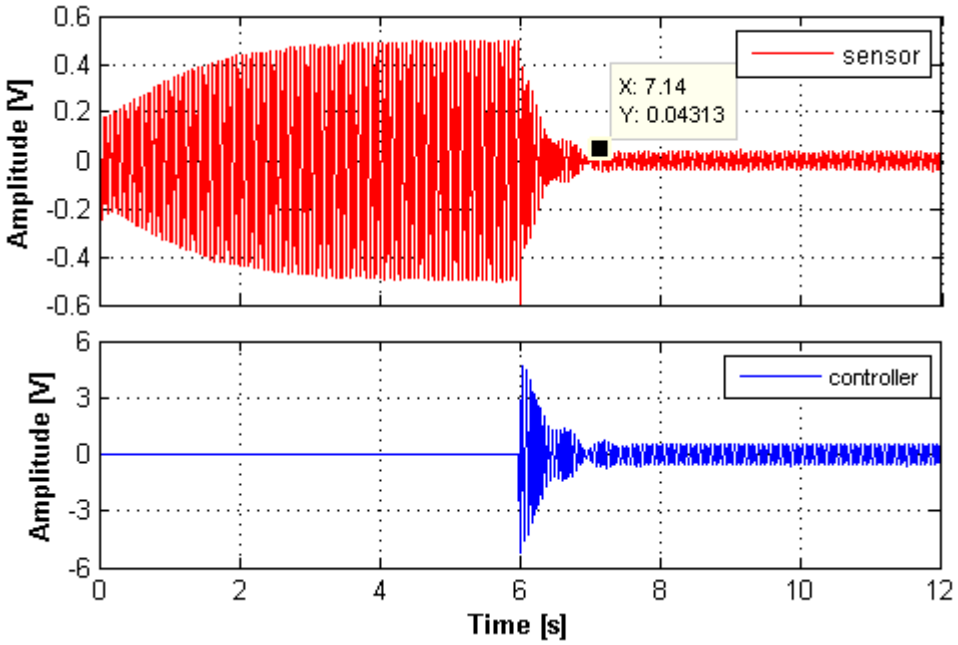

Figure 3.25. The Time Response of Forced Vibration of the Piezo-Beam at the First Resonance Frequency (Experimental Study)

When results of the simulation and the experimental studies are compared, the trends of the responses in time domain of the controlled piezo-beam at the first resonance frequency are similar. Also, the ratio of the forced vibration suppression in both studies are very close to each other with 0.05% of difference. The times to reach the stabilization point are found as 1.14 seconds in both studies.

In the previous study, the LQR controller which was designed for the piezo-beam also decreased the forced vibration amplitude by 92% in both simulation and experimental studies [50]. It is shown that the FLC reaches almost the same performance as the LQR controller on the forced vibration suppression.

3.4.3. Studies for the Forced Vibration within the Frequency Span covering the First Resonance

The Simulink model in Figure 3.26 is created by adding a chirp signal as a disturbance in order to obtain the FRF of the controlled plant within the frequency span from 5 to 35 Hz by the simulation study. The chirp signal as the one in the previous chapter is

applied with the range of frequency from 5 to 35 Hz. The time and frequency responses are plotted for both uncontrolled and controlled plant in Figure 3.27 and Figure 3.28, respectively. The FLC increases the resonance frequency of the piezo-beam from 14.5 to 16.33 Hz and decreases the magnitude at resonance from -0.43 to -16.39 dB.

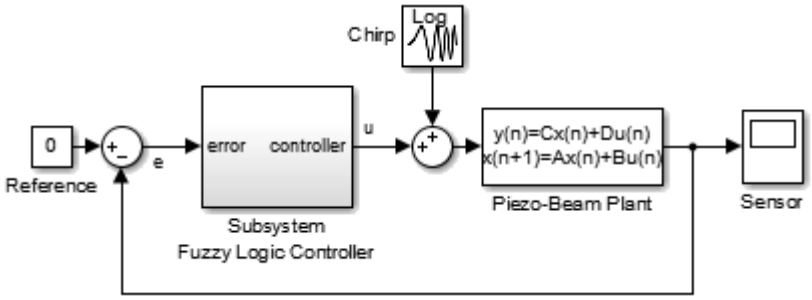

Figure 3.26. Simulink Model of the Closed Loop System for Forced Vibration within the Frequency Span covering the First Resonance (Simulation Study)

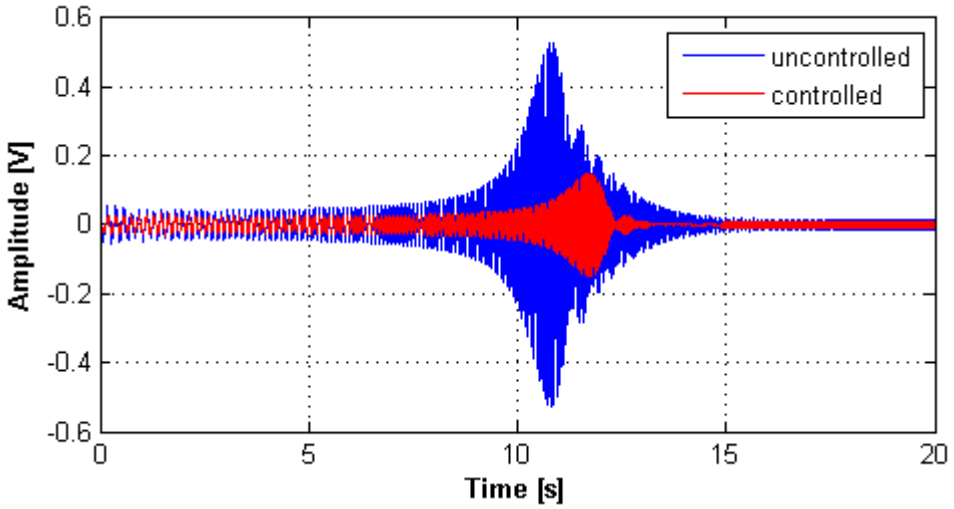

Figure 3.27. Time Response of Forced Vibration Suppression within the Frequency Span covering the First Resonance (Simulation Study)

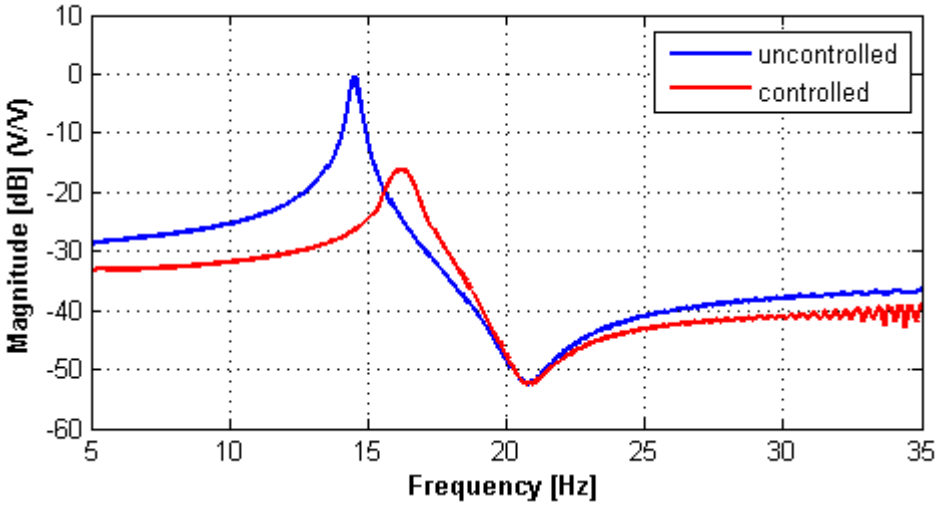

Figure 3.28. FRF of Uncontrolled and Controlled Piezo-Beam (Simulation Study)

On the other hand, the Simulink model in Figure 3.29 is created in order to obtain experimentally the FRF of the piezo-beam controlled by FLC. The piezo- beam is excited by controller PZT with addition of a chirp signal within the frequency span from 5 to 35 Hz to the controller signal.

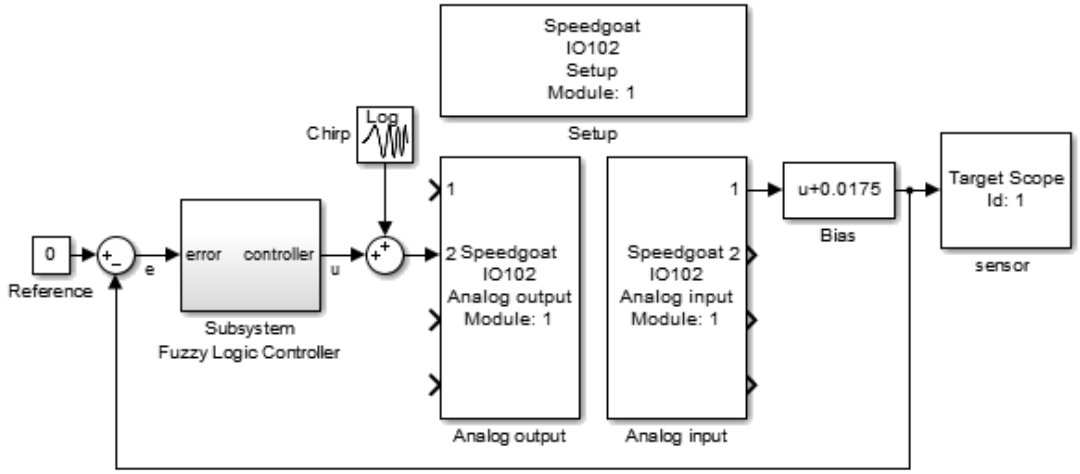

Figure 3.29. Simulink Model of the Closed Loop System for Forced Vibration within the Frequency Span covering the First Resonance (Experimental Study)

The responses of the sensor signals of uncontrolled and controlled piezo-beam are plotted in both time and frequency domain in Figure 3.30 and Figure 3.31,

respectively. The FLC increases the resonance frequency of the piezo-beam from 14.5 to 16.25 Hz and decreases the magnitude at resonance from -2.32 to -17.8 dB.

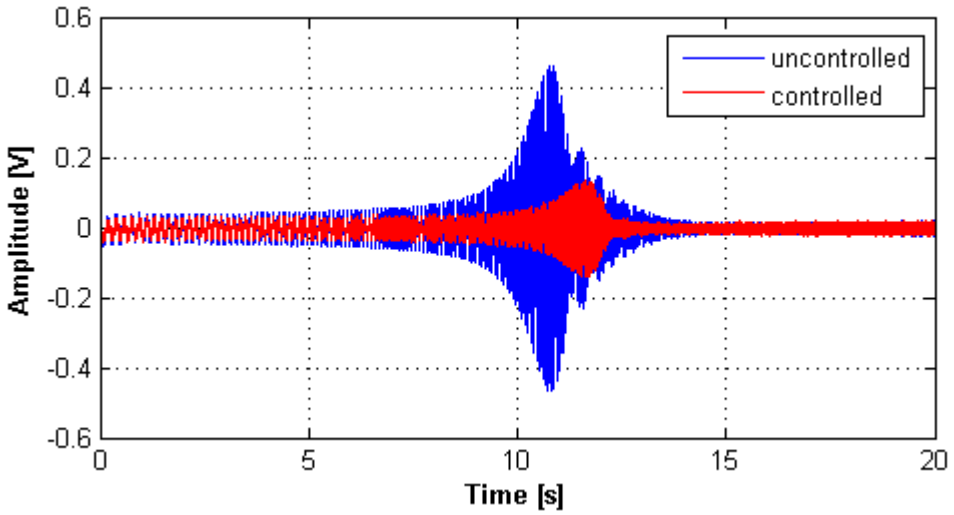

Figure 3.30. Time Response of Forced Vibration Suppression within the Frequency Span covering the First Resonance (Experimental Study)

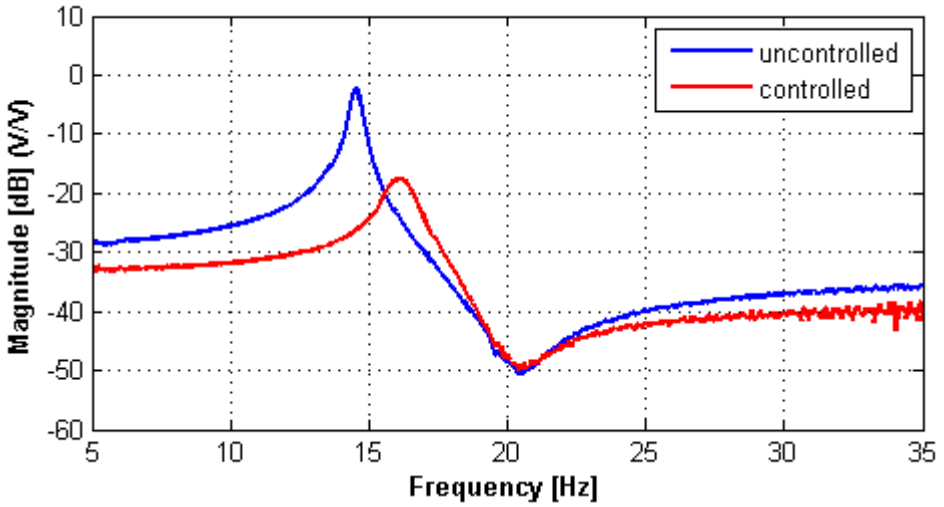

Figure 3.31. FRF of Uncontrolled and Controlled Piezo-Beam (Experimental Study)

The results of the experimental and simulation studies are consistent. The resonance frequency of the piezo-beam is increased by the percentage of 12.6% and 12.1% in simulation and experimental studies, respectively when the FLC is applied. The magnitude at the resonance is decreased by the ratio of 84.1% and 79.9% in the

simulation and experimental results, respectively. In other words, when controller is applied, the resonance frequency of the piezo-beam is increased as well as the magnitude at the resonance frequency is decreased.

In the previous study, the FRF of the piezo-beam controlled by LQR controller was obtained. The magnitude at the resonance was decreased by the ratio of 91% and the resonance frequency was decreased by 5% [50]. Therefore, it is also shown that the FLC's performance is not good enough in decreasing the magnitude at the resonance. However, it is observed that the FLC is good at shifting resonance frequency to a higher one.

Although suppressing of the fundamental resonance is of interest in this research work, performances of the designed FLC in the higher modes of the piezo-beam in the range of the frequencies up to 150 Hz are also observed in Appendix C. The minimal increase in the magnitude which is around a difference of 7 dB is observed at the higher modes when the FLC is applied for the forced vibration suppression within the frequency span covering the aforementioned higher modes.

3.5. Conclusion

In this chapter, the design stages of FLC are introduced. In the meantime, the FLC is designed for free and the forced vibration at the first resonance of the piezo-beam when the arm position of the mass location variation mechanism is 0°.

After designing stage, performance of the controller is evaluated in both in simulation and experimental studies. In the free vibration suppression, the settling time is decreased from 4.75 to 1.35 seconds according to the simulation results, whereas in the experimental study, the settling time is decreased from 4.7 to 1.3 seconds. In the forced vibration suppression at the first resonance, the performance of the controller is evaluated by the suppression ratio of 91.9% and 91.4% in simulation and experimental studies, respectively. Additionally, the FRFs of the piezo-beam with controller are obtained for the both studies by the chirp signal in the range of frequency

from 5 to 35 Hz. The obtained FRFs have similar trends in both studies. The resonance frequency of the piezo-beam with the FLC is increased by the percentage of 12.6% and 12.1% in the simulation and experimental studies, respectively. It can be deduced that the FLC adds some stiffness to the piezo-beam. Additionally, the magnitude at the resonance is decreased by the ratio of 84.1% and 79.9% in the simulation and experimental results, respectively.

Furthermore, the results obtained from three different cases which are free vibration time domain response, forced vibration time domain response at the resonance and the forced vibration frequency domain response are compared with the previous studies where LQR controller was applied on the same piezo-beam. Although the settling time for the free vibration suppression is longer than the one obtained via LQR, the FLC has shown a similar performance on the forced vibration suppression and an excellent performance on shifting the resonance frequency to a higher one.

Since the results are consistent in the free and forced vibration suppression at the frequency span covering the first resonance, the simulation studies will not be used in the following chapters and only the experimental results will be presented.

CHAPTER 4

THE PARAMETRIC STUDY USING VARIOUS FUZZY LOGIC CONTROLLERS FOR EVALUATING THE ROBUSTNESS PERFORMANCE

4.1. Introduction

In this chapter, the robustness performance of the FLC which is designed in the previous chapter is evaluated by performing the experimental study for different arm positions. Then, various FLC is designed by using different number of rules and rearranging the overlap ratio and the core location of the membership functions in order to analyze the effect on the robustness of those controllers.

4.2. Experimental Result for Different Arm Positions

In the previous chapter, the FLC is designed and used in order to suppress free and forced vibration of the piezo-beam for the arm position of the mass location variation system is 0°. In this section, performance of the same controller is evaluated on forced vibration suppression at the corresponding resonance frequency of the piezo-beam for various arm positions of the mass location variation mechanism.

Time responses of the forced vibration at their resonance frequencies for different arm positions are plotted in Figure 4.1. For all cases, the controller is successful in forced vibration suppression at their corresponding resonance frequencies. The controller has suppression performances with the ratios of 92%, 92%, 91% and 63% for the cases where arm positions are -64°, -32°, +32° and +64°, respectively. For all cases except the case where the arm position is +64°, the controller has almost the same performance at the case where the controller is designed.

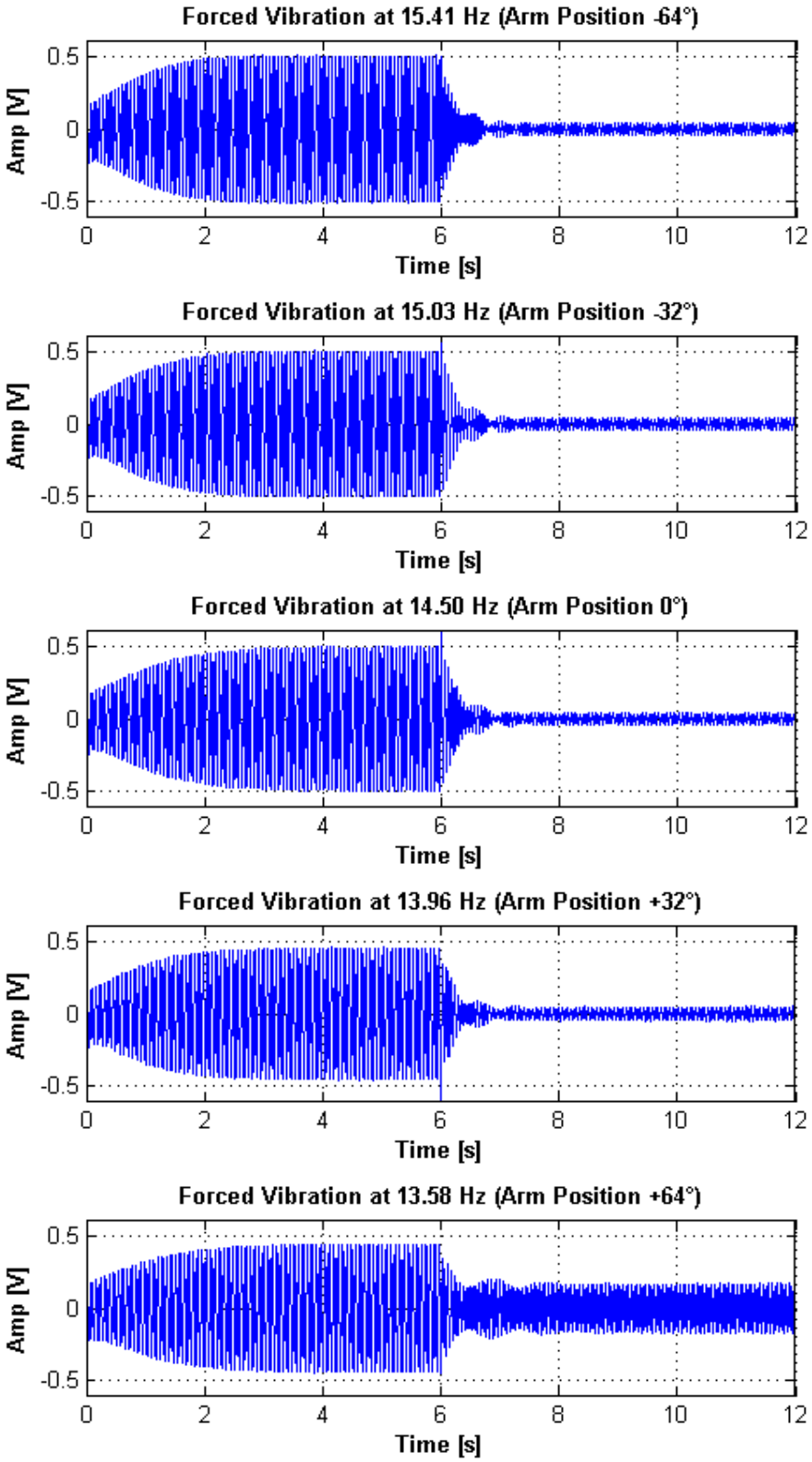

Figure 4.1. Forced Vibration at Corresponding Resonance Frequency for the Different Arm Positions

There is a sharp decrease in the performance for the arm position of +64°. The performances of the FLC where the arm positions are closer to +64° such as the arm position of +80°, +72°, +56° and +48° are also checked in Appendix D to analyze the trend of the decrease in the performance for the case where the arm is positioned at the tip of the piezo-beam. Time responses for the intermediate and extreme arm positions are plotted in Appendix D.

The all results are tabulated in Table 4.1 and it is observed that the suppression level decreases from ratio of 92% to level around 63% by rotating arm from a certain position towards to tip of the piezo-beam. Although the performance of the controller decreases, it has the success in the suppression at the forced vibration of the piezo-beam with the ratio of 63%.

Table 4.1 *The Result of the Suppression Ratios for Different Arm Positions*

The Arm Position	**Suppression Ratios**
-64°	92%
-32°	92%
0°	92%
+32°	91%
+48°	87%*
+56°	85%*
+64°	63%
+72°	63%*
+80°	61%*

For further studies, intermediate and extreme arm positions are not considered and in order to determine the robustness performance of designed FLCs, a robustness ratio is

* The suppression ratios for the intermediate and extreme arm positions are obtained from the time responses in Appendix 0

calculated by taking the average of the forced vibration suppression ratios for the arm positions of -64°, -32°, 0°, +32° and +64°. According to this calculated ratio, the performance comparison of designed FLCs are made by the robustness ratio which is obtained as 86% by taking average of the ratios of 92%, 92%, 92%, 91% and 63%.

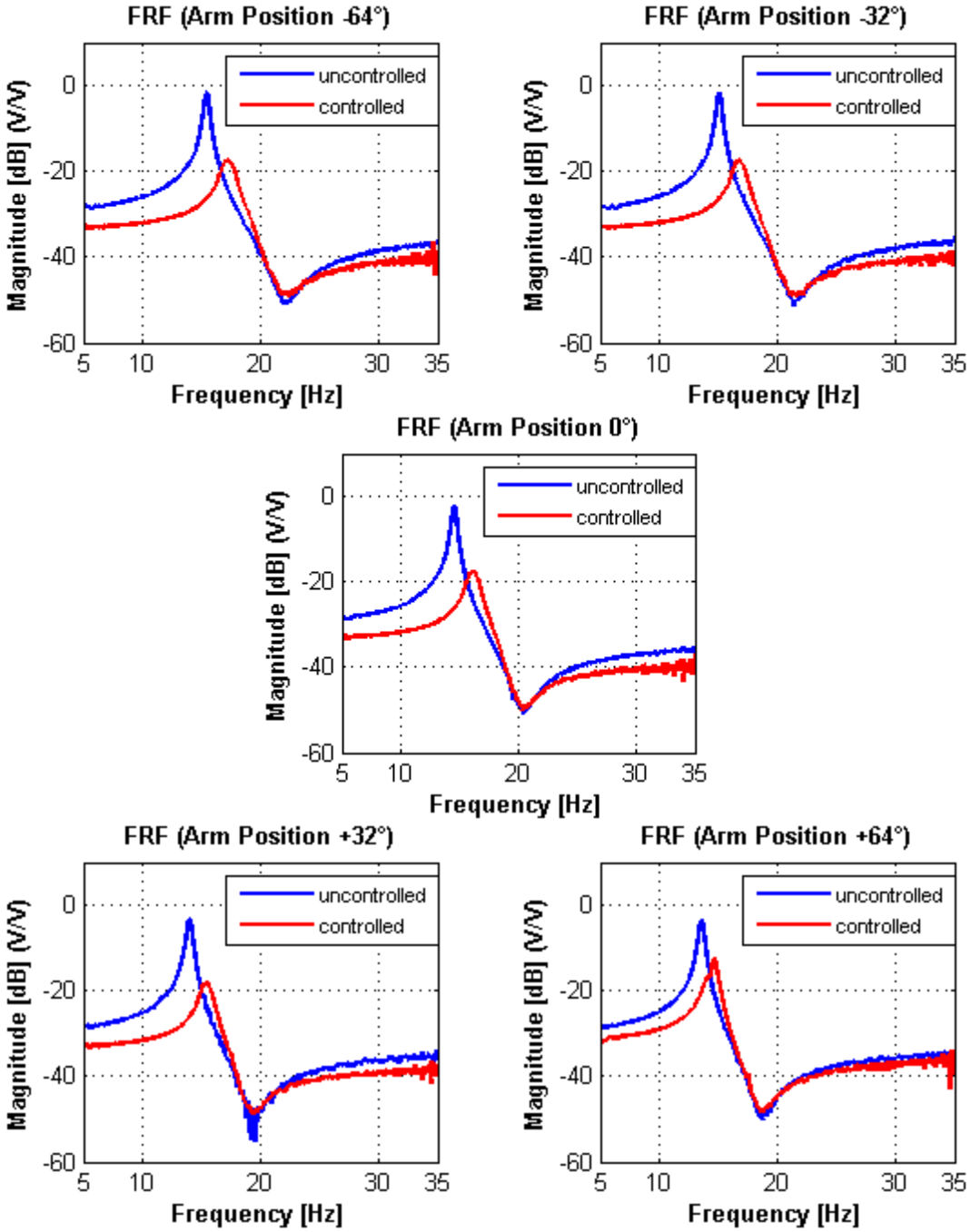

Figure 4.2. FRFs for the Different Arm Positions

FRFs of the piezo-beam for the different arm positions are given in Figure 4.2. The resonance frequencies are increased by 1.91, 1.75, 1.67, 1.45 and 1.07 Hz and the magnitudes are decreased by 16.0, 15.8, 15.3, 15.1 and 8.8 dB in the cases where the arm position -64°, -32°, 0°, +32° and +64°, respectively. In the case where arm position is +64°, although the trends of the change is similar as the other cases, the amount of suppression level is lower than the ones where the arm position is away from the tip of the piezo-beam.

4.3. Parametric Studies on the Designed FLC for the Investigation of the Robust Performances

In the previous section, the robust performance of the designed FLC is evaluated by changing the arm position of the piezo-beam. Although the controller has a great performance, in this section, on the other hand, various FLCs with different number of rules, overlap ratios and core locations are used for observing the effect of these parameters on the robustness performance.

4.3.1. Experimental Study for Different Number of Rules

In the previous chapter, the FLC is designed with 25 rules. Those fuzzy rules are composed of the combinations of five linguistic values of both inputs which are NB, NS, ZE, PS and PB. The number of the fuzzy rules affects the computation time and the output value of the controller. Therefore, in this section, for observing the effect of different number of rules, the FLCs with 9 and 49 rules are created by decreasing the linguistic values to 3 which are NS, ZE and PS and increasing the linguistic values to 7 which are NB, NM, NS, ZE, PS, PM and PB, respectively. The other design parameters of the FLC remain the same.

In the previous study, Şenöz and Şahin have compared the performances of the FLC with different rule numbers via simulations [56]. Therefore, in this study, the experimental setup is used to compare the performances of the FLC with different rule numbers.

For the FLC with 9 rules, the linguistic values NS, ZE and PS are used. The membership functions of these linguistic values are modified according to the same range of the chirp inputs and output values as shown in Figure 4.3. The fuzzy rules are created by removing the first and the last columns and rows as shown by crossing out the rules from the rule table of the FLC with the 25 rules in Table 4.2. The rule table for 9 rules is shown by indicating with green color in Table 4.2.

(a)

(b)

(c)

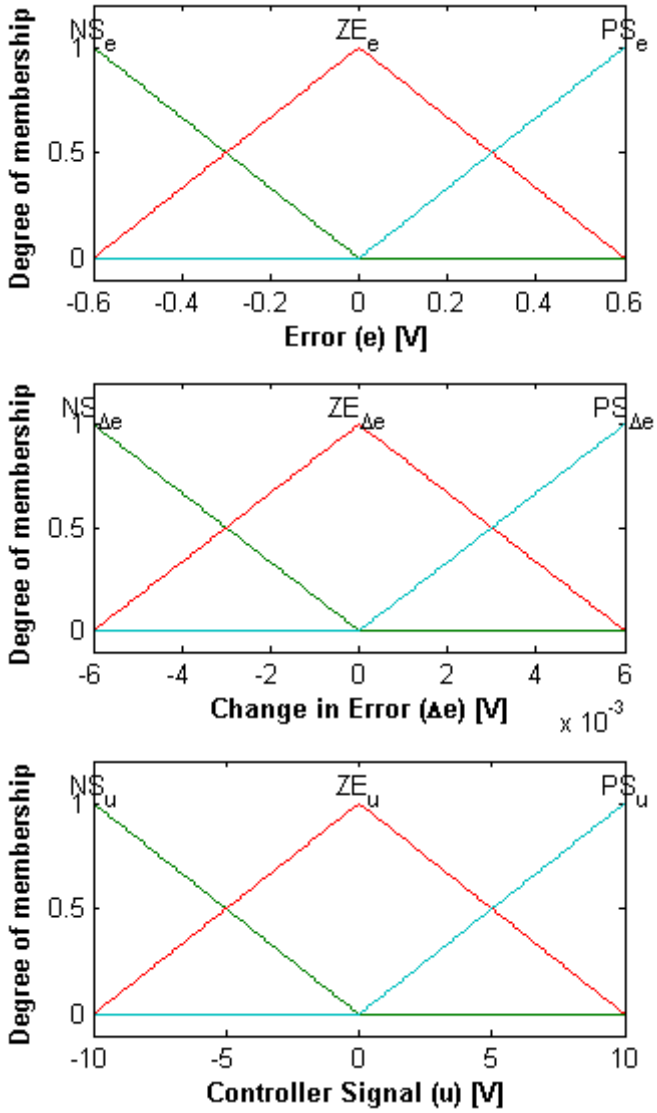

Figure 4.3. Membership Functions of the Inputs as (a) the Error and (b) the Change in Error and the Output as (c) the Control Signal for the 9 Rules

Table 4.2. *Fuzzy Logic Rule Table for the FLC with 9 rules*

Controller signal (x_u)		**change in error ($x_{\Delta e}$)**				
		NB	***NS***	***ZE***	***PS***	***PB***
error (x_e)	***NB***	*NB*	*NB*	*NB*	*NS*	*NS*
	NS	*NS*	*NS*	*NS*	*ZE*	*ZE*
	ZE	*NS*	*NS*	*ZE*	*PS*	*PS*
	PS	*ZE*	*ZE*	*PS*	*PS*	*PS*
	PB	*PS*	*PS*	*PB*	*PB*	*PB*

The relationship between the inputs and the output of the FLC is plotted as a surface graph which is shown in Figure 4.4.

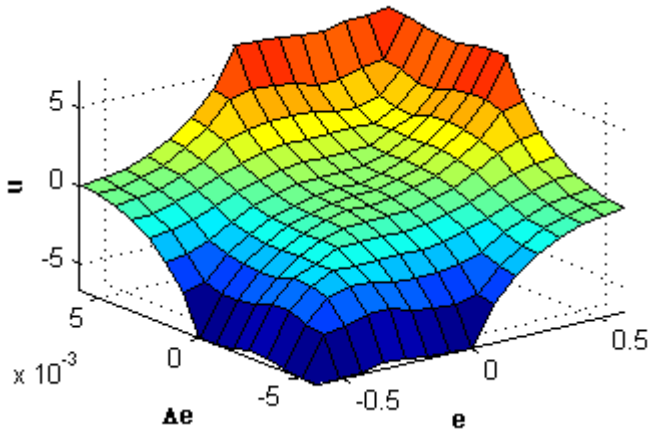

Figure 4.4. The Surface View of the FLC with 9 Rules

Time responses of the forced vibration suppression at their corresponding resonance frequencies via the FLC with the 9 fuzzy rules for different arm positions are plotted in Figure 4.5. For all the cases, the FLC with 9 rules has almost same performance on the forced vibration suppression at their corresponding resonance frequencies. It has the suppression ratios between 55% and 61% for all the cases. Although they do not have enough suppression level when compared the FLC with the 25 rules, suppression performances for all the cases are similar to each other.

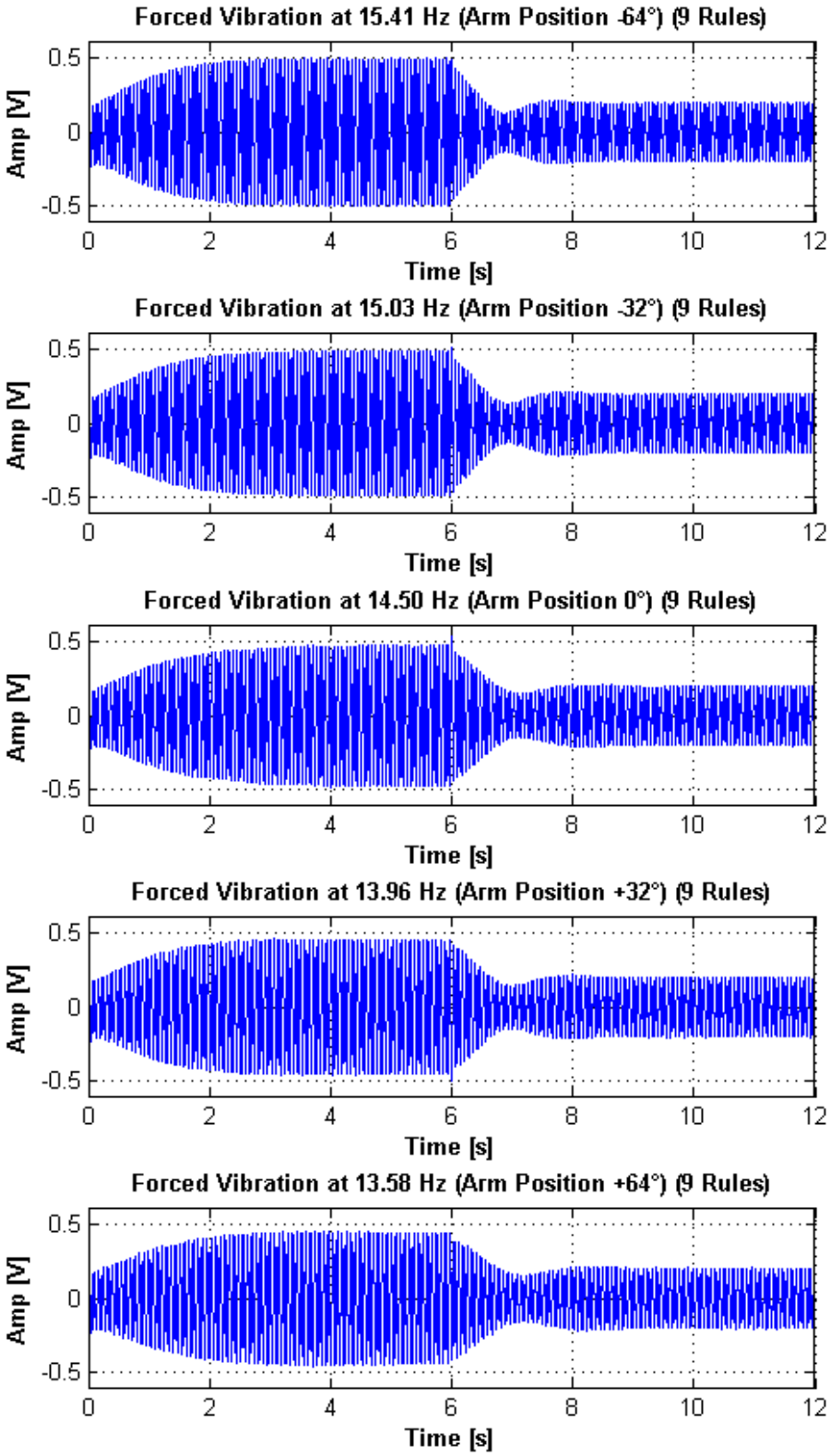

Figure 4.5. Forced Vibration Suppression at Corresponding Resonance Frequency via the FLC with the 9 Rules for the Different Arm Positions

For the FLC with 49 rules, the linguistic values NB, NM, NS, ZE, PS, PM and PB are used. The newly adding linguistic values NM and PM ("negative medium" and "positive medium") are substituted for the linguistic values NB and PB of the FLC with the 25 rules. As in the other FLCs, the membership functions of these linguistic values are arranged according to the same range of the chirp inputs and output values as shown in Figure 4.6. The fuzzy rules are created by adding the rules for NB and PB into the first and the last columns and rows of the rule table of the FLC with 25 rules. The rule table for 49 rules is shown in Table 4.3. Additionally, the common fuzzy rules shared with the rules in the FLC with the 25 rules are indicated in Table 4.3 with green color. The relationship between the inputs and the output of the FLC with 49 rules is plotted as a surface graph and shown in Figure 4.7.

Time responses of the forced vibration suppression at their resonance frequencies via the FLC with the 49 fuzzy rules for different arm positions are plotted in Figure 4.8. For all the cases except only the case where arm position is +64°, the FLC with 49 rules has a great performance on the forced vibration. It has the suppression ratio at around 92% for these cases. On the other hand, it has suppression ratio of 69% for the case where arm position is +64°. In comparison to the results with the FLC with 25 rules, the results of one with the 49 rules are very close to each other.

Table 4.3. *Fuzzy Logic Rule Table for the FLC with the 49 rules*

Controller signal (x_u)		**change in error** $(x_{\Delta e})$						
		NB	***NM***	***NS***	***ZE***	***PS***	***PM***	***PB***
error (x_e)	***NB***	*NB*	*NB*	*NB*	*NM*	*NM*	*NS*	*ZE*
	NM	*NB*	*NM*	*NM*	*NM*	*NS*	*NS*	*ZE*
	NS	*NM*	*NS*	*NS*	*NS*	*ZE*	*ZE*	*ZE*
	ZE	*NS*	*NS*	*NS*	*ZE*	*PS*	*PS*	*PS*
	PS	*ZE*	*ZE*	*ZE*	*PS*	*PS*	*PS*	*PM*
	PM	*ZE*	*PS*	*PS*	*PM*	*PM*	*PM*	*PB*
	PB	*ZE*	*PS*	*PM*	*PM*	*PB*	*PB*	*PB*

(a)

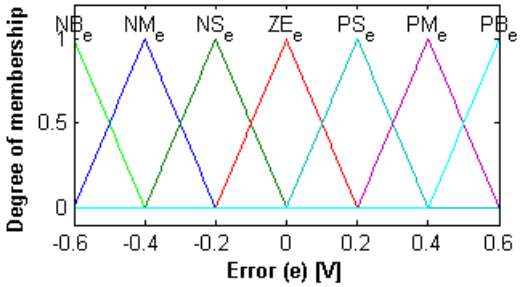

(b)

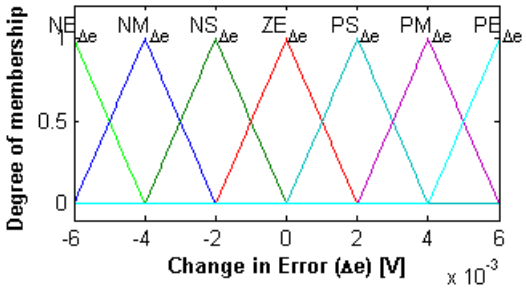

(c)

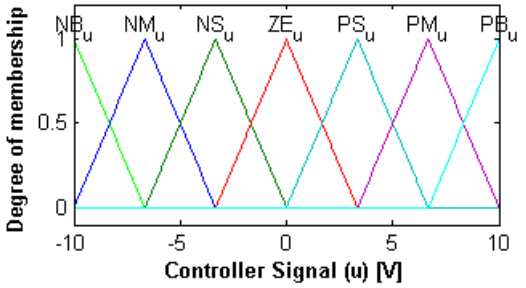

Figure 4.6. Membership Functions of the Inputs as (a) the Error and (b) the Change in Error and the Output as (c) the Control Signal for the 49 Rules

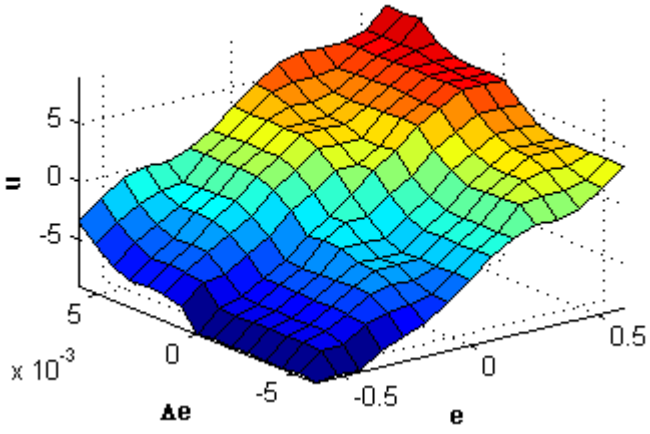

Figure 4.7. The Surface View of the FLC with 49 Rules

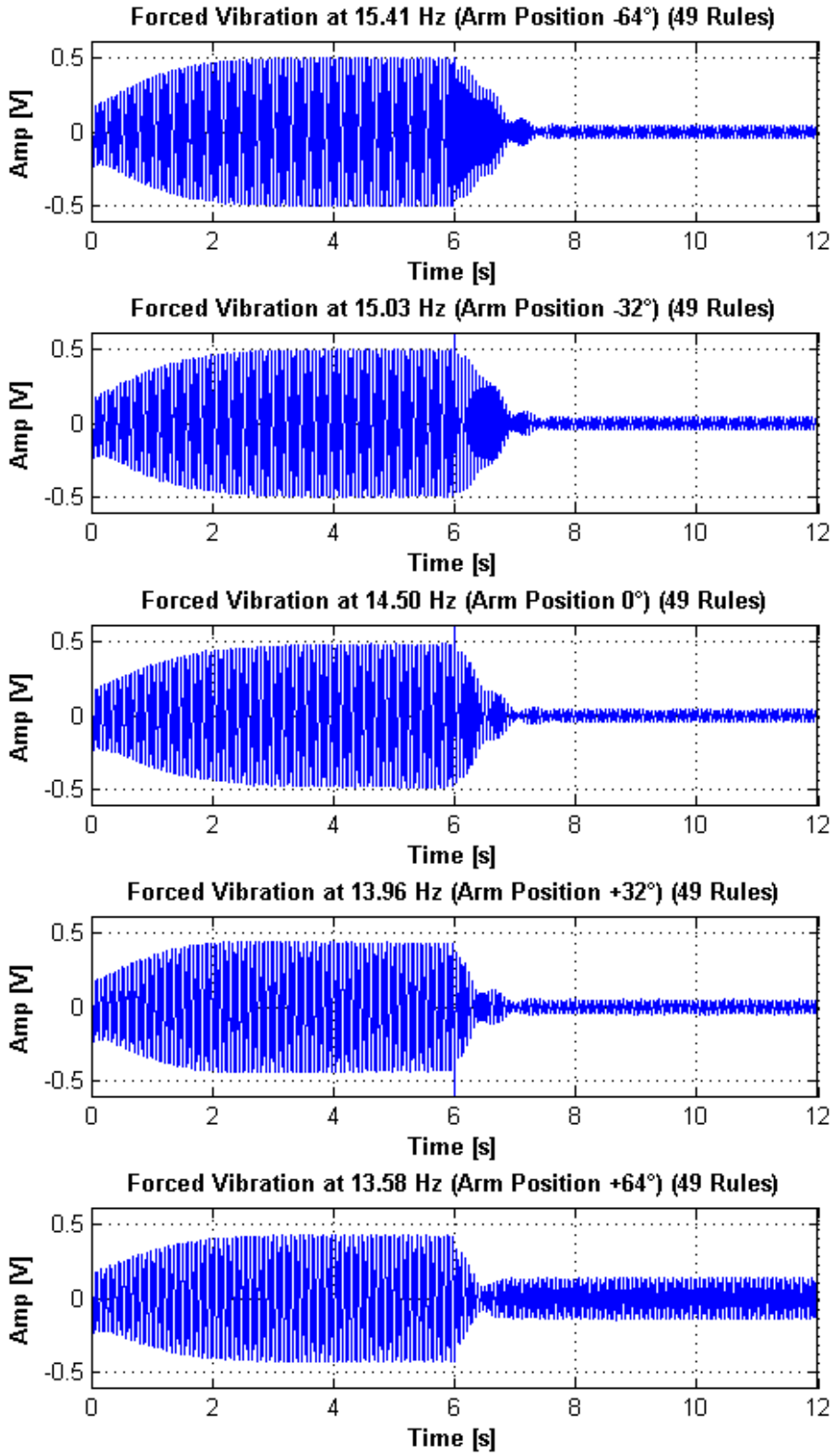

Figure 4.8. Forced Vibration Suppression at the Corresponding Resonance Frequency via the FLC with the 49 Rules for Different Arm Positions

In order to compare the robustness performance of the FLC with different number of rules, robustness ratios are calculated from the suppression ratios for different arm positions as given in Table 4.4. The robustness performance of the FLC with 9 rules shows a fairly low performance. On the other hand, the best robustness performance is obtained in the FLC with 49 rules with a minor difference of 1.4% from the FLC with 25 rules. However, increasing the number of rules is not preferred because it will increase the controller complexity and the load on the processor.

Table 4.4. The Results of the Suppression Ratios for Different Arm Positions via the FLC with Different Number of Rules and the Robust Ratios

Number of Rules	**The Arm Positions**					**Robustness Ratios**
	-64°	**-32°**	**0°**	**+32°**	**+64°**	
9 rules	61%	59%	57%	56%	55%	57.6%
25 rules	92%	92%	92%	91%	63%	86.0%
49 rules	92%	92%	92%	92%	69%	87.4%

For comparing the FLCs with different numbers of rules, FRFs of the piezo-beam for different arm positions are shown in Figure 4.9. It is shown that the performances of the FLC with 25 rules and the FLC with 49 rules are almost the same for all the cases. However, the FLC with 9 rules has much lower performance than the others.

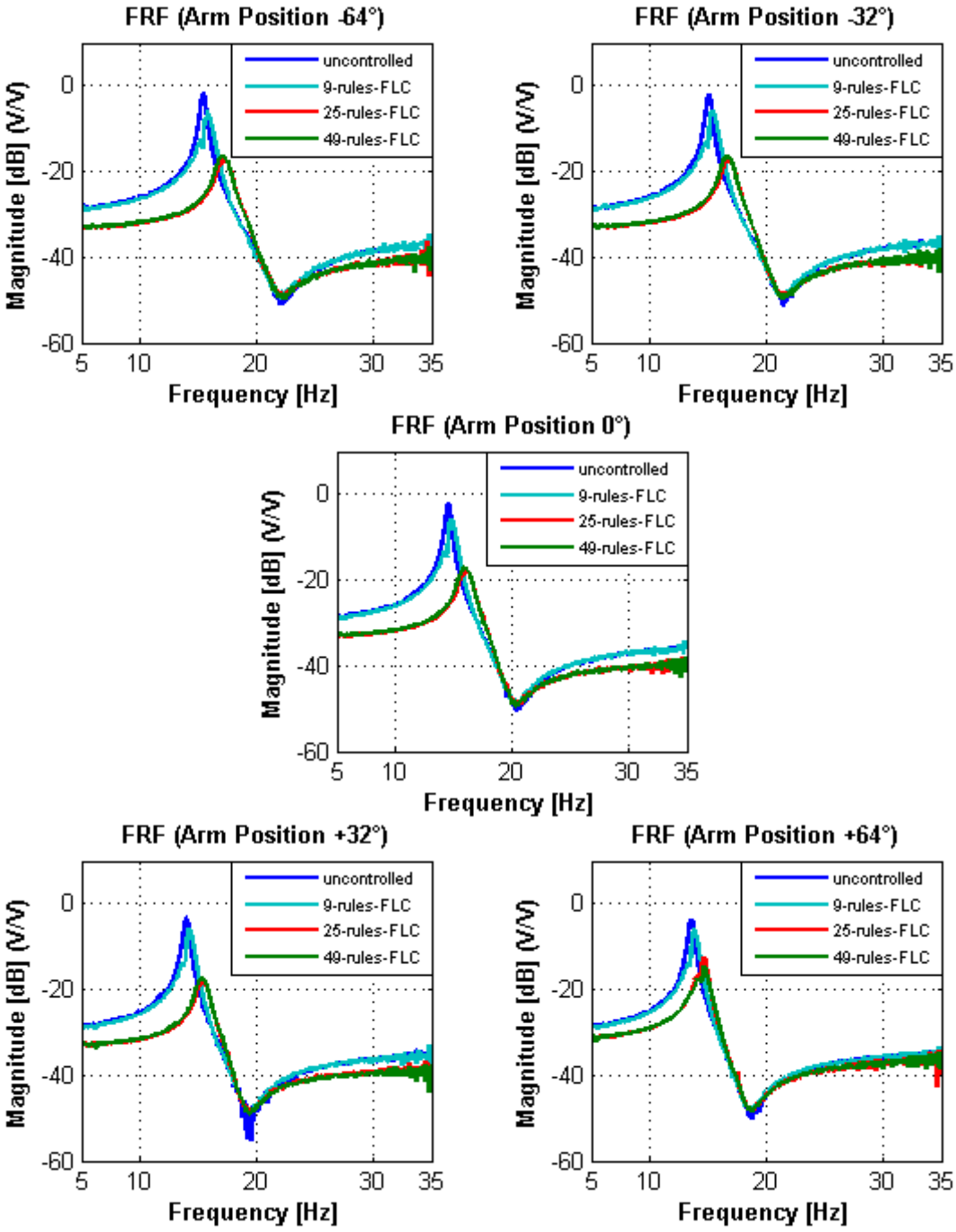

Figure 4.9. FRFs of Piezo-Beam for the Different Arm Positions via the FLCs with Different Number of Rules

Consequently, whereas decreasing the number of the rules of the FLC results in loss of performance in the forced vibration suppression, it is found that the controller consisting of more rules is not effective in improving the performance. Şenöz and Şahin have found the similar results in their simulation study [56]. Therefore, the FLC

with 25 rules is more convenient to use in this thesis due to reducing the complexity of the controller and not increasing the computation time.

4.3.2. Experimental Study for Different Overlap Ratios

In the FLC, a membership function is generally overlapped to another membership function. The intersection of two membership functions is placed between two points. One point is the lower member of the first membership function, fuzzy set 1, (LM_1) and other point is the upper member of the other membership function, fuzzy set 2, (UM_2) as shown in Figure 4.10. The overlap ratio is calculated by dividing the intersection of the membership functions by the interval of the membership function as shown in Equation 4.1.

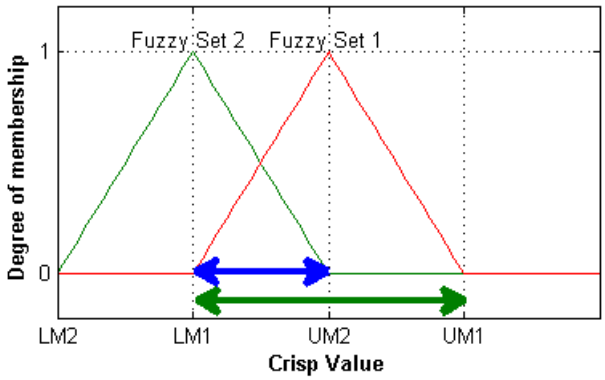

Figure 4.10. Representation of Overlap Ratio of the Fuzzy Set 1

$$Overlap\ Ratio = \frac{UM_2 - LM_1}{UM_1 - LM_1} \tag{4.1}$$

In the previous designed FLC, the overlap ratio is 50% for all the membership functions. The overlap ratio of two membership functions affects the output value of the controller directly. Therefore, in order to observe the effect of the overlap ratio, in this section, various FLCs are created by changing the overlap ratio of the membership function. The effect of the overlap ratios of 0%, 25% and 33% (i.e. ratios less than 50%) and the overlap ratios of 57%, 63% and 67% (i.e. ratios higher than 50%) are also used in the FLC applications. The overlap ratios are changed only for the membership function of the input fuzzy sets and the membership function of the output

fuzzy set remains the same. The FLCs with different overlap ratios are performed for the forced vibration suppression at the corresponding resonance frequency for different arm positions.

For the FLC with the overlap ratio of 0%, the membership functions of the input fuzzy sets are formed as in Figure 4.11.

(a)

(b)

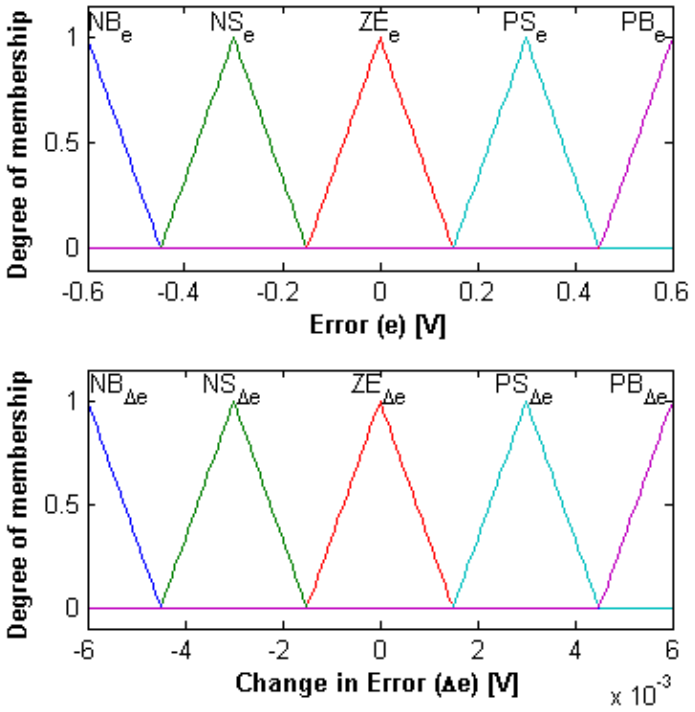

Figure 4.11. Membership Functions with Overlap Ratio of 0% (a) Error and (b) Change in Error

The time responses for the forced vibration suppression at the first corresponding resonance frequencies for different arm positions are shown in Figure 4.12 when the FLC with overlap ratio of 0% is used. The suppression ratio of forced vibration at the first corresponding resonance frequencies of the piezo-beam for all the cases except the arm position of +64° is also almost the same as for the FLC with the other overlap ratios. However, the suppression ratios for the four cases decrease to a value of at around 67%. In addition to this, the suppression ratio for the case where arm position is +64° decreases to a lower value of 53%.

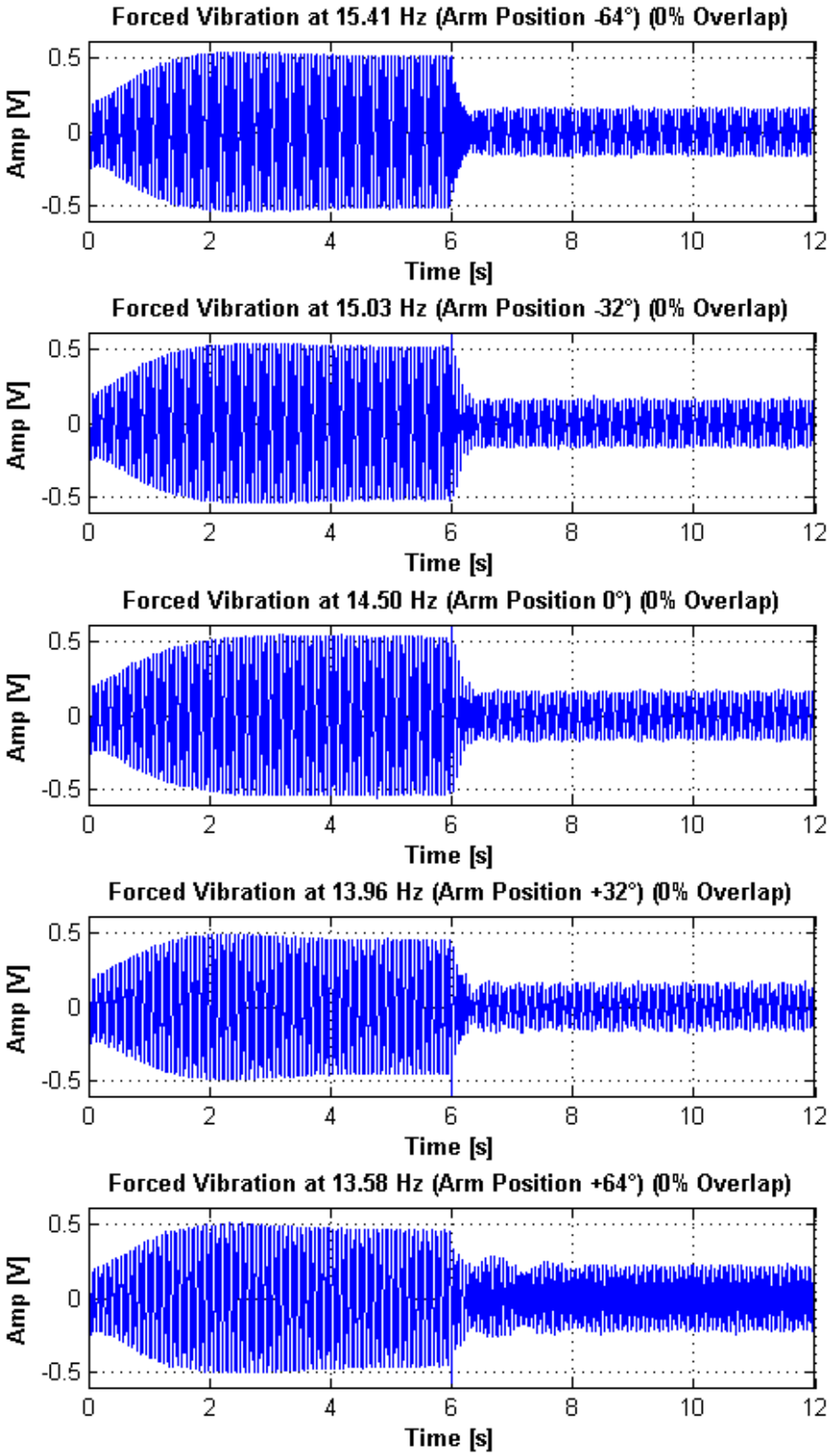

Figure 4.12. Forced Vibration Suppression at the Corresponding Resonance Frequency via the FLC with Overlap Ratio of 0% for Different Arm Positions

For the FLC with the overlap ratio of 25%, the membership functions of the input fuzzy sets are given in Figure 4.13.

(a)

(b)

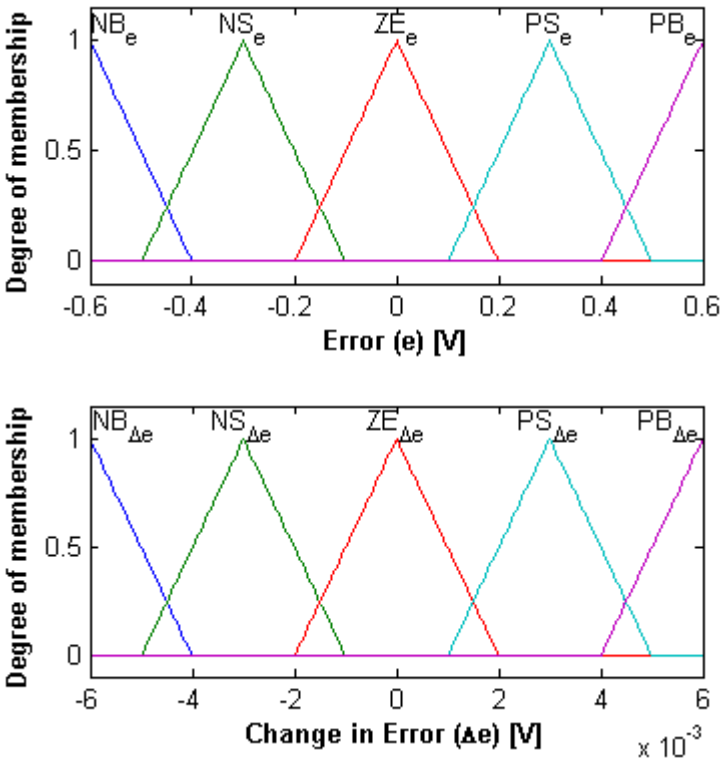

Figure 4.13. Membership Functions with Overlap Ratio of 25% (a) Error and (b) Change in Error

The time responses for the forced vibration suppression at the first corresponding resonance frequencies for different arm positions are shown in Figure 4.14 when the FLC with overlap ratio of 25% is used. As the result of the FLCs with the other overlap ratios, the suppression ratio of forced vibration at the first corresponding resonance frequencies of the piezo-beam for all the cases except the arm position of +64° are almost the same with each other. However, the suppression ratios for the four cases decrease to a value of at around 71%. For the case where the arm position is +64°, the suppression ratio also decreases to a value of 57%.

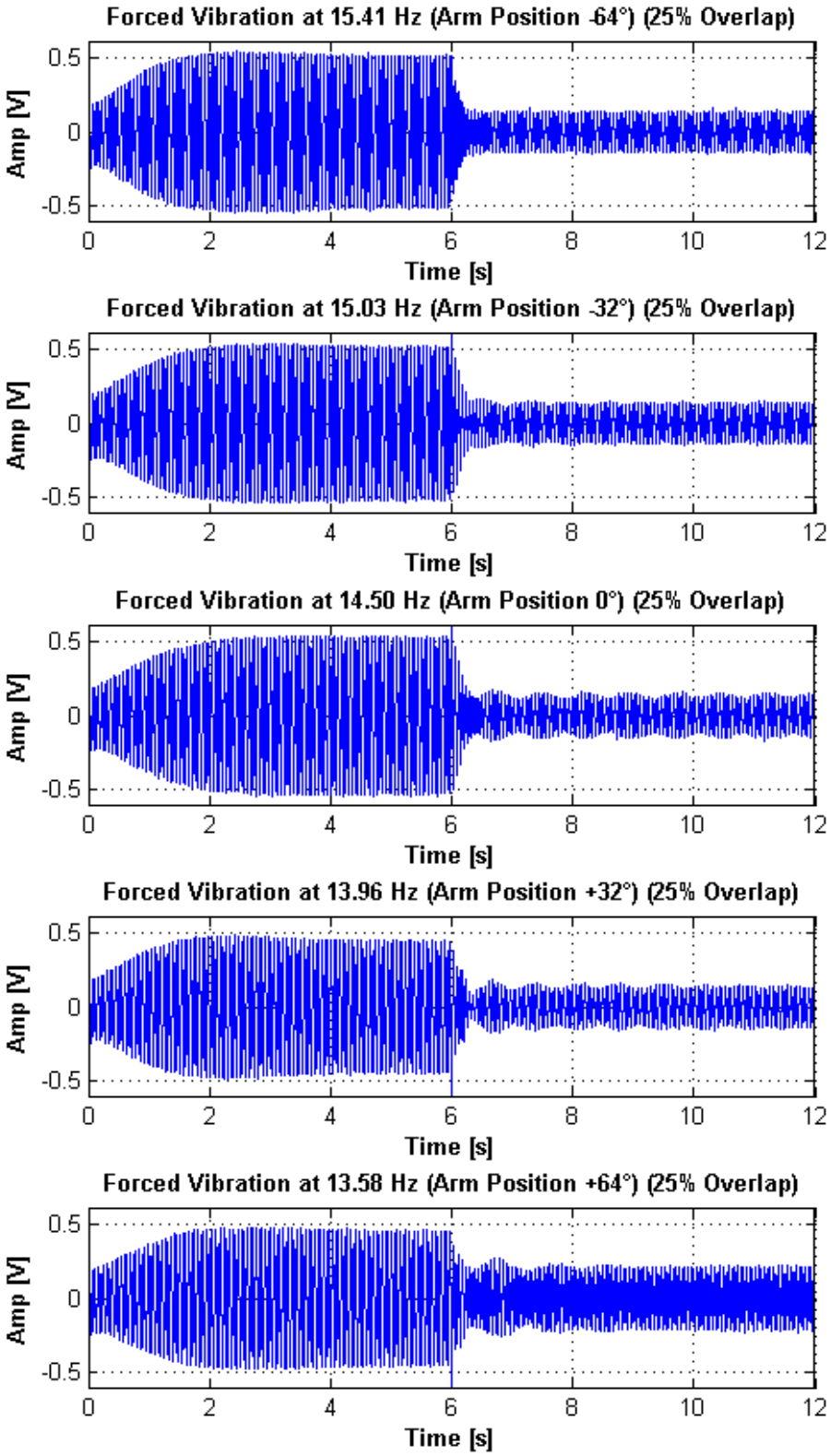

Figure 4.14. Forced Vibration Suppression at the Corresponding Resonance Frequency via the FLC with Overlap Ratio of 25% for Different Arm Positions

For the FLC with the overlap ratio of 33%, the membership functions for the error and the change in error are given in Figure 4.15.

(a)

(b)

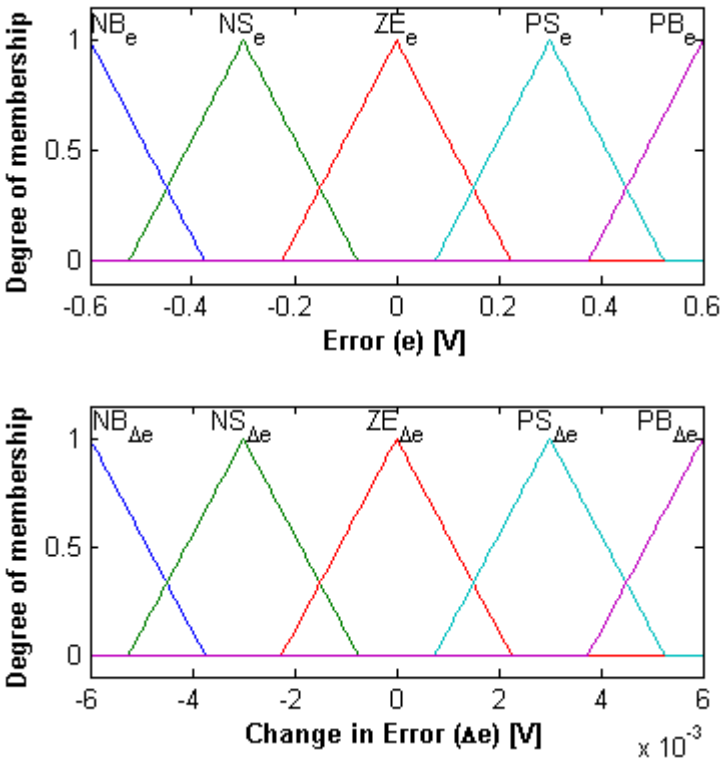

Figure 4.15. Membership Functions with Overlap Ratio of 33% (a) Error and (b) Change in Error

The time responses for the forced vibration suppression at the first corresponding resonance frequencies for different arm positions are shown in Figure 4.16 when the FLC with overlap ratio of 33% is used. The suppression ratios of the forced vibration at the first corresponding resonance frequencies of the piezo-beam for all the cases except the arm position of +64° are almost the same with a value of at around 78%. On the other hand, the suppression ratio for the case where the arm position is +64° decreases to a value of 59%.

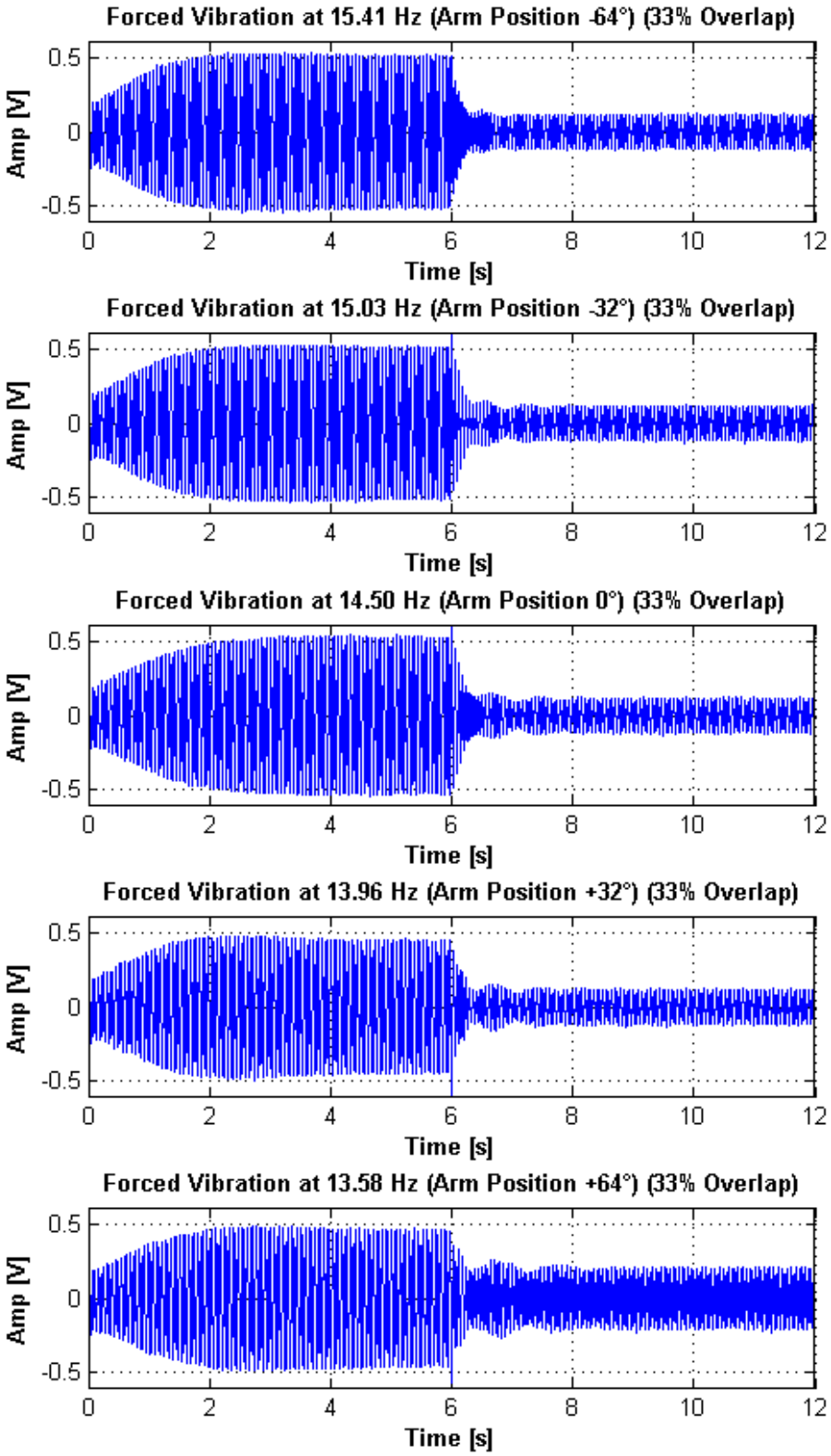

Figure 4.16. Forced Vibration Suppression at the Corresponding Resonance Frequency via the FLC with Overlap Ratio of 33% for Different Arm Positions

After the FLCs with overlap ratios below the ratio of 50% are performed for forced vibration suppression, the FLCs with overlap ratios above the ratio of 50% should be analyzed. For the FLC with the overlap ratio of 57%, the membership functions for the error and the change in error are given in Figure 4.17.

(a)

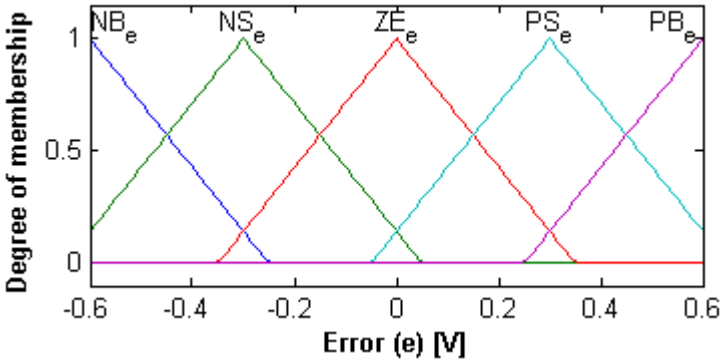

(b)

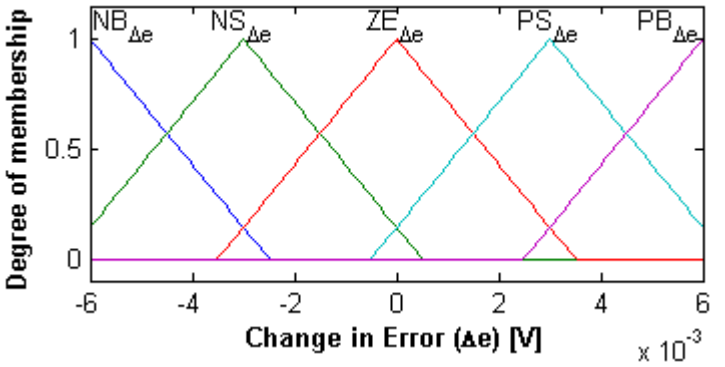

Figure 4.17. Membership Functions with Overlap Ratio of 57% (a) Error and (b) Change in Error

The time responses for the forced vibration suppression at the first corresponding resonance frequencies for different arm positions are shown in Figure 4.18 where the FLC with overlap ratio of 57% is used. The suppression of the forced vibration at the first corresponding resonance frequencies of the piezo-beam for all the cases except the arm position of +64° are obtained with a better ratio of 93%. On the other hand, the suppression ratio for the arm position of +64° is also obtained with a better ratio of 83%.

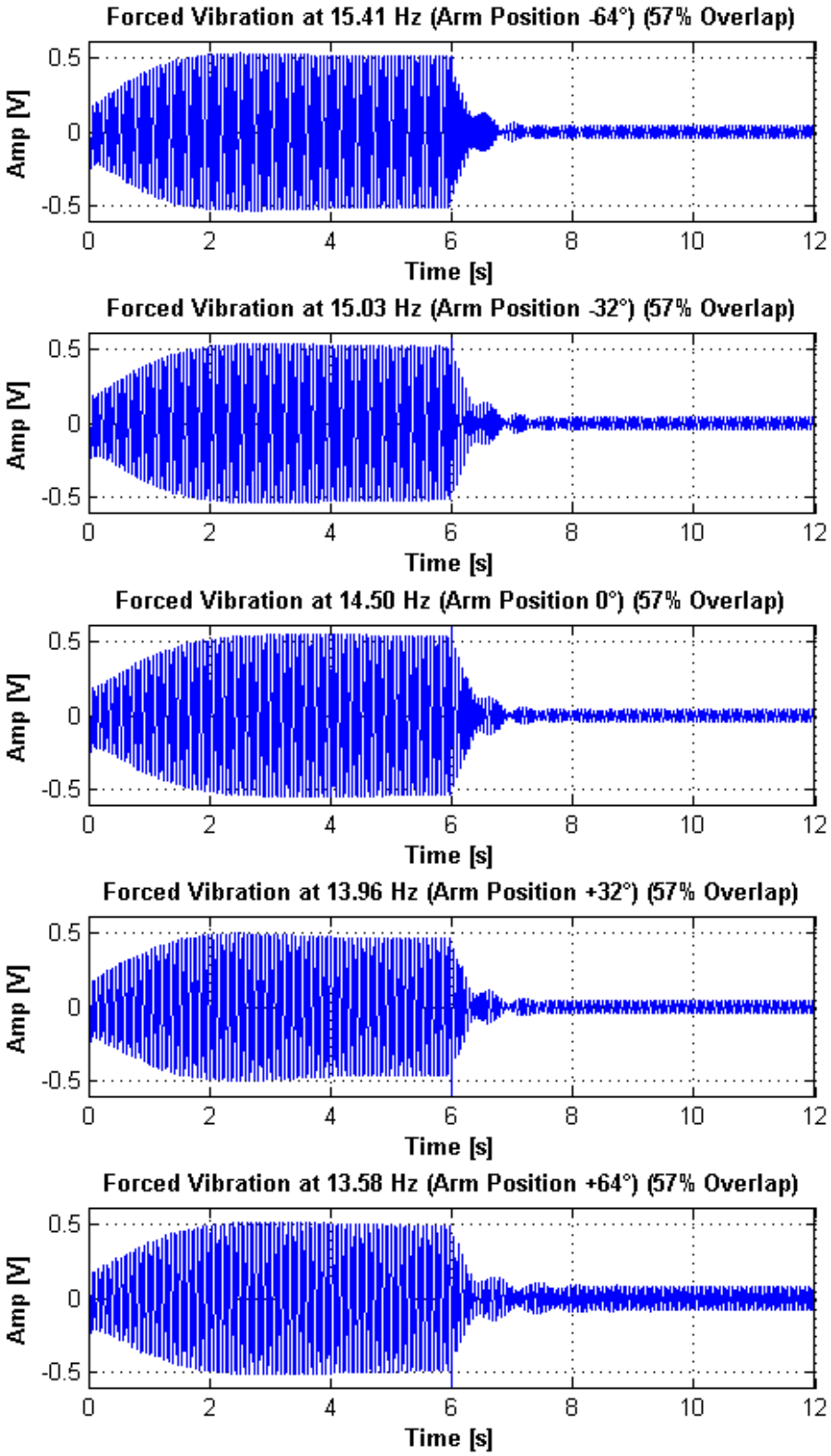

Figure 4.18. Forced Vibration Suppression at the Corresponding Resonance Frequency via the FLC with Overlap Ratio of 57% for Different Arm Positions

For the FLC with the overlap ratio of 63%, the membership functions for the error and the change in error are given in Figure 4.19.

(a)

(b)

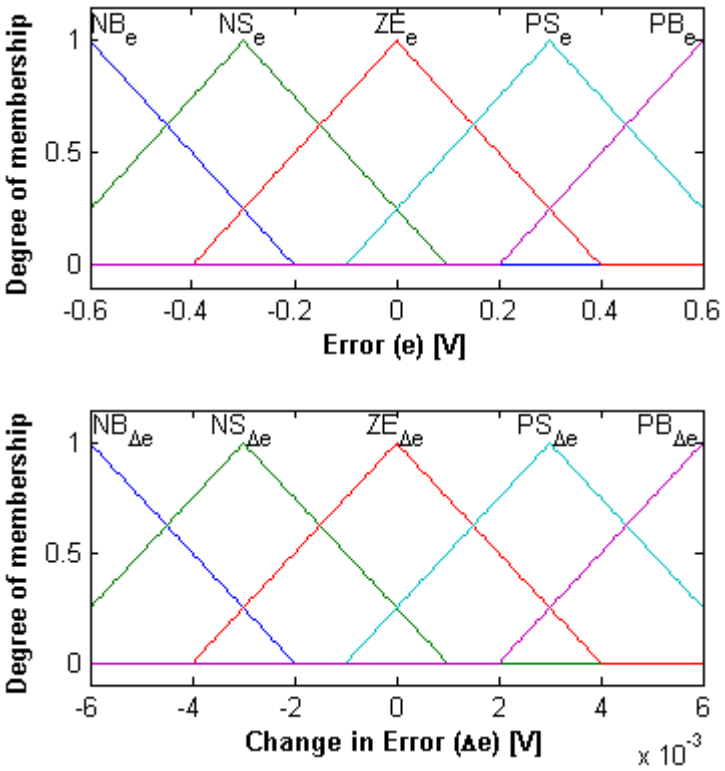

Figure 4.19. Membership Functions with Overlap Ratio of 63% (a) Error and (b) Change in Error

The time responses for the forced vibration suppression at the first corresponding resonance frequencies for different arm positions are shown in Figure 4.20 where the FLC with overlap ratio of 63% is used. It is shown that the suppression ratios of the forced vibration at the first corresponding resonance frequencies of the piezo-beam for all the cases are almost the same ratio of at around 89%. Although there is a slight decrease in the suppression ratio, it is shown that the consistent results are obtained for all the arm positions.

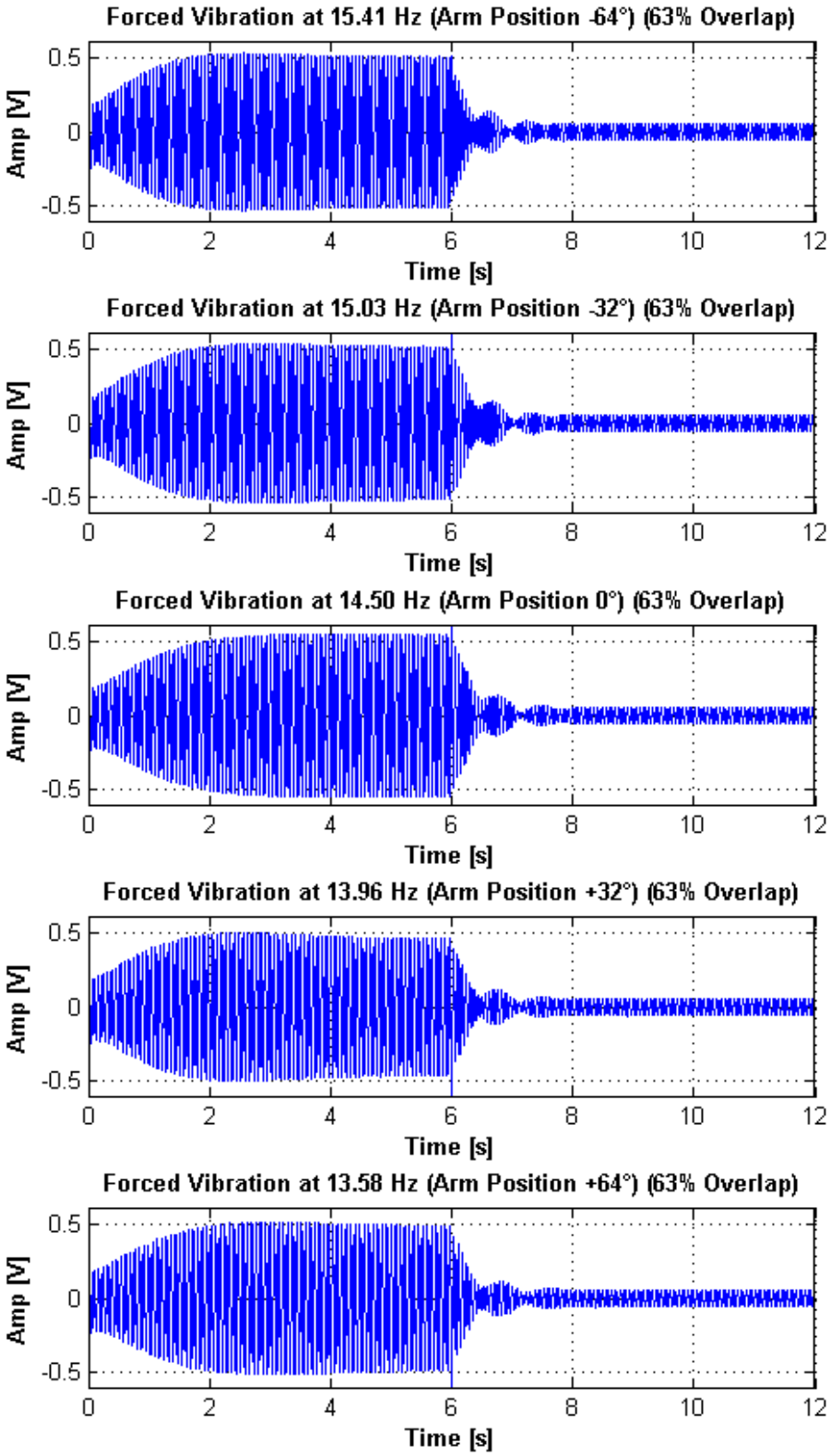

Figure 4.20. Forced Vibration Suppression at the Corresponding Resonance Frequency via the FLC with Overlap Ratio of 63% for Different Arm Positions

For the FLC with the overlap ratio of 67%, the membership functions for the error and the change in error are given in Figure 4.21.

(a)

(b)

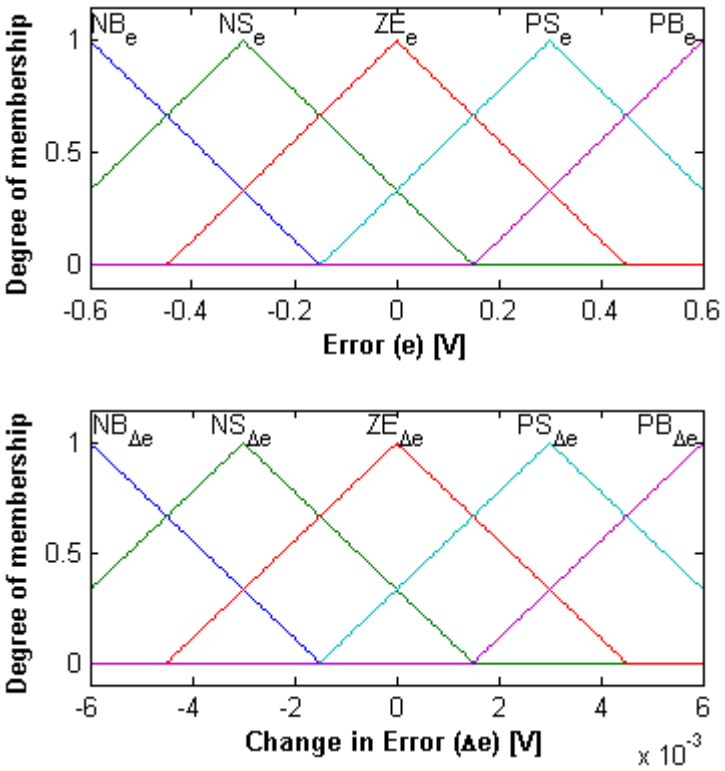

Figure 4.21. Membership Functions with Overlap Ratio of 67% (a) Error and (b) Change in Error

The time responses for the forced vibration suppression at the first corresponding resonance frequencies for different arm positions are shown in Figure 4.22 where the FLC with overlap ratio of 67% is used. The suppression ratios for all the cases are almost the same ratio of at around 86%. There is also a small decrease in the suppression ratio when the overlap ratio is slightly increased. However, the consistent results are obtained for all the arm positions.

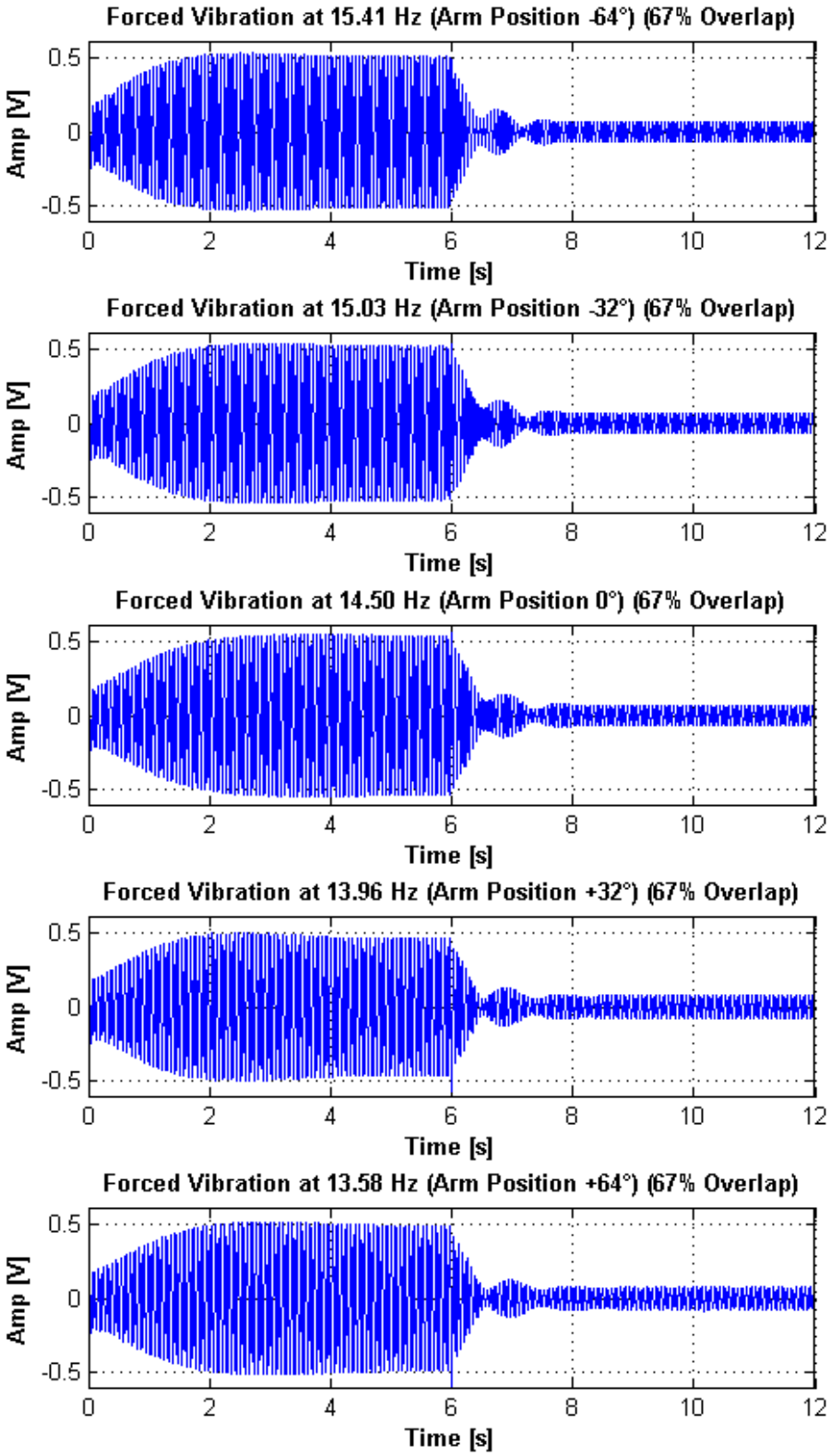

Figure 4.22. Forced Vibration Suppression at the Corresponding Resonance Frequency via the FLC with Overlap Ratio of 67% for Different Arm Positions

The suppression performances for different overlap ratios are compared in Table 4.5. It is found that decreasing the overlap ratio of the membership functions less than the ratio of 50% affects adversely the performances of the controller for all the arm positions. In contrast to this observation, the increase in the overlap ratio higher than the ratio of 50% provides consistent results for all the arm positions. However, it is observed that increase in the overlap ratio more than a certain overlap ratio around 57% results as a drop in the maximum suppression ratios. Moreover, almost the same suppression ratios for all arm positions are obtained via the FLC with overlap ratios of 63% and 67%. In the other cases where different overlap ratios are used, the suppression ratios are lower in values for the arm position of 64°.

According to the robustness ratios, the best FLC is obtained as the FLC with overlap ratio of 57% with a robustness ratio of 90.6%. In the further study, the FLC with overlap ratio of 57% is taken and used to change the various parameters in order to obtain the best FLC from performance point of view.

Table 4.5. *The Results of the Suppression Ratios for Different Arm Positions via the FLC with Different Overlap Ratios and the Robust Ratios*

Overlap Ratios	**The Arm Positions**					**Robustness Ratios**
	-64°	**-32°**	**0°**	**+32°**	**+64°**	
0%	67%	67%	67%	67%	53%	64.2%
25%	71%	71%	71%	71%	57%	68.2%
33%	78%	78%	78%	78%	59%	74.2%
50%	92%	92%	92%	91%	63%	86.0%
57%	93%	93%	93%	91%	83%	90.6%
63%	89%	90%	91%	88%	88%	89.2%
67%	87%	87%	87%	85%	85%	86.2%

4.3.3. Experimental Study for Different Core Location

The designed FLCs have symmetrical triangular membership functions whose *cores*[1] are located in the middle of the boundaries of the membership functions. However, in the literature, there are some examples of non-symmetrical triangular membership functions which are used in active vibration control application [42], [43]. Therefore, in this section, the effect of non-symmetrical membership functions on the performance of the fuzzy controller is evaluated by comparing three fuzzy controllers which are composed of different core location of membership functions NS and PS. Two FLCs are created by changing the core location of the membership functions. One has a core location for membership function closed to zero, and the other one has a core location away from zero.

The membership functions NS and PS of input fuzzy sets of the designed FLC with overlap ratio of 57% are rearranged by shifting the core locations towards to zero as shown in Figure 4.23. The core of NS_e and PS_e is located -0.2 and 0.2, respectively. Similarly, the core of $NS_{\Delta e}$ and $PS_{\Delta e}$ is located -0.002 and 0.002, respectively. The boundaries and the other membership functions remain unchanged.

[1] *Core* of a membership function for the fuzzy set A is defined as that region or value of the universe that is characterized by complete and full membership in the set A [57].

(a)

(b)

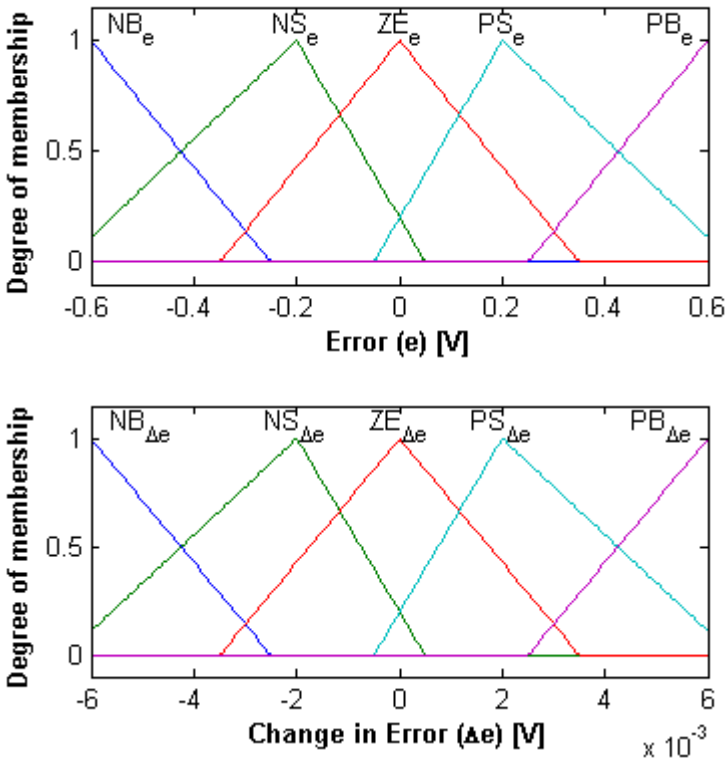

Figure 4.23. Membership Functions with Core Location Closed to Zero and Overlap Ratio of 57%
(a) Error and (b) Change in Error

The time responses for the forced vibration suppression at the first corresponding resonance frequencies for different arm positions are shown in Figure 4.24 when the FLC with membership functions where core location is closed to zero is used. Comparing the suppression ratio of forced vibration at the first corresponding resonance frequencies of the piezo-beam, they are almost the same with a ratio of 93% for the arm positions of -64°, -32° and 0°. The suppression ratio decreases as the arm rotates towards the tip of the piezo-beam after the arm position of 0°. The suppression ratio for the arm positions of +32° and +64° are found as 88% and 80%, respectively.

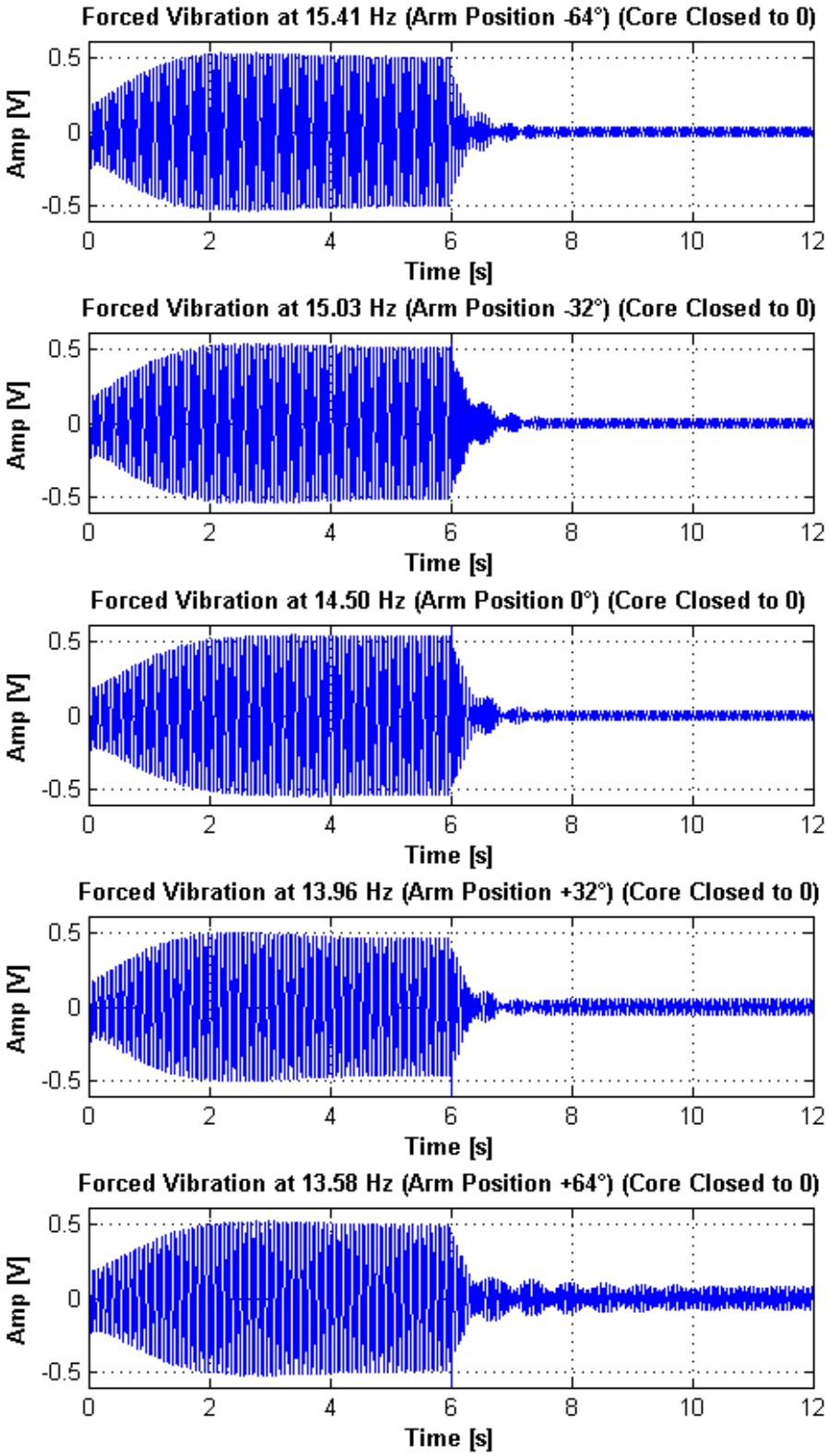

Figure 4.24. Forced Vibration Suppression at the Corresponding Resonance Frequency via the FLC with Core Location Closed to Zero and Overlap Ratio of 57% for Different Arm Positions

On the other hand, the membership functions are recreated by removing the core locations from zero as shown in Figure 4.25. The core of NS_e and PS_e is located -0.4 and 0.4, respectively. Similarly, the core of $NS_{\Delta e}$ and $PS_{\Delta e}$ is located -0.004 and 0.004, respectively.

(a)

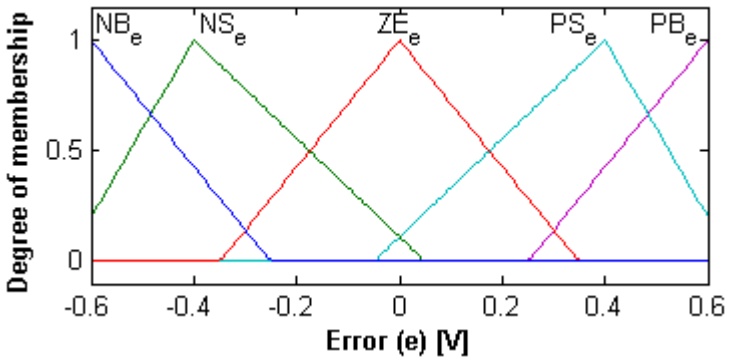

(b)

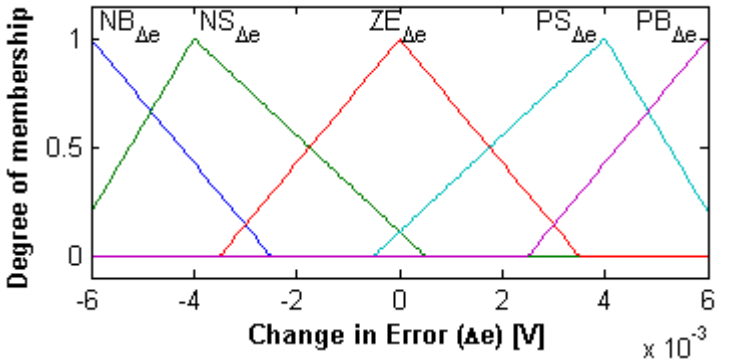

Figure 4.25. Membership Functions with Core Location Away from Zero and Overlap Ratio of 57% (a) Error and (b) Change in Error

When the FLC with membership functions where core location is away from zero is used, the time responses for the forced vibration suppression at the first corresponding resonance frequencies for different arm positions are shown in Figure 4.26. The suppression ratio of forced vibration at the first corresponding resonance frequencies of the piezo-beam are almost the same with a ratio of 91% for the arm positions of -64°, -32° and 0°. The suppression ratio for the arm position of +32° and +64° are found as 89% and 84%, respectively.

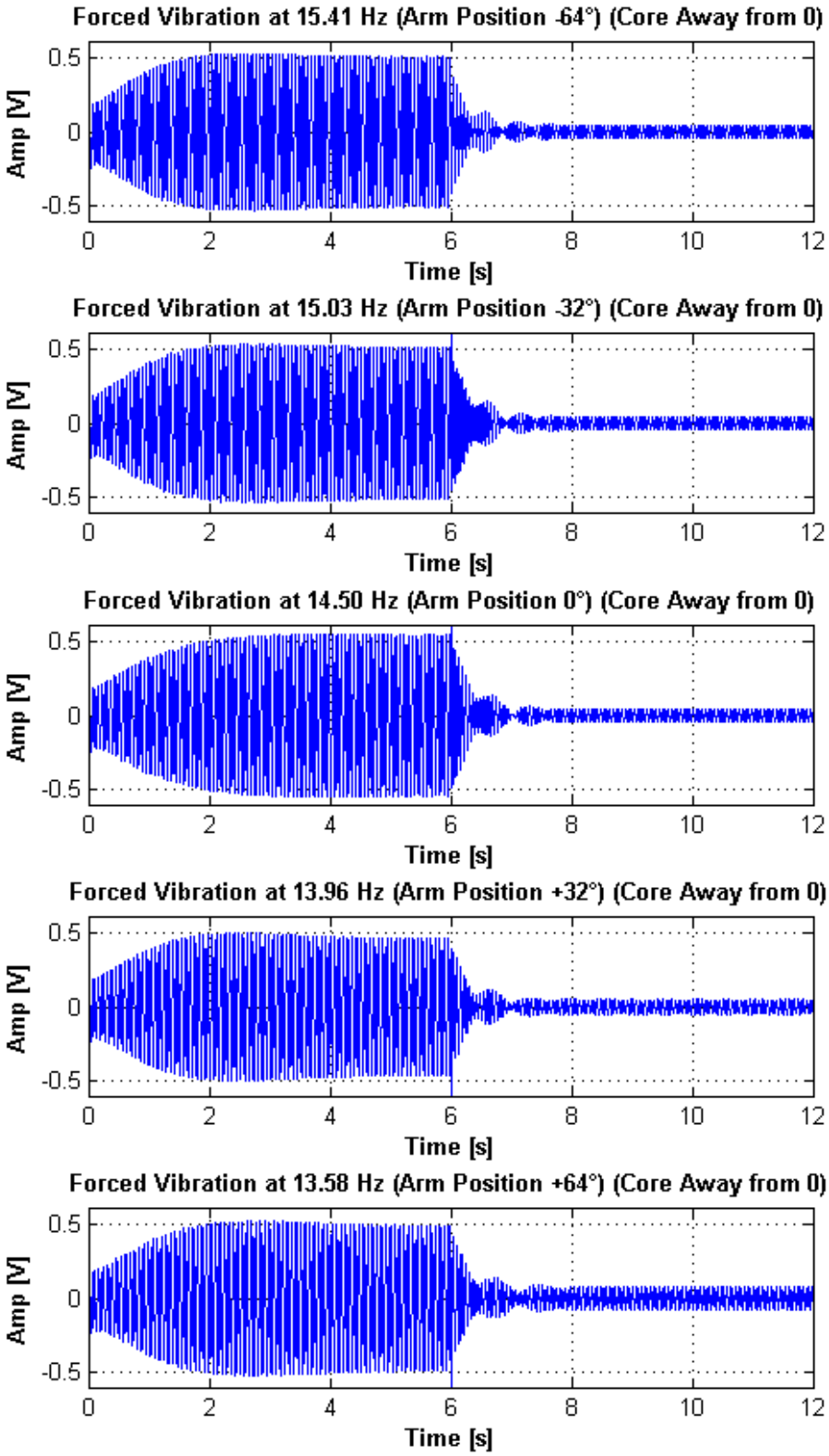

Figure 4.26. Forced Vibration Suppression at the Corresponding Resonance Frequency via the FLC with Core Location Away from Zero and Overlap Ratio of 57% for Different Arm Positions

The suppression performances in this section are summarized and compared in Table 4.6. It is observed that the performances of the FLC with core location closed to zero are almost the same as the performances of the designed FLC with symmetric membership functions. However, for the arm positions of +32° and +64°, there is a slight difference in the suppression ratio with a ratio difference of 3%. Robustness ratio for the FLC with core location closed to zero is only 1% lower than the designed FLC with symmetric membership functions. On the other hand, the FLC with core location away from zero has slightly low performances. Although it has slightly better performance among for the arm position of +64°, its robustness ratio is lower than the FLCs with the other core locations.

Table 4.6. *The Results of the Suppression Ratios for Different Arm Positions via the FLC with Different Core Locations*

Core Locations	**The Arm Positions**					**Robustness Ratios**
	-64°	**-32°**	**0°**	**+32°**	**+64°**	
Closed to 0	94%	93%	93%	88%	80%	89.6%
Middle	93%	93%	93%	91%	83%	90.6%
Away from 0	91%	91%	91%	89%	84%	89.2%

4.4. Conclusion

In this chapter, various parametric studies on the FLC which is designed in the previous chapter for 0° arm position are performed in order to analyze its robustness.

At first, performance of the controller is analyzed for different arm positions of the mass location variation mechanism when the piezo-beam is vibrated at the corresponding resonance frequency. For the cases where the arm positions are -64°, -32° and +32°, the performance of the controller remains almost the same as the performance in the case where the controller is designed. However, the performance of the controller is getting decreased at the arm position of +64°. Therefore, the FLCs is also performed for the arm positions nearby +64°. The decrease is also observed in the intermediate and extreme arm positions which are closer to +64°.

Then, in order to observe the effect of the number of fuzzy rules on the performance of the controller, the FLCs with 9 and 49 rule controllers are obtained additionally. The forced vibration suppression is then investigated experimentally via the FLCs for all cases. It is found that the FLC where the number of rules is decreased to 9 rules has a lower performance than the FLC with 25 rules on the vibration suppression. However, the FLC where the number of rules is increased to 49 rules has almost the same performance as the FLC with 25 rules. Therefore, the FLC with 25 rules is preferred in this study. Thus, a high performance FLC is obtained without over-increasing the number of rules due to complexity.

Following that, in order to observe the effect of the overlap ratio of the membership function, the FLCs are obtained by changing with overlap ratio to the values of 0%, 25%, 33%, 57%, 63% and 67%. The results of the FLC performances are obtained experimentally and it is observed that decreasing the overlap ratio of the membership functions below the ratio of 50% adversely affects the performances of the controller for all arm positions. Comparing the robustness ratios of the FLCs with different overlap ratios, the FLC with overlap ratio of 57% has the best robustness performance.

Lastly, the effect of the core location of the membership functions is observed on the vibration suppression performance. The FLC with overlap ratio of 57% which is selected as the best is used in this study. Although the performances of the FLC with core location closed to zero and the FLC with core location away from zero are almost the same as the performance of the FLC with symmetric membership functions. However, when the robustness ratios are compared, the FLC with symmetric membership functions has the best ratio with a difference of 1%.

Consequently, it is observed that the FLC which is designed in Chapter 3 is converted by changing overlap ratio from 50% to 57% to obtain the best robust performance among the FLCs alternatively designed in this chapter for the forced vibration suppression at their first corresponding resonance frequencies of the piezo-beam for different arm positions.

CHAPTER 5

CONCLUSION

5.1. General Conclusions

In this thesis, active vibration control of a piezo-beam comprising a mass location variation mechanism is achieved for free and forced vibration suppression at the first resonance frequency through a designed FLC. The robustness performance of various FLCs is evaluated by changing various design parameters at the various arm position of the mass location variation mechanism.

At first, the piezo-beam having the mass location variation mechanism and the hardware platform for controlling the PZT patches on the surface of the piezo-beam are introduced. The FRFs of the piezo-beam between the sensor and the controller PZT patch pairs are investigated for various arm positions and the first resonance frequencies of the piezo-beam corresponding to these arm positions are then obtained. Additionally, the transfer functions are also obtained so as to observe the performance of the designed FLCs through the simulation studies.

The FLC which is designed via Fuzzy Logic Toolbox in Matlab, is tested experimentally for free and the forced vibration suppression at the fundamental resonance frequency of the piezo-beam at the middle arm position provided by the mass location variation mechanism. The simulation studies are performed in order to compare their results with the experimental ones. The obtained results are consistent with each other and the suppression ratio of 92 % is obtained for both studies.

Finally, by chancing the number of the rules, the overlap ratio and core location of the membership functions of the FLCs, the robust performance of the FLCs is then evaluated for the forced vibration suppression of the piezo-beam for different arm

positions at their first corresponding resonance frequencies. It is observed that the FLC with 25 rules is more suitable than the FLCs with 9 and 49 rules and also the FLC with overlap ratio of 57% has the best performance among the FLCs with overlap ratio of 0%, 25%, 33%, 50%, 63% and 67%. Also, although the performances of the FLCs with core locations closed to zero and away from zero are almost the same as the performance of the FLC with symmetric membership functions, the FLC with symmetric membership functions has the best robustness ratio. Therefore, the FLC with the symmetric membership function is more desirable for the robust performance for vibration suppression.

Consequently, the FLC is obtained as a robust controller to suppress the free and the forced vibration at the first resonance of the piezo-beam with changing mass location through various different parameters. It is also observed that the excessive variation in the parameters investigated in this particular study does not substantially affect the suppression performances. Therefore, it can be said that the designed FLCs provide robust performance in active vibration control of the piezo-beam.

5.2. Recommendation for Future Work

The free and the first resonance vibrations of the piezo-beam are of interest in this particular thesis study. The vibration suppression of the higher modes can also be investigated through the changes in the parameters of the FLCs.

The parametric study performed in this thesis for the design of a robust FLC can be further developed by using a global optimization method in order to achieve a better robustness performance in the vibration suppression of a piezo-beam structure.

REFERENCES

[1] R. F. Keltie and C. C. Cheng, "Vibration reduction of a mass-loaded beam," *J. Sound Vib.*, vol. 187, no. 2, pp. 213–228, 1995.

[2] A. J. Keane and A. P. Bright, "Passive vibration control via unusual geometries: Experiments on model aerospace structures," *J. Sound Vib.*, vol. 4, no. 7, pp. 713–719, 1996.

[3] S. N. Shevtsov and V. A. Akopyan, "Active and passive vibration control of aircraft composite structures using power piezoelectric patch-like actuators," in *Piezoceramic Materials and Devices*, I. A. Parinov, Ed. Nova Science Publisher, Inc, 2010.

[4] X. Jin, M. Z. Q. Chen, and Z. Huang, "Minimization of the beam response using inerter-based passive vibration control configurations," *Int. J. Mech. Sci.*, vol. 119, no. October, pp. 80–87, 2016.

[5] J. Philip and L. John, "Impact of Smart Materials in Aero Industry," in *International Conference on Challenges and Opportunities in Mechanical Engineering, Industrial Engineering and Management Studies*, 2012, pp. 440–446.

[6] G. Takács and B. Rohal'-Ilkiv, "Algorithms in Active Vibration Control," in *Model Predictive Vibration Control: Efficient Constrained MPC Vibration Control for Lightly Damped Mechanical Structures*, 2012, pp. 105–140.

[7] I. Nagasaka, Y. Ishida, and T. Koyama, "Vibration Suppression of Helicopter Blades By Pendulum Absorbers," *Trans. Japan Soc. Mech. Eng. Ser. C*, vol. 73, no. 725, pp. 129–137, 2007.

[8] P. J. Murtagh, A. Ghosh, B. Basu, and B. M. Broderick, "Passive control of wind turbine vibrations including blade/tower interaction and rotationally sampled turbulence," *Wind Energy*, vol. 11, no. 4, pp. 305–317, 2008.

[9] B. Shafer, "An overview of constrained-layer damping theory and application," *J. Acoust. Soc. Am.*, vol. 133, no. 5, pp. 1–5, 2013.

[10] M. Ciminello, A. Calabr, S. Ameduri, and A. Concilio, "Synchronized switched shunt control technique applied on a cantilevered beam: Numerical and experimental investigations," *J. Intell. Mater. Syst. Struct.*, vol. 19, no. 9, pp.

1089–1100, 2008.

[11] J. T. Pearson, R. M. Goodall, and I. Lyndon, “Active control of helicopter vibration,” *Comput. Control Eng. J.*, no. December, pp. 277–284, 1994.

[12] F. Casella, A. Locatelli, and N. Schiavoni, “Modeling and control for vibration suppression in a large flexible structure with jet thrusters and piezoactuators,” *IEEE Trans. Control Syst. Technol.*, vol. 10, no. 4, pp. 589–599, 2002.

[13] J. Dosch, D. Leo, and D. Inman, “Modelling and Control for Vibration Suppression of a Flexible Active Structure,” *J. Guid. Control Dyn.*, vol. 18, no. 2, pp. 340–346, 1995.

[14] A. A. Ali, H. Y. Mahmood, and M. W. Saeed, “Active Vibration Control of Aircraft Wing Using Piezoelectric Transducers,” *Int. J. Sci. Eng. Res.*, vol. 7, no. 5, pp. 977–984, 2016.

[15] N. Fadhilah, M. Ros, M. S. Saad, and I. Z. Mat Darus, “Dynamic Modeling and Active Vibration Control of a Flexible Beam : A Review,” *Int. J. Eng. Technol.*, vol. 15, no. 05, pp. 12–17, 2015.

[16] U. Aridogan and I. Basdogan, “A review of active vibration and noise suppression of plate-like structures with piezoelectric transducers,” *J. Intell. Mater. Syst. Struct.*, vol. 26, no. 12, pp. 1455–1476, 2015.

[17] K. M. Gupta, “Introduction to Some Recent and Emerging Materials,” in *Engineering Materials: Research, Application and Advances*, 2015, pp. 11–20.

[18] M. Z. Sariman, M. H. Harun, A. K. M. Yamin, F. Ahmad, and M. R. Yunos, “Magnetorheological Fluid Engine Mounts : A Review on Structure Design of Semi Active Engine Mounting,” *Int. J. Mater.*, vol. 2, p. 76100, 2015.

[19] L. Xu and Z. Fu, “Multifield coupled analysis for a harmonic movable tooth drive system integrated with shape memory alloys,” *Appl. Math. Model.*, vol. 69, pp. 493–505, 2019.

[20] W.-G. Drossel, H. Kunze, A. Bucht, L. Weisheit, and K. Pagel, “Smart3 - Smart Materials for Smart Applications,” *Procedia CIRP*, vol. 36, pp. 211–216, 2015.

[21] S. Mishra, L. Unnikrishnan, S. K. Nayak, and S. Mohanty, “Advances in Piezoelectric Polymer Composites for Energy Harvesting Applications: A Systematic Review,” *Macromol. Mater. Eng.*, vol. 304, no. 1, pp. 1–25, 2019.

[22] J. Sirohi and I. Chopra, “Fundamental understanding of piezoelectric strain

sensors," *J. Intell. Mater. Syst. Struct.*, vol. 11, no. 4, pp. 246–257, 2000.

[23] G. Zuo and L. Wong, "A Review on Recent Active Vibration Control Techniques," 2016.

[24] C. M. A. Vasques and J. Dias Rodrigues, "Active vibration control of smart piezoelectric beams: Comparison of classical and optimal feedback control strategies," *Comput. Struct.*, vol. 84, no. 22–23, pp. 1402–1414, 2006.

[25] Q. Hu and G. Ma, "Variable structure control and active vibration suppression of flexible spacecraft during attitude maneuver," *Aerosp. Sci. Technol.*, vol. 9, no. 4, pp. 307–317, 2005.

[26] T. Caliskan, "Piezoelectric ceramics and their applications in smart aerospace structures," M.S. thesis, Department of Aeronautical Engineering, Middle East Technical University, Ankara, 2002.

[27] A. Alavinasab, H. Moharrami, and A. Khajepour, "Active control of structures using energy-based LQR method," *Comput. Civ. Infrastruct. Eng.*, vol. 21, no. 8, pp. 605–611, 2006.

[28] J. Zhang, L. He, and E. Wang, "Active vibration control of piezoelectric intelligent structures," *J. Comput.*, vol. 5, no. 3, pp. 401–409, 2010.

[29] Y. Wang and D. J. Inman, "Comparison of control laws for vibration suppression based on energy consumption," *J. Intell. Mater. Syst. Struct.*, vol. 22, no. 8, pp. 795–809, 2011.

[30] N. R. Fisco and H. Adeli, "Smart structures: Part II - Hybrid control systems and control strategies," *Sci. Iran.*, vol. 18, no. 3 A, pp. 285–295, 2011.

[31] O. F. Kircali, Y. Yaman, V. Nalbantoğlu, M. Şahin, and F. M. Karadal, "Application of spatial H∞ control technique for active vibration control of a smart beam," in *4th International Conference on Informatics in Control, Automation and Robotics*, 2007, pp. 322–328.

[32] M. Sahin, F. M. Karadal, Y. Yaman, O. F. Kircali, and V. Nalbantoglu, "Smart structures and their applications on active vibration control: Studies in the Department of Aerospace Engineering, METU," *J. Electroceramics*, vol. 20, pp. 167–174, 2008.

[33] Z. Qiu, X. Zhang, and C. Ye, "Vibration suppression of a flexible piezoelectric beam using BP neural network controller," *Acta Mech. Solida Sin.*, vol. 25, no.

4, pp. 417–428, 2012.

[34] M. K. Kwak and D. Sciulli, “Fuzzy-Logic Based Vibration Suppression Control Experiments on Active Structures,” *J. Sound Vib.*, vol. 191, pp. 15–28, 1996.

[35] L. A. Zadeh, “Fuzzy Sets-Information and Control-1965,” *Inf. Control*, 1965.

[36] E. H. Mamdani, “Application of fuzzy algorithms for control of simple dynamic plant,” *Proc. Inst. Electr. Eng.*, 1974.

[37] Q. Wenzhong, S. Jincai, and Q. Yang, “Active control of vibration using a fuzzy control method,” *J. Sound Vib.*, vol. 275, no. 3–5, pp. 917–930, 2004.

[38] T.-L. Teng, C.-P. Peng, and C. Chuang, “A study on the application of fuzzy theory to structural active control,” *Comput. Methods Appl. Mech. Eng.*, vol. 189, no. 2, pp. 439–448, 2000.

[39] J. Lin and W. Z. Liu, “Experimental evaluation of a piezoelectric vibration absorber using a simplified fuzzy controller in a cantilever beam,” *J. Sound Vib.*, vol. 296, no. 3, pp. 567–582, 2006.

[40] G. Tairidis, G. Foutsitzi, P. Koutsianitis, and G. E. Stavroulakis, “Fine tuning of a fuzzy controller for vibration suppression of smart plates using genetic algorithms,” *Adv. Eng. Softw.*, vol. 101, pp. 123–135, 2016.

[41] M. Marinaki, Y. Marinakis, and G. E. Stavroulakis, “Fuzzy control optimized by PSO for vibration suppression of beams,” *Control Eng. Pract.*, vol. 18, no. 6, pp. 618–629, 2010.

[42] N. D. Zoric, A. M. Simonovic, Z. S. Mitrovic, S. N. Stupar, A. M. Obradovic, and N. S. Lukic, “Free vibration control of smart composite beams using particle swarm optimized self-tuning fuzzy logic controller,” *J. Sound Vib.*, vol. 333, no. 21, pp. 5244–5268, 2014.

[43] J. Wei, Z. Qiu, J. Han, and Y. Wang, “Experimental Comparison Research on Active Vibration Control for Flexible Piezoelectric Manipulator Using Fuzzy Controller,” *J. Intell. Robot. Syst.*, vol. 59, no. 1, pp. 31–56, 2010.

[44] Y. T. Aksoy, “Active Vibration Control of a Smart Sandwich Plate via Piezoelectric Sensor and Actuators,” M.S. thesis, Aerospace Engineering Department, Middle East Technical University, Ankara, 2015.

[45] M. Itik, M. U. Salamci, F. Demet Ulker, and Y. Yaman, “Active vibration suppression of a flexible beam via sliding mode and H ∞ control,” in

Proceedings of the 44th IEEE Conference on Decision and Control, and the European Control Conference, CDC-ECC '05, 2005, pp. 1240–1245.

[46] Y. Yaman *et al.*, "Application of H∞ Active Vibration Control Strategy in Smart Structures," in *3rd International Conference on Advanced Enginnering Design*, 2003.

[47] C. Onat, M. Sahin, and Y. Yaman, "Active Vibration Suppression of a Smart Beam by Using an LQG Control Algorithm," in *2nd International Conference of Engineering Against Fracture (ICEAF II)*, 2011, pp. 22–24.

[48] C. Onat, M. Şahin, and Y. Yaman, "Fractional controller design for suppressing smart beam vibrations," *Aircr. Eng. Aerosp. Technol.*, vol. 84, no. 4, pp. 203–212, 2012.

[49] C. Onat, M. Sahin, Y. Yaman, S. E. Prasad, and S. Nemana, "Design of an LPV Based Fractional Controller for the Vibration Suppression of a Smart Beam," in *Smart Materials & Structures and NDT in Aerospace*, 2011, pp. 1–10.

[50] O. Akın, "Active Neuro-Adaptive Control of a Smart Beam Having Uncertainties in Structural Dynamics," M.S. thesis, Aerospace Engineering Department, Middle East Technical University, Ankara, 2015.

[51] O. Akın and M. Sahin, "Active neuro-adaptive vibration suppression of a smart beam," *Smart Struct. Syst.*, vol. 20, no. 6, pp. 657–668, 2017.

[52] V. Gupta, M. Sharma, and N. Thakur, "Optimization criteria for optimal placement of piezoelectric sensors and actuators on a smart structure: A technical review," *J. Intell. Mater. Syst. Struct.*, vol. 21, no. 12, pp. 1227–1243, 2010.

[53] N. Sabri, S. A. Aljunid, M. S. Salim, R. B. Badlishah, R. Kamaruddin, and M. F. A. Malek, "Fuzzy Inference System: Short Review and Design," *Int. Rev. Autom. Control*, vol. 6, no. 4, 2013.

[54] K. Sinthipsomboon, I. Hunsacharoonroj, J. Khedari, W. Pongaen, and P. Pratumsuwan, "A hybrid of fuzzy and fuzzy self-tuning PID controller for servo electro-hydraulic system," *Proc. 2011 6th IEEE Conf. Ind. Electron. Appl. ICIEA 2011*, pp. 220–225, 2011.

[55] O. A. M. Ali, A. Y. Ali, and B. S. Sumait, "Comparison between the Effects of Different Types of Membership Functions on Fuzzy Logic Controller Performance," *Int. J. Emerg. Eng. Res. Technol.*, vol. 3, no. 3, pp. 76–83, 2015.

[56] E. R. Senoz and M. Sahin, “Kiriş Benzeri Bir Yapinin Farkli Sayida Kural İçeren Bulanik Mantik Kontrolcüsü Kullanarak ve Pizeoelektrik Uyaricilar ile Aktif Titreşim Kontrolünün Performans Kiyaslamasi,” in *VI. Ulusal Havacılık ve Uzay Konferansı*, 2016, pp. 1–7. (In Turkish)

[57] T. J. Ross, “Properties of Membership Functions, Fuzzification, and Defuzzification,” in *Fuzzy Logic with Engineering Applications*, Second., 2004, pp. 90–119.

APPENDICES

A. Selection of a Low-Pass Filter for Eliminating the Sensor Noise

The noise in the sensor signal should be eliminated by a low-pass filter in order to obtain better derivative or difference in the sensor signal. The Simulink model is created for experimental study to observe the sensor signal with various low-pass filters, as shown in Figure A.1. A sine wave excites the piezo-beam at the first resonance of the piezo-beam for the arm position of 0°.

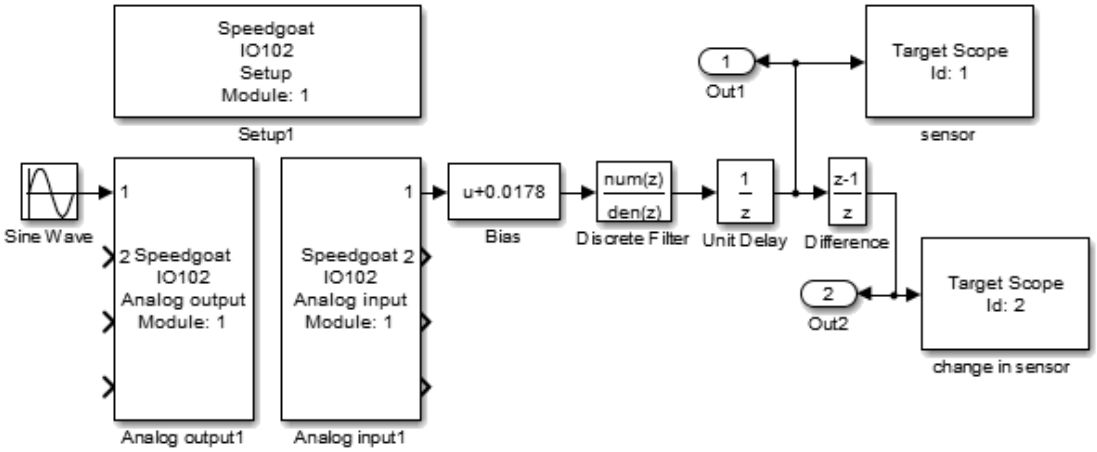

Figure A.1. Simulink Model for the Time Response at the First Resonance of the Piezo-Beam with a Low-Pass Filter

Three different low-pass filters are applied at the same excitation signal. The low-pass filters have cut-off frequencies of 50 Hz, 100 Hz and 400 Hz. Time responses of the sensor signal (Figure A.2 and Figure A.3) and the change in sensor signal (Figure A.4) for these particular low-pass frequencies are plotted respectively. As shown in Figure A.2 and Figure A.3, the low-pass filter with cut-off frequency of 50 Hz creates the biggest delay in the signal. The low-pass filter with cut-off frequency of 400 Hz is not enough to reduce noise in the change in sensor signal as shown in Figure A.4. Therefore, the low-pass filter with cut-off frequency of 100 Hz is selected to reduce noise in the signal.

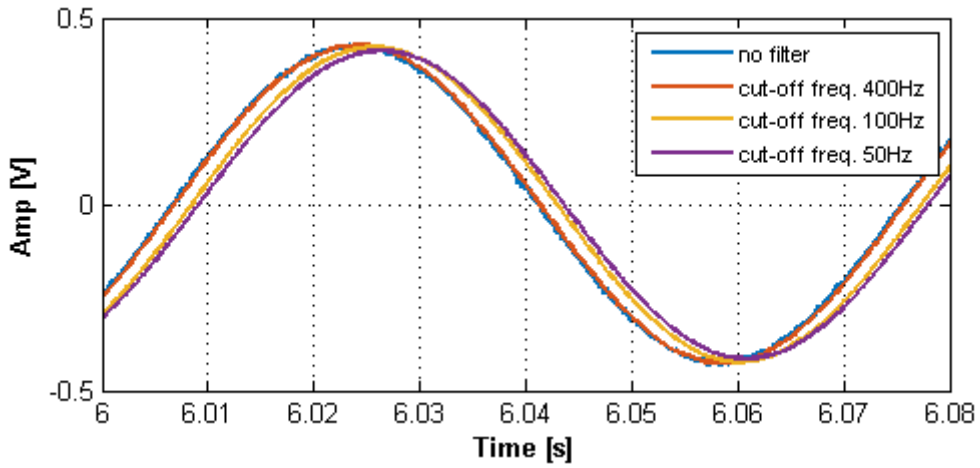

Figure A.2. Time Response of the Sensor Signal with Various Low-Pass Filters

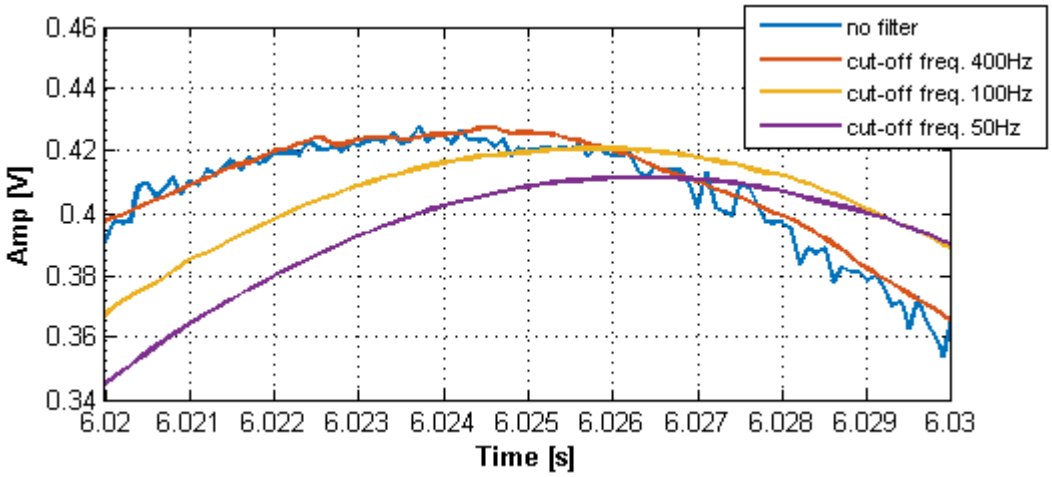

Figure A.3. Zoomed Plot of Time Response of the Sensor Signal with Various Low-Pass Filters

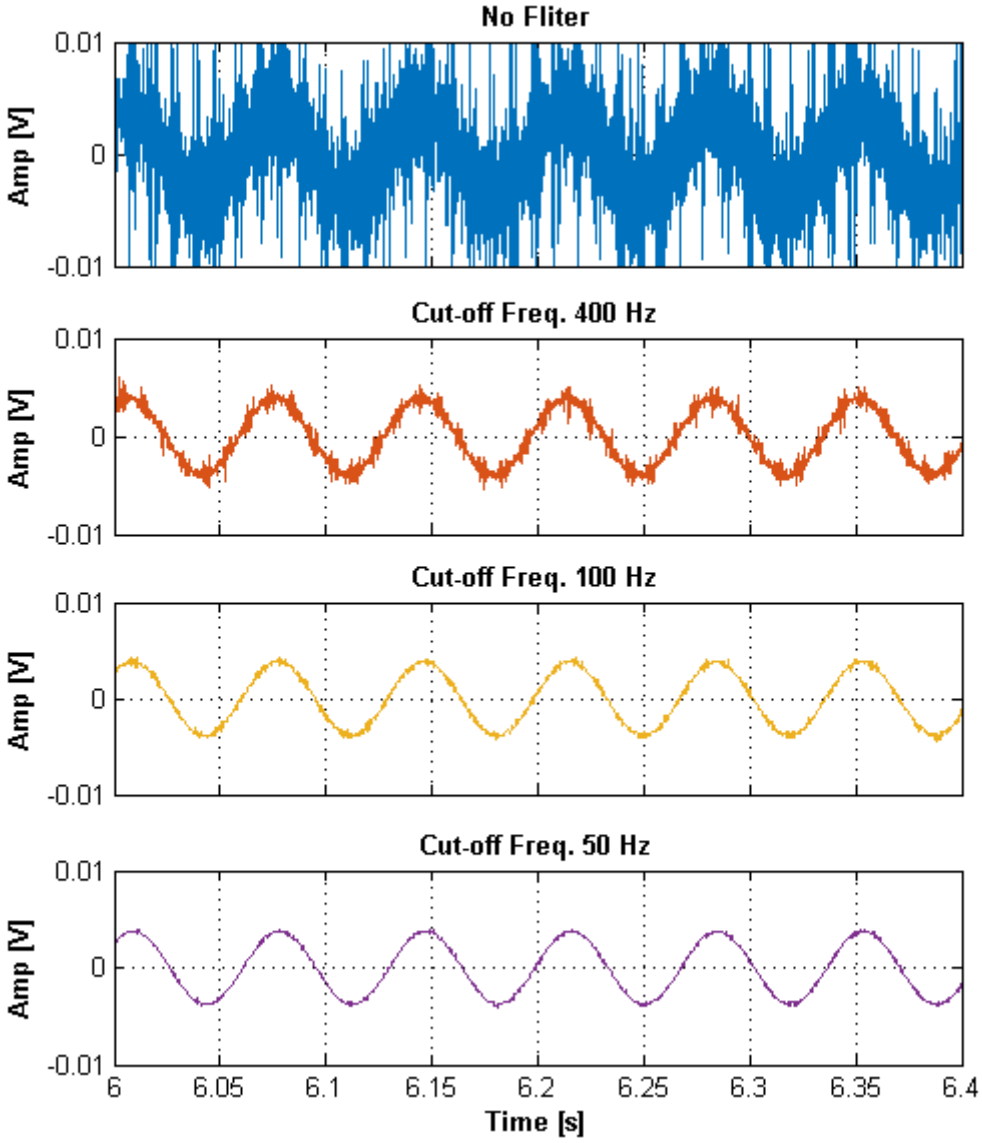

Figure A.4. Time Response of the Change in Sensor Signal with Various Low-Pass Filters

B. Selection of a Low-Pass Filter for Eliminating High-Order Frequency Content of Controller Output

FLC is a non-linear controller. The output of the controller may include high-order frequency content. The high-order frequency may stimulate the higher resonance mode of the piezo-beam. Therefore, a low-pass filter is used for defining the effective range of the controller.

At first, the low-pass filter having the cut-off frequency of 100 Hz is applied to output of the controller for forced vibration at the first resonance of the piezo-beam. The time response is given in Figure B.1. Then, in order to analyze the time domain data, the time response can be zoomed in the region where controller is switched on as shown in Figure B.2. After the controller is switched on at 6th second, another sine wave is appeared on the sine wave at the resonance frequency. For better understanding, frequency domain analysis should be made by taking FFT of the signal after the 6th second and the FFT is plotted in Figure B.3. The frequency of 92 Hz which is nearby the second resonance frequency of the piezo-beam is another dominant frequency in the sensor signal except the first resonance frequency. The reason is that the controller signal can stimulate the second resonance mode of the piezo-beam.

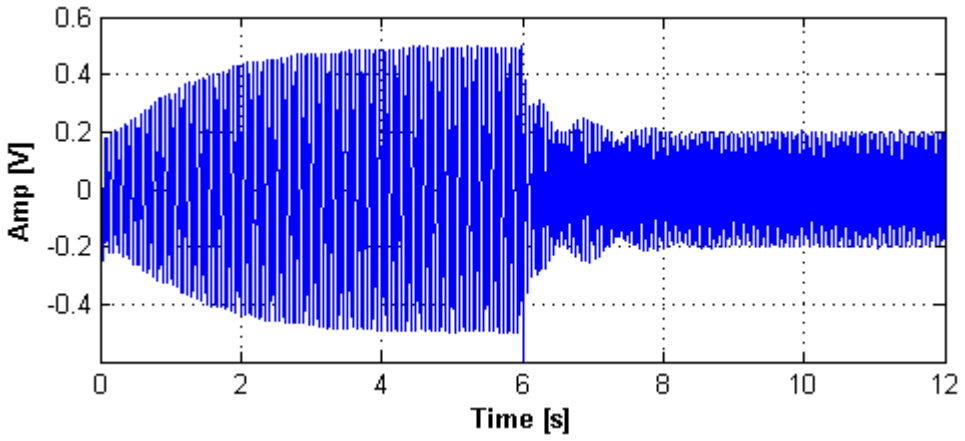

Figure B.1. Time Response of Forced Vibration at the First Resonance with the Low-Pass Frequency at cut-off Frequency of 100 Hz

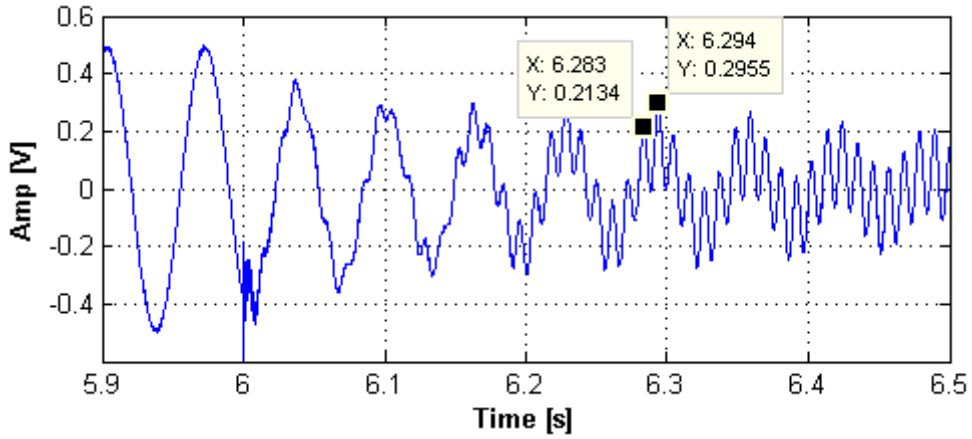

Figure B.2. Zoomed Plot of Forced Vibration at the First Resonance with the Low-Pass Frequency at cut-off Frequency of 100 Hz

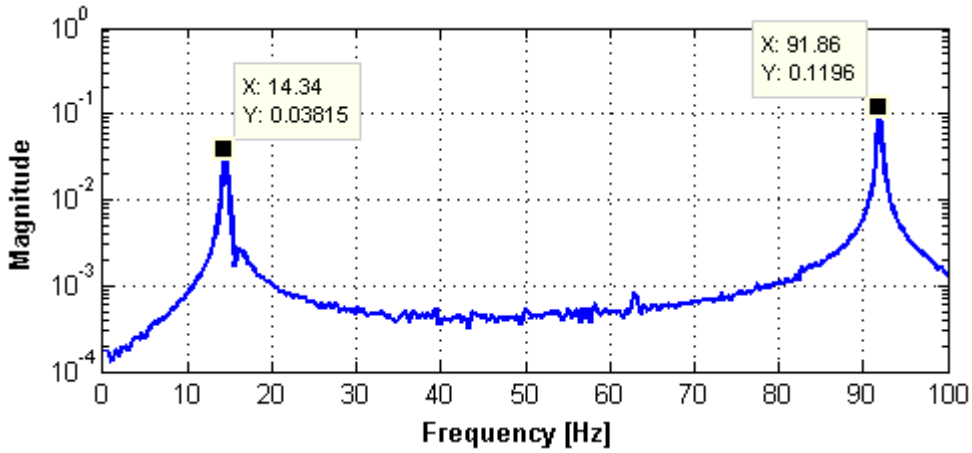

Figure B.3. FFT of the Sensor Signal with the Low-Pass Frequency at cut-off Frequency of 100 Hz after the Controller is switched on

Then, another low-pass filter having the cut-off frequency of 50 Hz which is between the frequencies occurring the maximum peaks is applied to output of the controller. The suppression performance at the forced vibration at the first resonance is much better than the previous filter as shown in Figure B.4. In order to compare the time domain results, the zoomed plot of time response in the region where controller is switched on is shown in Figure B.5. The FFT of the signal after the 6th second is also plotted as shown in Figure B.6.

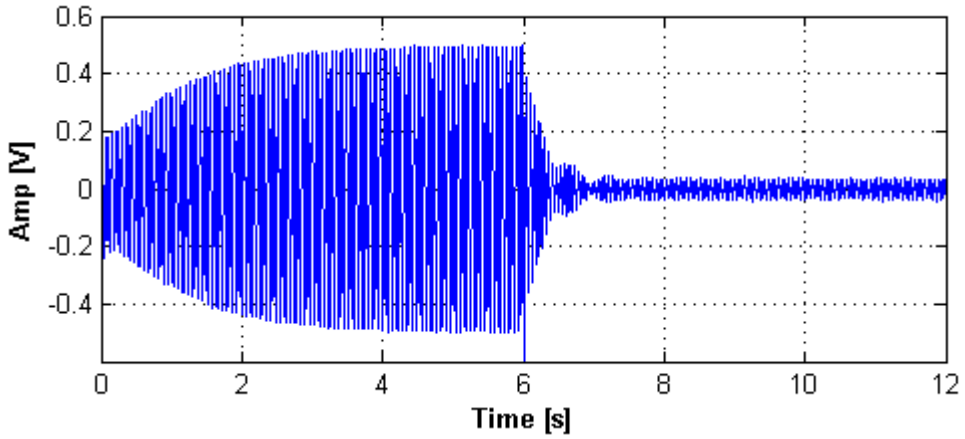

Figure B.4. Time Response of Forced Vibration at the First Resonance with the Low-Pass Frequency at cut-off Frequency of 50 Hz

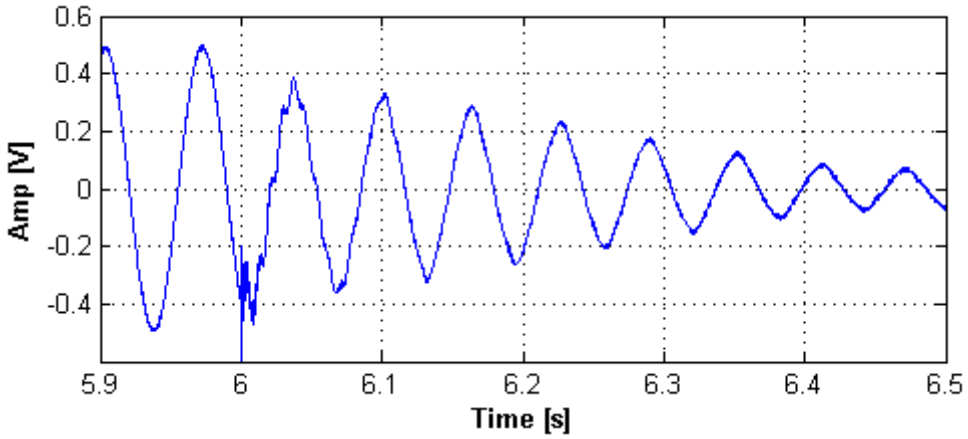

Figure B.5. Zoomed Plot of Forced Vibration at the First Resonance with the Low-Pass Frequency at cut-off Frequency of 50 Hz

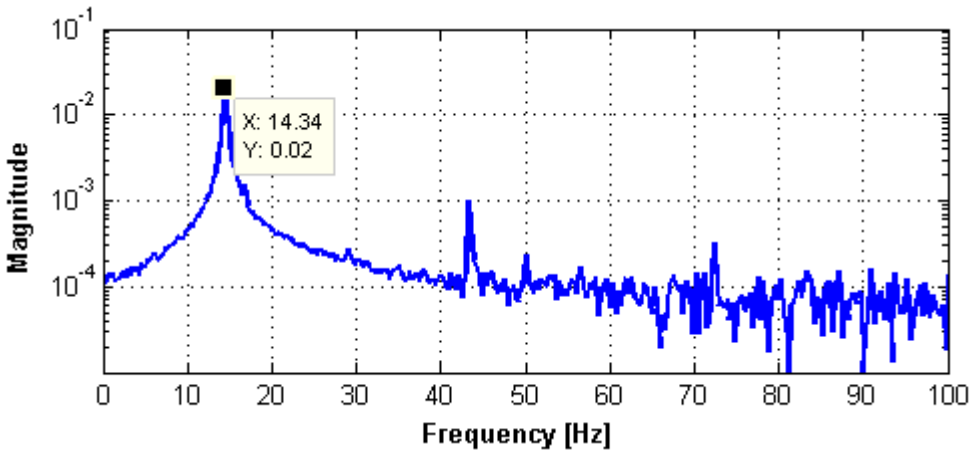

Figure B.6. FFT of the Sensor Signal with the Low-Pass Frequency at cut-off Frequency of 50 Hz after the Controller is switched on

Consequently, high-order frequency content in the sensor signal can be eliminated by the low-pass frequency with an appropriate cut-off frequency. When the cut-off frequency is selected in the middle of the first and second resonance frequencies, the effect of the second resonance mode disappears on the sensor signals.

C. Performance Analysis of the FLC for the Higher Modes

The designed FLC is performed for observing the higher modes at the frequencies up to 150 Hz. A chip signal from 5 Hz to 150 Hz is applied as an excitation signal. Then, the FRF of the piezo-beam which is controlled with the FLC is obtained for the arm position of 0° as shown in Figure C.1. At the higher frequencies between 60 Hz and 100 Hz, the magnitude of vibration is increased when the FLC is applied. However, the magnitude remains almost the same at the mode with frequency at about 120 Hz. Therefore, although the FLC does not improve the suppression of vibrations at higher modes, it does not create any instability.

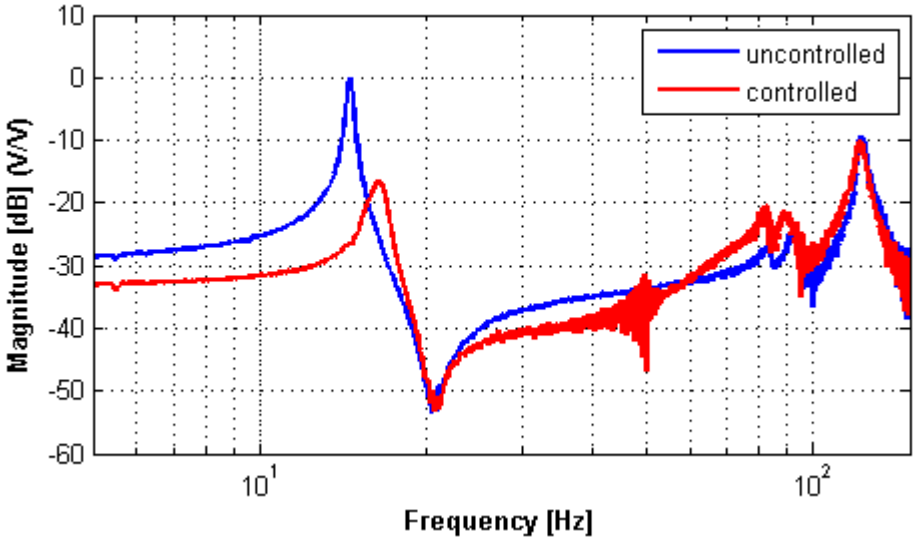

Figure C.1. FRF of Controlled Piezo-Beam for Higher Modes

D. Performance Analysis of the FLC for Near Arm Positions of +64°

In the robustness analysis for the designed FLC for different arm positions, it is shown that there is a sharp decrease in suppression ratio for the arm position of +64°. Therefore, in order to observe this decrease, tests should be performed in small intervals around the aforementioned arm position. The arm position of +48°, +56°, +72° and +80° are selected as further test cases.

The control unit of the mass location variation mechanism can only manipulate the arm to certain positions. Therefore, the arm is rotated manually to the intermediate positions by measuring with spirit level.

In order to excite the piezo-beam for different arm positions at their first corresponding resonance frequencies, the resonance frequencies are found as 13.78 Hz, 13.66 Hz, 13.52 Hz and 13.48 Hz by obtaining FRF for the arm position of +48°, +56°, +72° and +80°, respectively.

Then, the piezo-beam is excited at their first corresponding resonance frequency and the designed FLC is activated after 6 seconds to suppress the forced vibration. The time responses for different arm positions are plotted in Figure D.1. The FLC is able to suppress the forced vibration sufficiently when the arm position is lower than +64°. However, when the arm is at the position of +64° or higher, a significant reduction in the suppression level of the forced vibration is observed.

The suppression ratios for different arm positions are tabulated in *Table D.1*. According to these results, it is also observed that the suppression level decreases by rotating arm towards to tip of the piezo-beam.

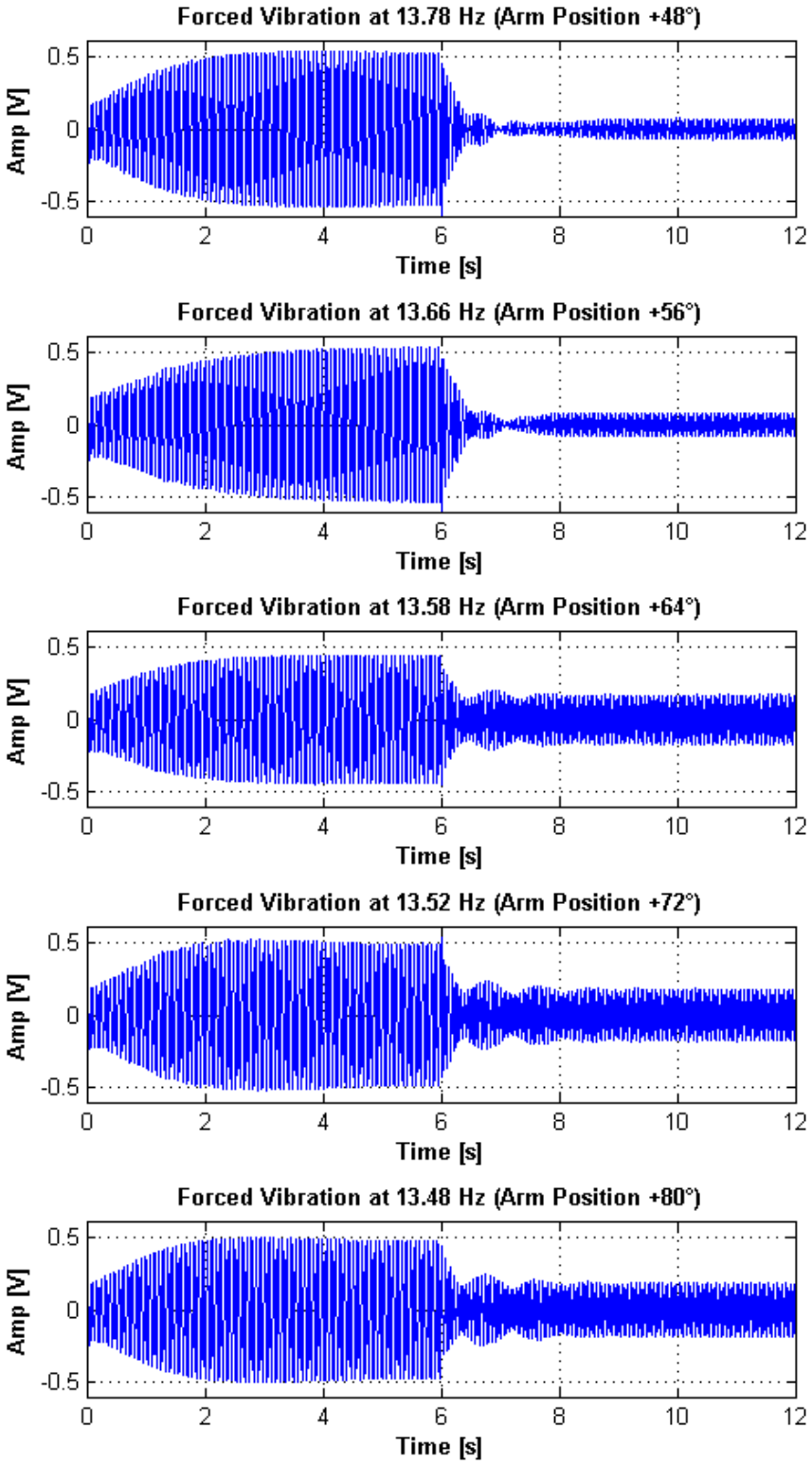

Figure D.1. Forced Vibration at Corresponding Resonance Frequency for the Different Arm Positions nearby +64°

Table D.1 *The Result of the Suppression Ratios for Different Arm Positions nearby +64°*

The Arm Position	**Suppression Ratios**
+48°	87%
+56°	85%
+64°	63%
+72°	63%
+80°	61%